INVESTIGATIONS INTO MICROGRID SIZING AND ENERGY MANAGEMENT STRATEGIES

Yara Jamil Khawaja

A Thesis Submitted for the Degree of

Doctor of Philosophy at Newcastle University

School of Engineering

Faculty of Science, Agriculture and Engineering

August 2019

DECLARATION

I hereby declare that this thesis is my own work and effort and that it has not been submitted anywhere for any award. Where other sources of information have been used, they have been acknowledged.

Newcastle upon Tyne, 2019

Yara Jamil Khawaja

CERTIFICATE OF APPROVAL

We confirm that, to the best of our knowledge, this thesis is from the student's own work and effort, and all other sources of information used have been acknowledged. This thesis has been submitted with my approval.

Dr. Damian Giaouris

Dr. Adib Allahham

Dr. Charalampos Patsios

Dr. Mohamed Dahidah

To Issa, Hani, Morad, and Bassel

— Yara

ACKNOWLEDGEMENTS

I would like to express my deep gratitude to my supervisors Dr. Damian Giaouris, Dr. Adib Allahham, Dr. Charalampos Patsios, and Dr. Mohamed Dahidah for their wisdom and guidance through my PhD journey. They have always been a source of motivation and my inspirational model as a researcher.

I am grateful to the Applied Science Private University in Jordan for funding my PhD study and for their support.

I would like also to express my gratefulness and appreciation to my colleagues and friends in the School of Engineering, especially those in Power System Research Group.

Thank you, my father, my mother and my mother-in-law, without your unconditional support, this thesis never would have come to be. Finally, and most importantly, I am thankful to my lovely family, Issa my wonderful husband and my lovely sons Hani, Morad and Bassel for all of their love, support, motivation and patience throughout my PhD. They were there to help me at difficult times, and to share in good times. Their encouragement has helped me with the research and with the writing of this thesis, and I am very grateful.

ABSTRACT

The evolution of microgrids represents a significant step towards the transition to more sustainable power systems. Recent trends in microgrids include the integration of renewable energy resources (RERs), alternative energy resources (AERs) and energy storage systems (ESSs). However, the integration of these systems creates new challenges on microgrid operation because of their stochastic and intermittent nature. To mitigate these challenges, determining the appropriate size together with the best energy management strategy (EMS) systems are essential to ensure economic and optimal performance.

This thesis presents an investigation into sizing and energy management of microgrids. In the first part of the thesis, an analytical and economic sizing (AES) approach is developed to find the optimal size of a grid-connected photovoltaic-battery energy storage system (PV-BESS). The proposed approach determines the optimal size based on the minimum levelised cost of energy (LCOE). Fundamental to this approach obtains an improved formula of LCOE which includes new parameters for reflecting the impact of surplus PV energy and the energy purchased from the grid.

In the second part of this thesis, an integrated framework is proposed for finding the best size-EMS combination of a stand-alone hybrid energy system (HES). The HES consists of PV, BESS, diesel generator, fuel cell, electrolyser, and hydrogen tank. The proposed framework includes three consecutive steps; first, performing the AES to obtain the initial size of the HES, second, implementing the initial EMS using finite automata (FA) and instantiating multiple EMSs; and third, developing an evaluation model to assess the instantiated EMSs and extract the featured conditions to produce an improved EMS. Then the AES approach is re-exercised using the improved EMS to obtain the best size-EMS combination. The core of this framework is utilising FA to implement various EMSs and capturing the impact of selecting the best EMS on the sizing of the HES.

Furthermore, a sensitivity analysis is performed to address the uncertainty in demand and solar radiation data showing their effect on the HES performance. The analysis is carried out by assuming variations in solar radiation and demand annual data. Several scenarios are generated from the sensitivity analysis, and a number of performance indices are computed for each scenario. Following that, a

fuzzy logic controller is designed using the performance indices as fuzzy input sets. The objective of this controller is to modify the EMS obtained from the integrated framework. This can be accomplished by detecting any changes in the demand and solar radiation and accordingly modify the operating conditions of the diesel generator, fuel cell, and electrolyser.

The performance of the proposed approaches is validated using real datasets for both demand and solar radiation. The results show the optimal size and EMS for both grid-connected and stand-alone microgrids. Moreover, the designed fuzzy logic controller enables the microgrid to mitigate the uncertainty in the demand and generation data.

The proposed approaches can be used with various scales of microgrids to extract manifold benefits where reliability, environmental and cost requirements can not be tolerated.

PUBLICATIONS AND CONTRIBUTIONS

The publications that were produced as a part of the research reported in this thesis are listed as follows:

Journal publications:

- **Yara Khawaja**; Adib Alhham; Damian Giaouris; Charalmpos Patsios; Sara Walker; Mohamed Dahadih; Issa Qiqieh; *An Integrated Framework for Sizing and Energy Management for Hybrid Energy System using Finite Automata*, Applied Energy, Elsevier, Volume 250, 2019, pp. 257-272.

- **Yara Khawaja**; Adib Alhham; Damian Giaouris; Charalmpos Patsios; *Modifying the Energy Management of a Hybrid Energy System using Fuzzy Logic* (to be submitted to Applied Energy, Elsevier).

Conference publications:

- **Yara Khawaja**; Damian Giaouris; Charalmpos Patsios; Mohamed Dahadih; *Optimal cost-based model for sizing grid-connected PV and battery energy system*, 2017 IEEE Jordan Conference on Applied Electrical Engineering and Computing Technologies (AEECT), Amman, 2017, pp. 1-6.

- **Yara Khawaja**; Adib Allahham, Damian Giaouris; Charalampos Patsios; and Mohamed Dahidah; *Supervision Control and Energy Management Strategies for Grid-Connected Microgrids Using Finite Automata*, UKES 2018.

CONTENTS

I Thesis Chapters 1

1 INTRODUCTION 2

1.1 Motivation . . . 2

1.1.1 Sizing of Microgrids . . . 3

1.1.2 Energy Management Strategies . . . 5

1.2 Thesis Scope and Contributions . . . 6

1.3 Thesis Overview . . . 8

2 BACKGROUND AND LITERATURE SURVEY 10

2.1 Introduction . . . 10

2.2 Microgrids . . . 10

2.2.1 Microgrid Benefits and Drawbacks . . . 11

2.2.2 Microgrids Modes . . . 13

2.3 Energy Storage Systems . . . 14

2.4 Hybrid Energy Systems . . . 16

2.5 Criteria for Microgrid Optimisation . . . 17

2.5.1 Reliability Assessment . . . 18

2.5.2 Economic Assessment . . . 20

2.5.3 Environmental Assessment . . . 21

2.6 Control and Energy Management of Microgrids . . . 22

2.7 Finite Automata and Fuzzy Logic . . . 25

2.7.1 Finite Automata and Discrete Event Systems . . . 26

2.7.2 Fuzzy Logic . . . 27

2.8 Microgrids Sizing Methods . . . 28

2.8.1 Graphical Construction Methods . . . 29

2.8.2 Analytical Methods 30
2.8.3 Iterative Methods 31
2.8.4 Probabilistic Methods 33
2.8.5 Artificial Intelligence Methods 33
2.8.6 Hybrid Methods 35
2.8.7 Software Tools 36
2.9 Concluding Remarks and Discussions 39

3 SIZING OF GRID-CONNECTED MICROGRID 40
3.1 Introduction 40
3.2 Grid-connected PV-BESS Architecture 41
3.3 Sizing Methodology of PV-BESS Grid-Connected 42
3.4 PV-BESS Analytical and Economic Model 46
3.4.1 PV System Analytical Model 47
3.4.2 BESS Analytical Model 49
3.4.3 The Economic Model of the Grid-connected PV-BESS . . . 50
3.5 Results and Discussion 54
3.6 Concluding Remarks 64

4 THE INTEGRATED FRAMEWORK 66
4.1 Introduction 66
4.2 HES Structure and Modelling in Finite Automata 68
4.2.1 HES Architecture 68
4.2.2 Modelling the BESS in Finite Automata 68
4.2.3 Implementing EMS using Finite Automata 71
4.3 Analytical Modelling of HES 77
4.3.1 Battery Energy Storage System 78
4.3.2 Diesel Generator 83
4.3.3 Fuel Cell 84
4.3.4 Electrolyser 85
4.3.5 Hydrogen Tank 87
4.4 The Economic Modelling 88

4.4.1 Photovoltaic . . . 89
4.4.2 Battery Energy Storage System . . . 90
4.4.3 Diesel Generator . . . 90
4.4.4 Objective Function and Constraints . . . 91
4.5 Initial Sizing . . . 93
4.6 Integrated Framework . . . 94
4.6.1 Instantiation of EMSs using Finite Automata . . . 95
4.6.2 Performance Indices . . . 99
4.6.3 Evaluation Model and $EMS_{initial}$ Replacement . . . 100
4.7 Results and Discussion . . . 102
4.8 Concluding Remarks . . . 108

5 MODIFYING ENERGY MANAGEMENT USING FUZZY LOGIC 110
5.1 Introduction . . . 110
5.2 Resizing the Hybrid Energy System using Forecasted Data . . . 111
5.3 Sensitivity Analysis . . . 113
5.4 Modify the EMS Using Fuzzy Logic . . . 119
5.4.1 The design of Fuzzy Logic Controller . . . 119
5.4.2 The Fuzzy Rules . . . 124
5.4.3 The Results of Fuzzy Logic Controller . . . 130
5.4.4 Validation Case Study . . . 133
5.5 Concluding Remarks . . . 136

6 CONCLUSIONS AND FUTURE WORK 137
6.1 Summary and Conclusions . . . 137
6.2 Critical Review and Future Work . . . 139

II Thesis Bibliography 141

BIBLIOGRAPHY 142

LIST OF FIGURES

Figure 1.1 The evolution of global total Photovoltaic (PV) installed capacity from 2012 to 2020 [1]. 4

Figure 2.1 Example of a microgrid including PV, Wind Turbine (WT), Battery Energy Storage System (BESS), Diesel Generator (DSL) for a residential and industrial demand. The presented microgrid can operate in both grid-connected and stand-alone modes. 12

Figure 2.2 Types of Energy Storage Systems (ESSs) used in microgrids and examples for each type. 16

Figure 2.3 General architecture of Hybrid Energy System (HES) that shows the diversity in the assets such as Renewable Energy Resources (RERs), inverters, AC demand, DC demand, ESSs and control unit representing the energy management strategy. 17

Figure 2.4 Evaluation criteria for sizing microgrids that classified into reliability, economic and environmental assessment. 18

Figure 2.5 Energy Management System. 23

Figure 2.6 Methods used for sizing microgrids with RERs and classified into seven methods. 29

Figure 3.1 Grid-connected PV-BESS system consisting of PV, BESS, inverter, and charge controller. 41

Figure 3.2 The flowchart of the proposed Analytical and Economic Sizing (AES) approach. 44

Figure 3.3 Solar radiation of the Isle of Wight for one calendar year [2]. 45

Figure 3.4 Hourly ambient temperature profile for the Isle of Wight for one calendar year [2] 45

Figure 3.5 Demand distribution of one calendar year [3]. 46
Figure 3.6 The relationship between different values $P_{PV,rated}$ and Levelised Cost of Energy (LCOE) for the three combinations; PV-Lead-Acid Battery (LAB), PV-Lithuim Ion Battery (LIB), and PV-Redox Flow Battery (RFB). 56
Figure 3.7 The relationship between different values $P_{PV,rated}$ and Levelised Cost of Delivery (LCOD) for the three BESSs; LAB, LIB, and RFB. 57
Figure 3.8 Energy purchased and extra PV energy sold to the grid for the combination PV-LAB and $P_{PV,rated} = 590\ kW$ and $Bat_C = 1\ MWh$. 59
Figure 3.9 State of charge for lead-acid BESS for one calendar year. . 60
Figure 3.10 Energy purchased and extra PV energy sold to the grid- for the combination PV-LIB and $P_{PV,rated} = 710\ kW$ and $Bat_C = 1\ MWh$. 61
Figure 3.11 State of charge for lithium-ion BESS for one calendar year. 62
Figure 3.12 Energy purchased and extra PV energy sold to the grid- for the combination PV-LIB and $P_{PV,rated} = 710\ kW$ and $Bat_C = 1\ MWh$. 63
Figure 3.13 State of charge for redox flow BESS for one calendar year. 64
Figure 4.1 Stylized demonstration of three-step proposed framework: (1) analytical and economic sizing; (2) using Finite Automata (FA) to generate various Energy Management Strategy (EMS); and 3) evaluation model and feedback. . . 67
Figure 4.2 The network diagram of a stand-alone HES which consists of PV, BESS, Fuel Cell (FC), Electrolyser (EL), Hydrogen Tank (HT), DSL, and multiple inverters. 69
Figure 4.3 Modelling BESS in finite automata. 70

Figure 4.4 Nine states describing $EMS_{initial}$ based on finite automata. Each state illustrates which asset is operating and whether the BESS and HT are charging or discharging. The PV and demand are considered always as ON state . . 72
Figure 4.5 Finite automata model for $EMS_{initial}$. 72
Figure 4.6 The flowchart of AES approach showing the steps of the EMS to find the initial size of the HES. 79
Figure 4.7 Hourly solar radiation profile for Newcastle upon Tyne city for one calendar year [4]. 80
Figure 4.8 Hourly ambient temperature profile for Newcastle upon Tyne city for one calendar year [4]. 81
Figure 4.9 Hourly demand profile for Newcastle upon Tyne citry for one calendar year [5]. 82
Figure 4.10 Levelised cost of energy for the HES when using AES approach. 93
Figure 4.11 Finite automata model for EMS_1. 96
Figure 4.12 Finite automata model for EMS_2. 97
Figure 4.13 Finite automata model for EMS_3. 99
Figure 4.14 Finite automata model for EMS_{new}. 101
Figure 4.15 Levelised cost of energy for the HES when using integrated framework. 104
Figure 4.16 BESS soc, FC and PV power values during 48 hours in June, the DSL output is zero during these hours. 105
Figure 4.17 BESS soc, FC, PV, DSL power and demand values during 48 hours in December. 106
Figure 4.18 HT $socHT$, EL,PV, and FC power values during 48 hours in June. 107
Figure 4.19 HT soc, EL,PV, and FC power values during 48 hours in September. 108

Figure 5.1 An illustrative diagram showing the three stages required to design a Fuzzy Logic Controller (FLC). Starting from resizing the assets of the HES, conducting the sensitivity analysis, then implementing the FLC to modify the original EMS based on the output conditions set. 111
Figure 5.2 Original and forecasted solar radiation of one calendar year.112
Figure 5.3 Original and forecasted demand distribution of one calendar year. 112
Figure 5.4 The effect of demand and solar radiation variations on the fuel cost. 117
Figure 5.5 The effect of demand and solar radiation variations on DSL working hours. 117
Figure 5.6 The effect of demand and solar radiation variations on PV contribution. 118
Figure 5.7 The configuration of the FLC introducing the input membership functions; fuel cost, WH_{DSL}, and PV contribution. The output membership function is the conditions sets that modify the EMS. 120
Figure 5.8 Membership function for fuel cost input fuzzy set. 121
Figure 5.9 Membership function for WH_{DSL} input fuzzy set. 121
Figure 5.10 Membership function for PV contribution input fuzzy set. 122
Figure 5.11 Membership function for output fuzzy sets. 124
Figure 5.12 The fuel cost before and after applying the FLC. 132
Figure 5.13 The DSL working hours before and after applying the FLC. 132
Figure 5.14 The percentage of the PV contribution before and after applying the FLC. 133

LIST OF TABLES

Table 2.1 Comparison of sizing methods available in the literature [6, 7, 8, 9]. 38

Table 3.1 Cost and technical specifications of PV system used for energy and cost calculations. 48

Table 3.2 Cost and technical specifications of the three types of BESS. 50

Table 3.3 Summary of the results obtained from Figure 3.6 regarding the minimum LCOE at $P_{PV,rated}$ = 710 kW and the value of PV rated power at minimum $LCOE_{system}$ for the three PV-BESS systems. 56

Table 3.4 LCOD for the three BESSs; LAB, LIB and RFB when $P_{PV,rated}$ = 710 kW. 56

Table 3.5 PV-LAB system, PV system only and Grid only scenarios, where $P_{PV,rated}$=590 kW and LAB Bat_C=1 MWh 59

Table 3.6 PV-LIB system, PV system only and Grid only scenarios where $P_{PV,rated}$=710 kW and LIB Bat_C=1 MWh 61

Table 3.7 PV-RFB system, PV system only and Grid only scenarios. $P_{PV,rated}$=710 kW and RFB Bat_C=1 MWh 62

Table 3.8 PV-RFB components sizes. 64

Table 4.1 Conditions for BESS operation. 70

Table 4.2 Conditions for $EMS_{initial}$. 73

Table 4.3 Data used for PV analytical modele [10, 11]. 80

Table 4.4 Data used for battery energy system modelling [10]. 83

Table 4.5 Data used for hydrogen system modelling (FC, EL, and HT). 88

Table 4.6 The cost and lifetime of the HES assets [10, 12]. 91

Table 4.7 Data used for the economic models of the PV, BESS, and DSL. 92

Table 4.8 The size of HES based on $EMS_{initial}$. 94
Table 4.9 Operating conditions for EMS_1. 97
Table 4.10 Operating conditions for EMS_2. 98
Table 4.11 Performance indices for the generated EMSs using finite automata. 100
Table 4.12 Operating conditions for EMS_{new}. 102
Table 4.13 The size of HES using the AES approach and integrated framework. 103
Table 4.14 Comparison between the results obtained using AES approach and the integrated framework. 105
Table 4.15 Performance indices for EMS_{new} and the generated EMSs using the sizes obtained from the integrated framework. . 108
Table 5.1 The optimal size of HES using the integrated framework and forecasted demand and solar irradiance. 113
Table 5.2 Results of sensitivity analysis for an annual change of ±5% and ±10% of P_{load}. 114
Table 5.3 Results of sensitivity analysis for an annual change of ± 5% and ± 10% of I_{PV}. 114
Table 5.4 Results of sensitivity analysis for an annual change of +5%, +10% of P_{load} and I_{PV}. 115
Table 5.5 Results of sensitivity analysis for an annual change of +5%, +10% of P_{load} and −5%, −10% of I_{PV}. 115
Table 5.6 Results of sensitivity analysis for an annual change of −5%, −10% of P_{load}, 5%, 10% for I_{PV}. 116
Table 5.7 Results of sensitivity analysis for an annual change of −5%, −10% of P_{load} and I_{PV}. 116
Table 5.8 Numerical ranges of the fuzzy sets 120
Table 5.9 The 24 sensitivity analysis scenarios interpreted into LOW, MED, and MAX with regarding to the fuzzy sets. 123
Table 5.10 Illustration of the relationship between the sensitivity analysis scenarios, the output fuzzy sets and the condition sets. 124

Table 5.11 Operating conditions for EMS_{new} produced by the integrated framework described in Chapter 4. 125
Table 5.12 Values of the parameters related to soc and $socHT$ mentioned in Table 5.11. 126
Table 5.13 The sets of modified conditions labeled from A to H. 127
Table 5.14 The values of fuel cost, WH_{DSL}, and PV contribution of the 24 scenarios after applying the FLC. 131
Table 5.15 Different scenarios used for the case study showing the effectiveness of applying the FLC. 135

ACRONYMS

AI Artificial Intelligence

AER Alternative Energy Resource

AES Analytical and Economic Sizing

BESS Battery Energy Storage System

COE Cost of Energy

DG Distributed Generation

DOD Depth of Discharge

DES Discrete Event System

DSL Diesel Generator

EENS Expected Energy Not Supplied

EL Electrolyser

EMS Energy Management Strategy

ESS Energy Storage System

FA Finite Automata

FC Fuel Cell

FLC Fuzzy Logic Controller

GA Genetic Algorithim

HA Hours of Autonomy

HES Hybrid Energy System

HT Hydrogen Tank

LA Level of Autonomy

LAB Lead-Acid Battery

LCC Life Cycle Cost

LCOE Levelised Cost of Energy

LCOD Levelised Cost of Delivery

LCOS Levelised Cost of Storage

LIB Lithuim Ion Battery

LPSP Loss of Power Supply Probability

MPPT Maximum Power Point Tracking

MT Microturbines

NPC Net Present Cost

NPV Net Present Value

PSO Particle Swarm Optimisation

PV Photovoltaic

RER Renewable Energy Resource

RFB Redox Flow Battery

SCDES Supervisory Control of Discrete Event Systems

WT Wind Turbine

NOMENCLATURE

β	temperature coefficient of solar cell efficiency $[\frac{1}{^\circ C}]$
η_{PV}	overall efficiency of the the PV [%]
η_{ch}	battery charge efficiency [%]
η_{dch}	battery discharge efficiency [%]
η_{inv}	inverter efficiency [%]
η_{module}	module efficiency [%]
η_{rt}	battery round trip efficiency [%]
η_{sys}	system overall efficiency [%]
η_{temp}	PV temperature efficiency [%]
A, B	diesel generator consumption curve coefficients $[Liter/kWh]$
A_{PV}	PV total area $[m^2]$
B_{DSL}	binary logic for the diesel generator operation
B_{DSL}	binary logic for the electrolyser operation
B_{FC}	binary logic for the fuel cell operation
Bat_C	battery energy storage system capacity $[kWh]$
$C_{BESS,OM}$	operation and maintenance cost for the battery $[£/kWh]$
C_{BESS}	total cost of the battery [£]
$C_{DSL,fuel}$	total fuel cost of the diesel generator $[£/L]$
$C_{DSL,OM}$	operation and maintenance cost of the diesel generator $[£/kW]$
C_{DSL}	total cost of the diesel generator [£]
$C_{PV,charge}$	cost of the PV arrays that generate energy used to charge the battery $[£/kWh]$
$C_{PV,Esold}$	cost of the PV arrays that generate energy sold to the grid $[£/kWh]$
$C_{PV,Extra}$	cost of the PV arrays that generate extra energy $[£/kWh]$
$C_{PV,OM}$	operation and maintenance cost for PV $[£/kW]$
C_{PV}	total cost of the PV [£]
C_{cc}	cost of charge controller $[kWh]$

$C_{E,purchase}$	cost of the energy purchased from the grid [£/kWh]
$C_{E,sold}$	cost of the energy sold to the grid [£]
$C_{inv,OM}$	operation and maintenance cost of the inverter [£/kW]
$C_{inv,PV}$	total cost of the PV inverter [£]
$C_{PV,load}$	cost of the PV arrays that generate energy used to supply the demand [£/kWh]
C_{system}	total cost of a system [£]
d	index for the number of batteries involved in the grid-connected PV-BESS system
DEG_{BESS}	battery degradation rate
DEG_{PV}	PV degradation rate [%]
E_{BESS}	energy produced by the battery [kWh]
E_{DSL}	energy produced by the diesel generator [kWh]
$E_{PV,charge}$	energy generated by the PV used to charge the battery [£/kWh]
$E_{PV,Extra}$	extra energy generated by the PV [£/kWh]
$E_{PV,load}$	energy generated by the PV to supply the demand [£/kWh]
E_{PV}	energy produced by the PV [kWh]
$E_{load,total}$	total energy of the demand [kWh]
$E_{purchase}$	energy purchased from the grid [kWh]
E_{sold}	energy sold to the grid [kWh]
E_{system}	total energy of generated by hybrid energy system [kWh]
F	Faraday constant [C/mol]
$F_{consume}$	fuel consumption of the diesel generator [$Liter$]
f_p	fuel unit cost [£/$Liter$]
H	yearly module reference in-plane radiation [kW/m^2]
$H_{2,cons,1kW}$	H_2 consumed by 1 kW fuel cell in 1 hour [$mol/hour$]
$H_{2,prod,1kW}$	H_2 produced by 1 kW electrolyser in 1 hour [$mol/hour$]
HA	hours of autonomy of the battery [$hours$]
HA_{H_2}	hours of autonomy of the hydrogen tank [$hours$]
I_{NOCT}	solar radiation at NOCT [W/m^2]
I_{PV}	solar radiation [kW/m^2]

IC_{BESS}	initial cost of the battery [£/kWh]
IC_{DSL}	initial cost of the diesel generator [£/kW]
IC_{PV}	initial cost of the inverter [£/kW]
IC_{inv}	initial cost of the inverter [£/kW]
j	index of years
k	index for the number of battery hours of autonomy involved in the hybrid energy system study
$LCOD$	levelised cost of delivery [£/kW]
$LCOE$	levelised cost of energy [£/kW]
$LCOE_{E_{out}}$	levelised cost of output energy from the battery [£/kWh]
$LCOS$	levelised cost of storage [£/kW]
LHV	low heat value of hydrogen [kWh/kg]
$Life_{DSL,h}$	lifetime of the diesel generators $hours$
$Life_{DSL}$	lifetime of the diesel generators $years$
N	system lifetime $years$
n	index of hours in a year
$N_{PVEsold_T}$	fraction of PV arrays that generate energy sold to the grid
$N_{PVextra_T}$	fraction of PV arrays that generate extra energy
N_{PVload_T}	fraction of PV arrays that generate energy to supply the demand
$NOCT$	normal operating cell temperature [$°C$]
$P_{DSL,rated}$	diesel generator rated power [kW]
$P_{DSL}(n)$	hourly generated power by the diesel generator [kW]
$P_{EL,min}$	electrolyser minimum power [kW]
$P_{EL,rated}$	electrolyser rated power [kW]
$P_{EL}(n)$	hourly power consumed by the electrolyser [kW]
$P_{FC,rated}$	fuel cell rated power [kW]
$P_{FC}(n)$	hourly power generated by fuel cell [kW]
P_{HT}	hydrogen tank final pressure [bar]
$P_{PV,rated}$	PV rated power [kW]
$P_{PV,surplus}$	surplus power generated by the PV [kW]
P_{PV-max}	maximum range of PV rated power [kW]

P_{PV-min}	minimum range of PV rated power $[kW]$
$P_{PV}(n)$	hourly power generated by the PV $[kW]$
$P_{input}(n)$	the sum of input power to the battery at a specific hour $[kW]$
$P_{load,avg}$	average hourly demand $[kW]$
$P_{load,max}$	maximum demand $[kW]$
$P_{load}(n)$	hourly demand $[kW]$
Pr_{cc}	charge controller cost per unit, $[£/kWh]$
$Pr_{e,purchase}$	unit price of energy purchased from the grid $[£/kWh]$
$Pr_{e,sold}$	unit price of energy sold to the grid $[£/kWh]$
Pr_{inv}	PV inverter cost per unit $[£/kWh]$
r	discount rate $[\%]$
RC_{BESS}	replacement cost for the battery $[£/kWh]$
RC_{DSL}	replacement cost for the diesel generator $[£/kWh]$
RC_{inv}	replacement cost for the inverter $[£/kWh]$
S_{HT}	hydrogen tank size $[kg]$
SFC	specific fuel consumption for the diesel generator $[Liter/kWh]$
soc_{DSL}	state of charge for diesel generator operation $[\%]$
soc_{FC}	state of charge for fuel cell operation $[\%]$
soc_{max}	maximum battery state of charge $[\%]$
soc_{min}	minimum battery state of charge $[\%]$
$socHT$	Hydrogen tank state of charge $[\%]$
$socHT_{max}$	maximum hydrogen tank state of charge $[\%]$
$socHT_{min}$	minimum hydrogen tank state of charge $[\%]$
$T_{amb,NOCT}$	ambient temperature of NOCT $[^{\circ}C]$
T_{amb}	ambient temperature $[^{\circ}C]$
T_{cell}	PV cell temperature $[^{\circ}C]$
T_{ref}	PV cell reference temperature $[^{\circ}C]$
V_{FC}	fuel cell working voltage $[V]$
V_b	battery voltage $[V]$
V_{el}	electrolyser working voltage $[V]$
WH_{DSL}	yearly working hours of the diesel generator $[hours/year]$

WH_{EL}	yearly working hours of the electrolyser	[$hours/year$]
WH_{FC}	yearly working hours of the fuel cell	[$hours/year$]

Part I

Thesis Chapters

1

INTRODUCTION

The existing electrical power network is dominated by centralised generation. The electricity is mainly produced at large generation facilities and transferred to the users through the transmission and distribution grids. Due to the increase in energy demand and the growing of greenhouse gas emissions, the existing centralised energy system is subjected to alterations to handle these changes. Microgrids have emerged as a competitive feature of the future energy systems and a promising superseding to the centralized generation. Therefore, optimising microgrids in terms of sizing and their energy management strategies have recently received considerable attention. This chapter presents the motivation and defines the key concepts and terms in the context of the research reported in this thesis. It highlights the necessity of determining the optimal size and energy management strategy of microgrids as a way to improve reliability and reduce the system's cost. Finally, the main contributions of this research together with the thesis organization are discussed.

1.1 MOTIVATION

Climate change and greenhouse gas emissions represent the main drivers for the development of the concept of a microgrid that incorporates Renewable Energy Resources (RERs) in Europe [13, 14]. According to the Paris climate agreement, all countries have to undertake serious efforts to avoid global average temperature rise exceeding 2 °C [15]. In consideration of this, the energy sector is experiencing a transition to more low-carbon energy systems by integrating more RERs into the existing grids. Renewable energy offers a clean and eco-friendly source of energy where the energy is generated by converting free natural energy

into other useful energy forms [16]. Efficient use of diverse RERs can pave a path for sustainable development, therefore, careful design and planning for utilising renewable energy sources is required. The motivation for this work is introduced as follows.

1.1.1 *Sizing of Microgrids*

Electricity generation is considered the largest contributor to greenhouse gas emissions, accounting for 25% of the global greenhouse gas emissions [17]. Previously, electricity production was completely dependent on fossil fuels. The power plants are designed on a large scale for continuous operation. The centralized power plants are responsible for delivering energy to distant places which may result in loss of energy through transmission. However, the increase in energy demand and the negative effects of burning fossil fuels as well as the concerns from their depletion, have encouraged countries to promote greater use of RERs.

Deploying RERs in the electrical grids offers great potential to reduce dependence on fossil fuels and greenhouse gas emissions. Photovoltaics (PVs) and Wind Turbines (WTs) are the most utilised RERs since they are getting cheaper and are abundant. Moreover, the orientations regarding electricity generation are moving towards decentralised systems with their benefits in reducing energy losses [13, 18, 19]. Today, microgrids constitute an effective solution for critical infrastructures, campuses, remote communities, island networks or single buildings such as factories, shopping malls or faculties [20]. A Microgrid is defined as a low-voltage distribution network that includes the integration of RERs and demand. Microgrids can operate as a stand-alone system, grid-connected or in transition between them [21]. The intensive research and development in this field have led to a huge growth in RERs installations that are today cost-competitive [8]. However, microgrids have some limitations such as high capital cost of RERs installations, optimal utilisation of these resources and control and management issues [22].

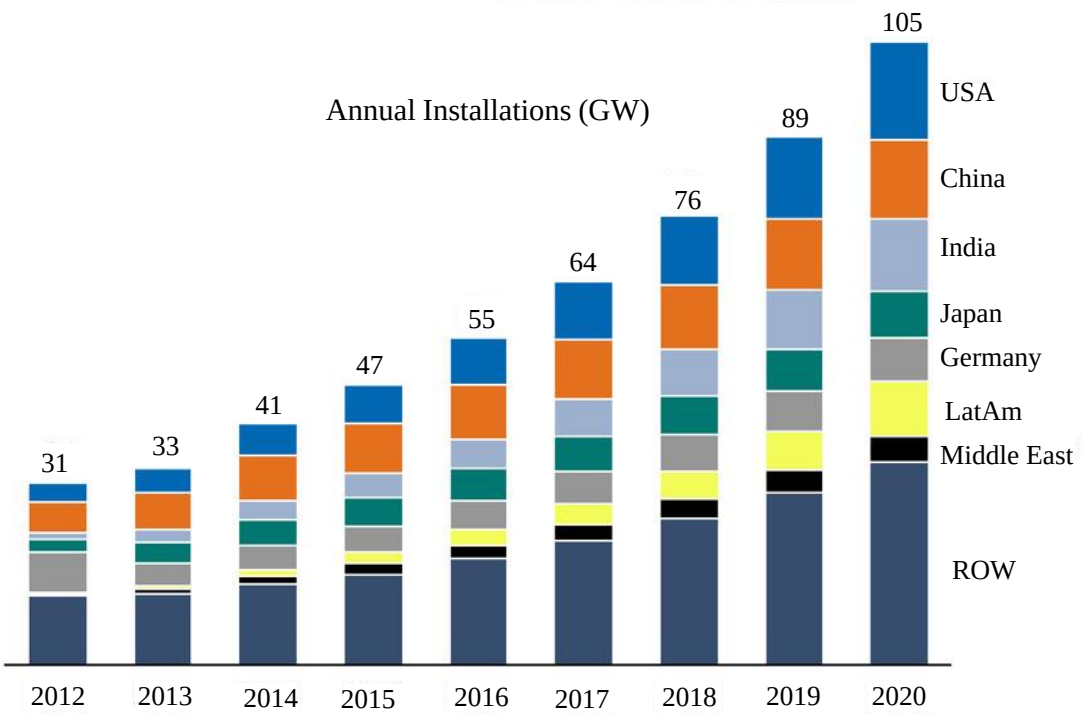

Figure 1.1: The evolution of global total PV installed capacity from 2012 to 2020 [1].

Among various RERs, PVs prove to be the most attractive option for electricity generation. This is due to their benefits such as noiseless, environmental advantages, simple operation and maintenance, and long lifespan [16]. Moreover, the PVs cost is currently on a fast reducing track and will continue decreasing for the coming years [23]. For these reasons, the RER under consideration in this thesis is PV. Figure 1.1 shows the fast growth of the PVs installations (in GW) applied widely in many countries from 2012 to 2020 [1]. The installed capacity of PVs has increased from 2012 to 2016 by 24 GW, while from 2016 to 2020 this value has doubled (50 GW).

Therefore, there is a genuine need to find the optimal sizing of the integrated RERs and Energy Storage System (ESS). The importance of ESSs emerges from their benefits in reducing the intermittent characteristics of the RERs. Finding the sizes of the microgrid assets represents the first step in designing any microgrid and is essential to mitigating the limitations of microgrids. Furthermore, the coordination between the integrated assets in microgrids represents

a challenging task in designing microgrids. This is introduced in the following section.

1.1.2 *Energy Management Strategies*

It is fundamental in designing any microgrid to obtain the sizes of the integrated assets. However, the optimal operation of the microgrid and the coordination between all the assets are also essential in every microgrid. One of the most promising means of reducing energy consumption and related energy costs while ensuring continuous demand supply is implementing an efficient Energy Management Strategy (EMS) [24]. An optimal microgrid sizing together with an appropriate EMS determines the overall system performance and both deserve similar attention.

The integration of RERs and ESSs in microgrids brings challenges to the operation and stability of the grid [22, 25, 26, 27]. Therefore, a proper control strategy is essential to ensure a smooth transition of energy in microgrids [27]. There are two essential options in controlling any microgrid; power management control and EMS. In power management strategies voltage, current and frequency are the main variables to consider. While in EMSs, the key parameters to optimise are the cost, fuel cost, maintenance cost, and the system lifetime [28]. The EMS serves several vital purposes such as [22]: (i) protects the ESSs by controlling the charging and discharging cycles, (ii) ensures maximum utilisation of RERs, (iii) ensures the continuous supply to the demand, (iv) and minimises the operation, maintenance, fuel and replacement costs by efficient use of all the assets in the microgrid. This thesis is interested in optimising the EMS along with the size.

The basic principle of existing optimisation approaches for microgrids are either determining the optimal size [29, 30, 31, 32] or obtaining the optimal EMS [33, 34, 35]. Few approaches tackled optimising both the size and EMS [36, 37, 38]. While these optimisation approaches have made piecemeal advances in different directions, they leave room for further improvements. For example, *how*

to redefine the optimal size-EMS by implementing various EMS, and how the obtained EMS can adopt any future changes and disturbances in the input data.

1.2 THESIS SCOPE AND CONTRIBUTIONS

This thesis attempts to address the above fundamental question by exploring the state-of-the-art of the optimisation methods in sizing and EMSs for microgrids. The work in this thesis is divided into three parts; the first part deals with sizing grid-connected PV-Battery Energy Storage System (BESS) system using an Analytical and Economic Sizing (AES) approach. The second part finds the optimal size-EMS of a stand-alone Hybrid Energy System (HES) through an integrated framework. The last part of the thesis investigates the ability of the obtained EMS to deal with the uncertainty in demand and solar radiation data.

The main contributions of this thesis are listed as follows:

- an AES approach is developed to determine the optimal size, minimum cost and best PV-BESS combination in a grid-connected microgrid. The energy demand is mainly covered by the PV-BESS system, or by purchasing energy from the grid whenever the energy generated by PV-BESS is insufficient to supply the demand. The surplus PV energy generated will be used to charge the BESS, and extra energy will be sold back to the grid. The selection of the optimal size of the PV and BESS type is based on the minimum Levelised Cost of Energy (LCOE) for the PV-BESS combination. A more accurate model for LCOE is proposed by including the impact of surplus energy sold to the grid and energy purchased from the grid. Three types of BESS are considered in the work which are Lead-Acid Battery (LAB), Lithuim Ion Battery (LIB), and Redox Flow Battery (RFB). This work has been published in IEEE in January 2018 (see [10]).

- an integrated framework is proposed for finding the optimal size-EMS combination for a stand-alone HES. The HES consisting of PV, BESS, Diesel Generator (DSL), Fuel Cell (FC), Electrolyser (EL), and Hydrogen

Tank (HT). In the first step, the proposed framework is used to determine the size of the assets in the HES based on an initial EMS. Then the obtained size is exercised through multiple EMSs produced using Finite Automata (FA). This is followed by an evaluation model to compare the performance indices of each instantiated EMS. The role of the evaluation model is to track the featured operating conditions in the instantiated EMSs. Then select the featured conditions that lead to an improvement in performance indices and retain them in the new EMS. As such, the new-optimised EMS will then replace the initial one leading to the optimal size-EMS combination. The novelty in this work can be summarized as taking the impact of selecting the right EMS on the sizing of the HES. This can lead to better performance and can be explained in our integrated framework by reducing the cost, reducing the DSL and FC working hours and increasing the PV utilisation. Moreover, using FA in implementing and instantiating multiple EMSs to attain an improved one has not been reported. This work has been published in Applied Energy/Elsevier in May 2019 (see [39]).

- a Fuzzy Logic Controller (FLC) is implemented for the purpose of modifying the selected EMS from the integrated framework. The main objective of this FLC is to maintain the HES performance under uncertainty in demand and solar radiation. A sensitivity analysis is conducted, and all possible scenarios are generated by making changes to the demand and solar radiation data. These scenarios are utilised as input to the FLC, and the fuzzy sets are the working hours of the DSL, fuel cost, and PV contribution. The fuzzy output sets of FLC represent condition sets that will cause modifications on the DSL, FC, and EL operating conditions in the original EMS. An article has been prepared for this work, and it is under submission to Applied Energy/Elsevier.

1.3 THESIS OVERVIEW

This thesis is organized into six chapters. The major contributions of this thesis are summarized as follows:

Chapter 2 presents an essential background on microgrids, their benefits and drawbacks, microgrids modes, and an illustration example of a microgrid consists of RERs, DSLs and BESS. Then an introduction on ESSs is provided showing the existing types of ESSs. The concept of HESs is introduced demonstrating an example of their general architecture. This is followed by an investigation of current EMSs in the literature up to date. Criteria for microgrid optimisation and the sizing methods used for the sizing are also discussed.

Chapter 3 proposes an AES approach for sizing a grid-connected PV-BESS. It demonstrates how the analytical models of the PV and BESS are employed with the LCOE model to optimise the size of the PV-BESS. Moreover, the LCOE model is modified from its original form to include the cost of the surplus energy sold to the grid and energy purchased from the grid. A comparison between the combinations of PV-BESS obtained by the AES approach is performed to show the effect of the LCOE on selecting the best combination.

Chapter 4 demonstrates an integrated framework for sizing a stand-alone HES. It describes the steps of the integrated framework in detail. A modified version of the AES approach implemented in Chapter 3 is used in the first step of the framework. The utilisation of FA in the framework to implement and generate multiple EMSs is also discussed. The evaluation model used to assess the instantiated EMSs and to select the featured conditions is explained. The process of resizing with the improved EMS is clarified and the obtained results from the AES and the framework are compared.

Chapter 5 investigates the effect of the demand and solar uncertainty on the performance of the HES introduced in Chapter 4. It shows how the system is resized using AES approach and forecasted data for demand and solar radiation. It introduces all possible sensitivity analysis scenarios for the new size of the HES. This chapter demonstrates how the obtained sensitivity scenarios are

utilised to perform a FLC. It explains how this FLC is designed in detail, and its application to modify the EMS. Moreover, a case study of one of the sensitivity analysis scenarios reporting the results after and before applying the FLC is discussed.

Chapter 6 summarizes the contributions and key highlights of this thesis, showing critical review of this research together with the potential future directions.

Overall, this thesis shows promising design and implementation approaches for finding the optimal size and EMS of microgrids. It can provide an addition to the existing literature in the field of optimisation of microgrids.

2

BACKGROUND AND LITERATURE SURVEY

2.1 INTRODUCTION

The drivers of integration RERs in microgrids is to combat climate change, environmental pollution, and increasing global demand. WT, PV, hydropower, geothermal energy, and biomass energy are examples of RERs. PV is one of the fastest growing technologies and widely applied in many countries. It is expected in the coming decade the PV installations in the world will be approximately doubled [40]. Efficient use of various RERs allows for more sustainable energy systems. As a consequence, design and planning for utilising RERs in microgrids are required.

This chapter highlights the basic concepts raised in the field of microgrids to understand the state of the art reported in the context of this work. First, the concept of microgrid and the assets that contribute to the microgrid is explained. Then the, multiple criteria for microgrid assessment are introduced to determine which RER and EMS are better to use. Following that, the importance of controlling and managing microgrids is clarified. Since microgrid design is the primary theme of this thesis, the second part of this chapter is made to emphasize the research efforts in the field of sizing methods found so far and its classification. Finally, a discussion is placed for the comparison between all the available methods.

2.2 MICROGRIDS

During the past decades, the deployment of Distributed Generations (DGs) in the existing power systems has been increasing rapidly. DG refers to any small-

scale power system that operates independently of the utility grid and located on the user side where it is utilised [41]. DGs include RERs such as PVs and WTs, and Alternative Energy Resources (AERs) such as FCs and Microturbiness (MTs)s [13, 22, 42]. In addition, DGs include non-renewable generators such as DSLs and gas turbines [43]. Microgrid has emerged as an attractive option to harness the benefits offered by the DGs to the existing power systems [44, 45]. The U.S. Department of Energy defines a microgrid as "a group of interconnected loads and distributed energy resources within clearly defined electrical boundaries that acts as a single controllable entity with respect to the grid. A microgrid can connect and disconnect from the grid to enable it to operate in both grid-connected and island mode [46]." Island or stand-alone microgrid are two terms for the same concept, the term stand-alone will be used in this thesis.

2.2.1 *Microgrid Benefits and Drawbacks*

The intuitive advantages of microgrids have been broadly classified into environmental and economical benefits. However, other advantages of microgrids are represented in a significant reduction in energy losses and improvement in the utilisation of RERs. The reliability of the systems is also improved by connecting multiple generating units to ensure continuous demand supply. Also, the decentralization of DGs allows the microgrid in the cases of outages to operate independently leading to a reduction in the adverse effects of outages. Moreover, one of the advantages of microgrids is to enhance EMS by properly matching the supply and demand to reduce the energy imported from the grid. [47, 48, 49]. Figure 2.1 shows an example of a microgrid that includes a PV farm, WT farm, various demand, DSLs and BESS. The presented microgrid can operate in both modes, stand-alone and grid-connected through the point of common coupling. In grid-connected mode, the PVs and WT will supply the residential and industrial demand during their availability. The BESS will store surplus energy from WT to supply when needed. However, any deficiency in energy will be covered by the

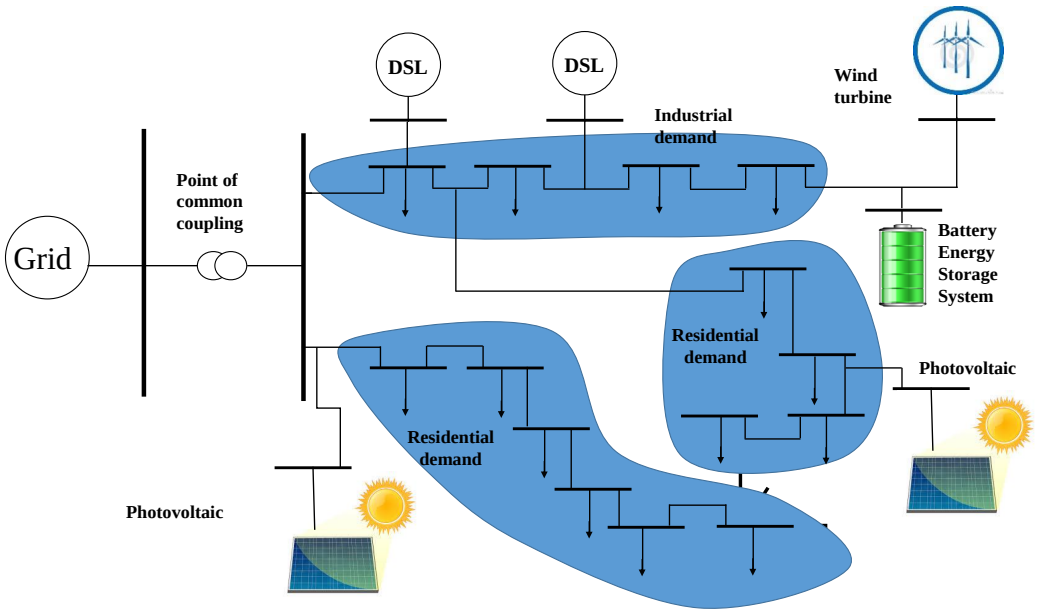

Figure 2.1: Example of a microgrid including PV, WT, BESS, DSL for a residential and industrial demand. The presented microgrid can operate in both grid-connected and stand-alone modes.

grid. In stand-alone mode, the DSLs acts as a backup generator and supply the demand.

In addition, RERs and AERs are environmentally friendly, these energy resources will never die out as they are continuously replenished. However, because of the stochastic and intermittent nature of RERs, affording continuous electricity from a power system with integrated RERs presents a challenge. One of the most efficient technologies providing anticipated unit cost reductions, which makes the investment in RERs/AERs looks extremely attractive, is ESSs. The integration of ESS along with RERs/AERs is assumed to provide fundamental advantages to the microgrid. This is represented by maintaining the balance between generation and consumption, and improving the reliability of the power grid [50]. Section 2.3 explains the benefits of ESSs in more details.

Another practical solution to overcome the intermittency of RERs is HESs. A HES combines two or more RERs with some conventional source like DSL along with an ESS (HESs are explained in Section 2.4).

To determine the optimal exploitation of RERs/AERs in microgrids, the system design must consider significant factors. These factors relate to the operation,

component selection, and applied methodology. Therefore, choosing an optimum sizing methodology is fundamental to meet the desired demand at a distinct level of security. Sizing and optimisation techniques allow the power system to operate efficiently and economically in different conditions [51], and Section 2.8 discusses the available sizing methods in the literature.

Stability and protection in microgrids are also issues that need to be investigated when integrating DGs in the electrical grid. However, these issues are out of the scope of this thesis.

2.2.2 *Microgrids Modes*

Whether a power system is based on single RER/AER or a HES, it can be configured either to be stand-alone or grid-connected. The selection of the possible configuration depends on key parameters: (i) the possibility of grid extension, (ii) the electricity cost of energy supplied from the grid and, (iii) the weather forecasting in the specific area. Grid-connected configurations are typically preferred for applications in urban areas, while stand-alone configurations may be suitable for remote locations [51].

The main priority of grid-connected microgrids is to cover local demand from available RERs/AERs; any surplus energy will be fed into the grid. In the case where there is a shortage of electricity, it will be drawn from the grid. In grid-connected systems, the grid acts a backup source. On the other hand, stand-alone microgrids produce energy independently from the grid, where DSLs can be used as a backup source. These systems are preferable for remote areas where the grid cannot penetrate and there is no other source of energy [18, 22].

A comparison between grid-connected and stand-alone microgrids, on which the decision of which mode to consider in the microgrid, is presented as follows [18]:

- The accessibility of the location where DGs installed, grid-connected systems are ideal for locations near to the grid where the grid extension is convenient. The stand-alone systems are suitable for remote areas because

of the irregularities in the topological structure of the area and the distance which makes the connection to the grid very difficult [51].

- The economic feasibility is critically important in deciding whether to make the system grid-connected or stand-alone. In grid-connected systems, the surplus energy will be used either to charge a battery or be fed back into the grid, which will be more profitable than stand-alone systems.

- The connectivity to the grid enables grid-connected systems to set up large-scale systems with high plant load factors (where a high load factor means that power usage is relatively constant) thereby improving the economic viability of the operation. On the other hand, stand-alone systems are required to operate with low plant load factors (low load factor shows that occasionally a high demand is set).

- In grid-connected systems the grid acts as a back-up for the system, accordingly increasing its efficiency. While the back-up in stand-alone systems could be an ESS or small-scale distributed generator.

- If the grid-connected system is incorporated with an ESS, it will be cost-effective by reducing the energy imported from the grid while selling the surplus energy to the grid. In stand-alone systems, the excess energy will be discarded, which will be considered as energy loses.

2.3 ENERGY STORAGE SYSTEMS

The ESS refers to the process of converting electrical energy from a power system into a form that can be kept in various types of storage. Then the stored energy can be used when needed by transforming it back to serve the intended purpose [52]. ESS technologies have been found to be the best solution for the challenges associated with the proliferation of DGs. An ESS has multiple functions when installed in a distribution system, and some of these functions can be summarised as follows [50, 53, 54, 55]:

- To facilitate the integration of the RERs into the grid, increasing their penetration rate, and enhance the quality of the energy supplied.
- To reduce peak demand problems by providing energy when needed and hence eliminating the extra operation of the traditional generators (such as DSL) during the peak periods.
- To provide a balance between generation and consumption and improving the management and reliability of the grid.
- To provide remote areas with their energy needs, in cases when it is challenging to set up new grid connection plans.
- To reduce the energy imported from the electrical grid in grid-connected systems.
- To improve the electrical system's overall stability and making the elimination of power disturbances possible.

Many ESS technologies are available in the market, and the selection of the appropriate storage technology depends on several factors. Power rating, discharge time, suitable storage duration, lifetime, life cycle cost, capital cost, round trip efficiency, and maturity represent the key factors in selecting the appropriate ESS [56]. ESSs can be categorized into: electrical, mechanical, thermal, electromechanical, magnetic, chemical and thermochemical [55, 57, 58, 59, 60], and Figure 2.2 shows different types of ESSs and examples on each type. Electrochemical BESS technologies, namely lead acid (LA), nickel-cadmium (NiCd), nickel-metal hydride (Ni-MH), lithium ion (Li-ion), and sodium-sulfur (NaS) batteries are widely used in microgrid energy systems [50]. Detailed reviews of ESS technologies can be found in [50, 55, 56].

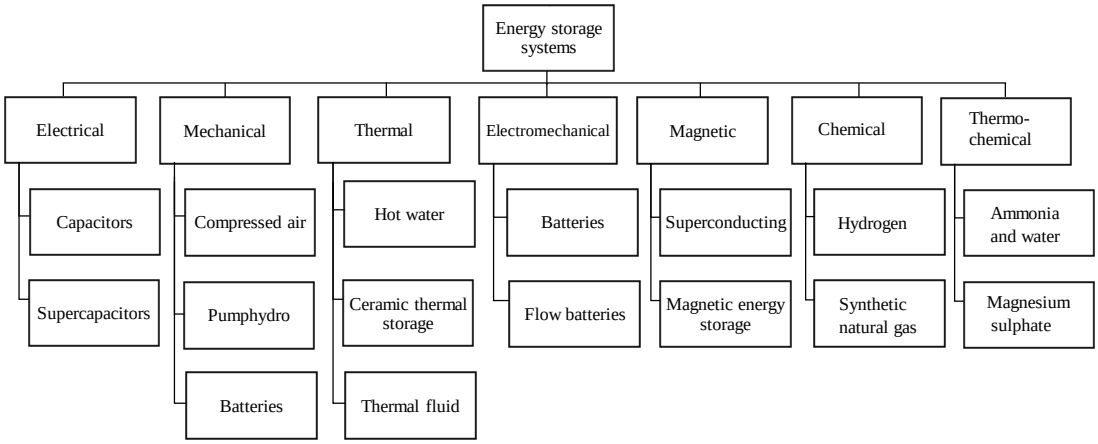

Figure 2.2: Types of ESSs used in microgrids and examples for each type.

2.4 HYBRID ENERGY SYSTEMS

RERs include among others PV, WT, and tidal. However, utilising PV energy gained more attention than others for many reasons: (i) infinite, (ii) needs minimal maintenance, and (iii) the running costs are extremely small and have zero carbon emissions [61]. To obtain the maximum benefits of solar energy or any other RERs, hybridization has emerged. A hybrid energy system (HES) combines two or more of RER/AER to feed a required demand and may include conventional energy resources and ESSs [62, 63, 24]. The primary role of the HES is to ensure maximum production of energy while maintaining the quality and continuity of the provided service [64]. Despite the unpredictable nature of RERs, introducing HES can present complementary patterns such that each resource provides energy if the other resources are unavailable. HES considered the most efficient option where grid connectivity is practically impossible or uneconomical [65]. Figure 2.3 demonstrates a general architecture of the HES.

The HES can be configured as grid-connected or stand-alone systems. The grid-connected HESs are designed in a way that the participating resources can cover the local demand, and any surplus energy will be stored or sold to the grid. In addition, installing ESSs in the grid-connected HES is not a necessity as the grid acts as a backup system. Whereas the stand-alone HESs need ESSs to store

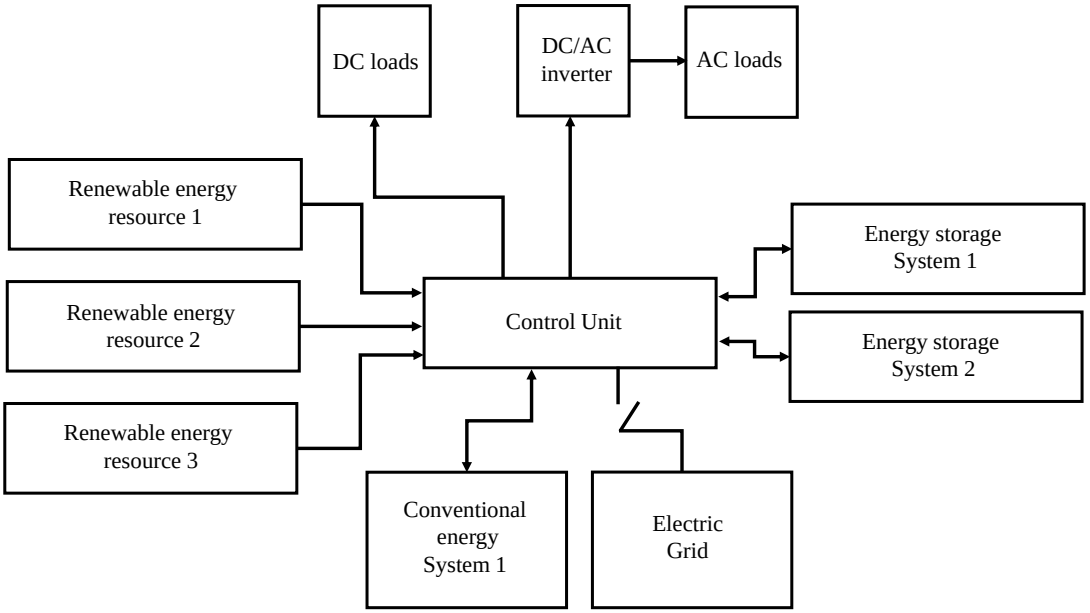

Figure 2.3: General architecture of HES that shows the diversity in the assets such as RERs, inverters, AC demand, DC demand, ESSs and control unit representing the energy management strategy.

the surplus energy and a backup system such as DSLs to maintain continuity of service.

On the environmental level, HESs can reduce the emissions of greenhouse gas through the increased use of RERs [66]. Moreover, it has been demonstrated that HESs can significantly reduce the total life-cycle cost of stand-alone systems in many situations, while at the same time providing a more reliable supply of electricity [63].

To obtain the best performance of HESs in terms of maximising the utilisation of the generated energy and minimizing the total cost, two crucial issues are considered: appropriate sizing and suitable energy management strategy [67, 68, 69]. These two issues are considered in this thesis.

2.5 CRITERIA FOR MICROGRID OPTIMISATION

The key objective of introducing microgrids with RERs/AERs is to satisfy the demand requirements at any time taking into consideration the growing demand and this is the reliability assessment. The economic side is also very important

in microgrid optimisation, in order to reach to the most cost-effective microgrid. Additionally, the environmental aspect is very essential to reduce global warming. Therefore, reliability, economics and environmental assessment are fundamental in any microgrid design [70].

To achieve the optimum performance of microgrids in terms of the above-mentioned objectives, there must be a criterion to evaluate the HES based on those aspects [71]. Figure 2.4 provides a classification of evaluation metrics.

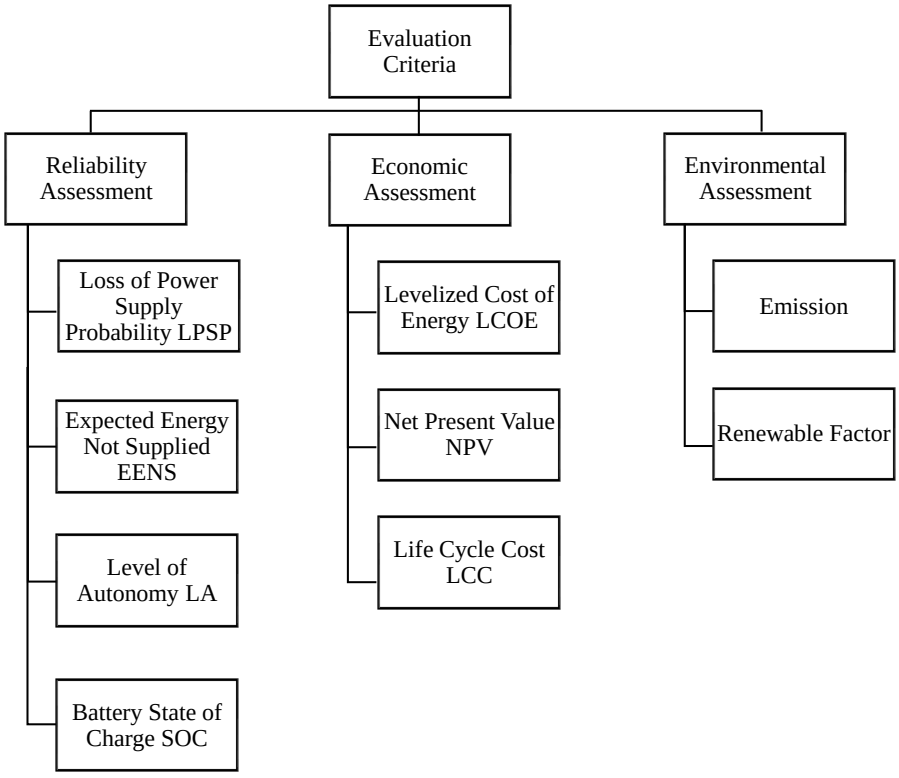

Figure 2.4: Evaluation criteria for sizing microgrids that classified into reliability, economic and environmental assessment.

2.5.1 *Reliability Assessment*

Reliability refers to the adequacy and security of the power supply in any microgrid. Adequacy means that the system should have the ability to meet the aggregate power and energy requirements of all consumers at all times. While security represents the ability of the system to deal with sudden interruptions [72].

There are several reliability indicators for microgrids that can asses their performance, and some of these are given below [73]:

- Loss of Power Supply Probability (LPSP): an electrical system is reliable when it is capable to supply enough power to the demand during a certain period. The most reliable indicator for that is the LPSP defined as the ratio of energy deficiency to demand during a certain period. The lower LPSP the more reliable operation of the power system, if LPSP equals zero means the installed DGs can cover the demand. Whereas if the LSPS is one, this indicates the demand is never fed [74]. Generally, LPSP is calculated as follows [73]:

$$LPSP = \frac{\sum_{t=1}^{T} DE(t)}{\sum_{t=1}^{T} P_{load}(t)} \quad , \tag{2.1}$$

  where $DE(t)$ and $P_{load}(t)$ represent the deficiency in energy and the demand during a certain time respectively.

- Expected Energy Not Supplied (EENS): this indicator measures the expected energy that cannot be supplied when the demand exceeds the available energy in the system. EENS can be obtained as follow [74, 73, 75]:

$$EENS = \begin{cases} P_{load} - \int_{P_{min}}^{P_{max}} P \,.\, f_P(P)\, dP & P_{load} > P_{max} \\ \int_{P_{min}}^{P_{max}} (P_{load} - P) \,.\, f_P(P)\, dP & P_{min} \le P_{load} \le P_{max} \\ 0 & P_{load} \le P_{min} \end{cases} , \tag{2.2}$$

  where P is the power generated by the microgrid, P_{load} refers to the demand, $f_P(P)$ is the probability density function for the power output of the microgrid. While P_{max} and P_{min} are the maximum and minimum power generated by the microgrid respectively.

- Level of Autonomy (LA): this indicator is defined as one minus the ratio between the total number of hours in which loss of load H_{LOL} occurs and the total hours of operation H_{tot} [73]:

$$LA = 1 - \frac{H_{LOL}}{H_{tot}} \quad , \tag{2.3}$$

where H_{LOL} represents the number of hours for which loss of load occurs and H_{tot} is the total operating hours of the system.

- Battery state of charge (soc): soc is related to the energy stored in the battery. It can help in determining the battery capacity to ensure that the constraints about system reliability are met and can be calculated using the following equation:

$$soc(t) = \begin{cases} soc(t-1) + \dfrac{[P_{input}(t) - P_{load}(t)] \cdot \eta_{ch} \cdot \Delta t}{\eta_{inv} \cdot Bat_C}, & P_{input}(t) > P_{load}(t) \, , \\ \\ soc(t-1) - \dfrac{(P_{load}(t) - P_{input}(t)) \cdot \Delta t}{\eta_{inv} \cdot \eta_{dch} \cdot Bat_C}, & P_{input}(t) \leq P_{load}(t), \end{cases} \tag{2.4}$$

where P_{input} is the sum of input power to the battery, P_{load} represents the demand, BAT_C is the battery capacity in kWh. Whereas η_{inv}, η_{ch}, and η_{dch} are the inverter, battery charging and discharging efficiency respectively. Δt is the time interval between this state and the previous one.

2.5.2 *Economic Assessment*

Economic analysis is essential for any power system and has a strong relationship with power system reliability. The inadequate reliability of power supply costs customers much more than adequate reliability [76]. It will be noted in the following section, that almost all sizing methods use economic assessment to

obtain the optimal size of the assets in a microgrid. Underneath are some of the economic indicators used to determine the economic feasibility of a power system:

- LCOE: is widely used to evaluate the economic feasibility of power systems and ESSs. The costs distributed over the project lifetime are considered and this provides a more accurate economic picture of the project under analysis [77, 78, 79]. The LCOE of the microgrid can be obtained by dividing the total cost of the assets in the microgrid by the total energy generated. Equation 2.5 represents the general form of LCOE [10]:

$$LCOE = \frac{Total\ System\ Costs}{Total\ Annualized\ Energy\ Production} \quad (£/kWh) \quad , \tag{2.5}$$

- Life Cycle Cost (LCC): is the total system cost calculated during the lifetime of the system. The LCC consists of three components, which represent the initial cost (IC_{system}), the annualized replacement cost (RC_{system}), and the annualized operation and maintenance cost (OM_{system}) [80]. It is calculated as follows:

$$LCC = IC_{system} + OM_{system} + RC_{system} \quad . \tag{2.6}$$

- Net Present Value (NPV): the NPV of a power system is the difference between the present values of the total profit and total cost of the system within its operational lifetime. Obviously, the higher the NPV, the higher economic benefit [81].

2.5.3 *Environmental Assessment*

Environmental assessment is a vital aspect of sustainability, that causes a direct effect on our planet. Environmental assessment is related to reducing the pollution that could result from some DGs. Two important indicators in the environmental assessment are emissions and the renewable factor.

- Emission: the emissions of a microgrid include carbon dioxide (CO_2), sulphur dioxide (SO_2) and nitrogen oxides(NOx). Based on the Tokyo Protocol, CO_2 and NOx are two types of the six main greenhouse gases. SO_2 is one of the most primary reasons for acid rain. The emissions of any microgrid are measured as yearly emissions of the emitted and the emissions into the air of different systems [72].

- Renewable Fraction: the renewable fraction means the amount of renewable energy generated divided by the total energy generated by the system, and it represents the extent of renewable energy in a microgrid. A higher value of this factor indicates that a great portion of RERs is used [72].

2.6 CONTROL AND ENERGY MANAGEMENT OF MICROGRIDS

Microgrid control is responsible for dealing with multiple aspects such as the voltage and frequency regulation, irregularity of the RERs, the imbalance between demand and generation, and the type of the integrated ESS [82, 83, 84]. The diversity in control issues led to the adoption of the hierarchical control scheme as a standardized solution in microgrids, especially when different time processing is required to execute the multiple tasks [82, 83]. Generally, the control in microgrids can be divided according to the hierarchical control into three levels. The primary level is responsible for local control of DGs, the secondary level deals with the frequency and voltage deviations. Finally, the tertiary level is identified as the EMS where it is responsible for managing the power and the energy between DGs and the demand. The scope of this thesis is oriented towards the third level of control [84, 83].

When combining one or more of RERs/AERs along with an ESS to supply a certain demand, the need for an effective EMS arises [85]. EMS represents a sequence of instructions to determine decisions regarding the operation of the assets in the microgrids and to guide the flow of energy in the microgrid. The need for an EMS is fundamental for both grid-connected and stand-alone systems.

The role of the EMS differs based on the microgrid configuration. For instance, in grid-connected systems the EMS controls the energy flow to and from the grid. However, in stand-alone systems, the EMS role is to ensure continuity of supply to the demand, improve the system performance, maximise the utilisation of RERs, reduce the system operation cost, and prolong system lifetime [25].

A generalized structure of EMS is presented in Figure 2.5. A typical EMS requires data input such as components costs, fuel price, demand and RERs profiles, and the assigned objectives. There are three types of microgrid assessment which are reliability, economic and environmental (explained in Section 2.5). The assessments are considered as objectives for EMS optimisation. Accordingly, the EMS provides output information such as the decision which DGs to operate, when to charge/discharge the ESS, whether to import/export energy from the grid. Moreover, indices to evaluate the microgrid performance are produced by the EMS.

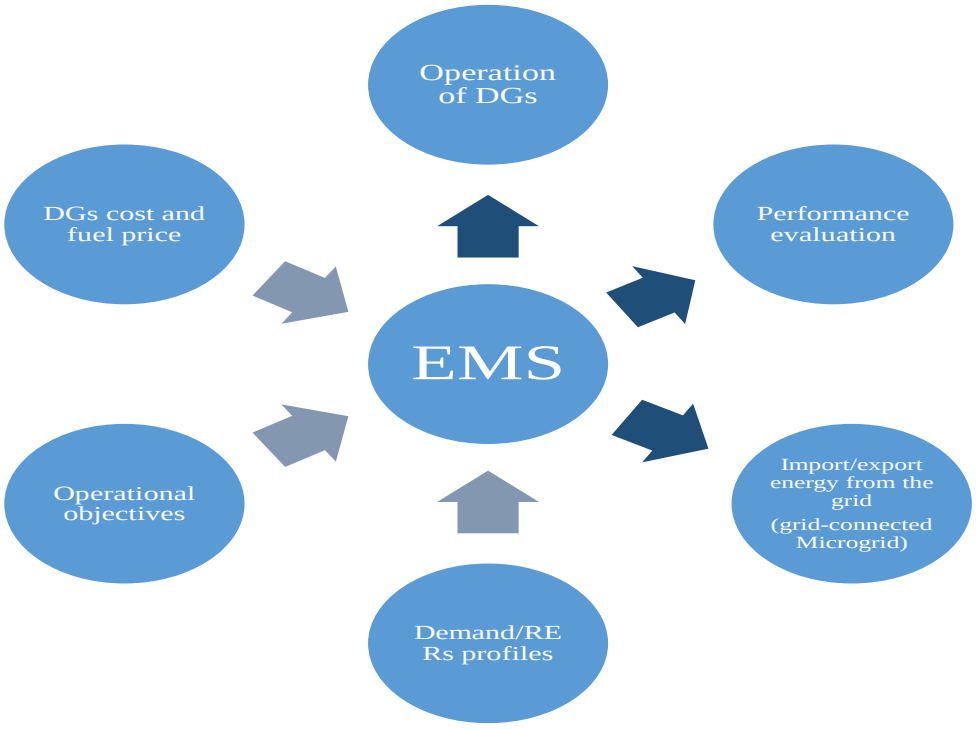

Figure 2.5: Energy Management System.

The EMS of a microgrid is a research topic widely tackled in literature in the past few years. In this thesis, the EMSs are classified into two groups based on

the algorithm or method used to implement the EMS. The two groups are EMSs based on classical approaches and EMSs based on intelligent approaches.

- EMSs based on classical approaches

  The EMS implemented by classical approaches is known for its simplicity in term of control and design. These approaches include rule-based, linear and nonlinear programming. Rule-based EMSs are governed by a series of rules and they are widely used due to their simplicity and practicality [22]. In [37], three rule-based EMSs are developed to find the size and suitable EMS for a stand-alone HES. The HES consists of PV, BESS, FC, EL, and HT. The three EMSs were designed based on operating modes and combining technical-economic aspects. The objective of the EMSs were mainly to satisfy the demand, then, maintain a certain level in the HT and BESS.

  Linear programming is one of the simplest methods for determination of the optimal solution in problems with several alternative solutions. The method is based on maximising or minimising an objective function according to constraints and bounded variables to obtain the unknown parameters. Nonlinear programming is the same as linear but the objective function contains a nonlinear function [86]. For example, linear programming was used to develop an EMS for a HES [87]. The objective of the EMS was to minimise the operation cost of the HES. The cost function integrates all associated degradation costs and the lifetime of all the assets in the HES. The HES includes PV, WT, FC, EL, and HT. The results showed an improvement of the EMS against conventional EMS.

  In general classical approaches are easy to implement and understand and commonly used in the literature. Nevertheless, these methods are not suitable for big and complex systems where the complexity and calculation time of the overall optimisation procedure are increased.

- EMSs based on intelligent approaches

  Recently, many studies have been conducted on EMS using Artificial Intelligence (AI) techniques, such as Genetic Algorithim (GA), artificial neural net-

work, particle swarm optimisation as well as hybrid approaches [22, 24, 88]. Implementing EMSs using AI approaches lead to enhance the efficiency and performance of microgrid and thereby meet the demand with maximum energy production [27]. Additionally, AI approaches are able to deal with nonlinear systems and multi-objective systems efficiently. However, the execution time for these approaches maybe longer in some cases and achieving a real-time control may not be possible [27]. Moreover, AI approaches require enough knowledge and experience for systems to be implemented efficiently.

A GA-memory based EMS is presented by Azkarzadeh [89] for optimal sharing of the power generation task between the DGs in a grid-connected microgrid. The objective of the EMS was to minimise the operating costs of PV, WT, and combined heat and power system. A multi-objective particle swarm optimisation EMS is introduced by Manbachi et al. [90] for real-time managing of a stand-alone microgrid. A new concept called the operation value factor was defined for each objective function to minimise the microgrid load shedding and increase achieve higher levels of performance and reliability.

2.7 FINITE AUTOMATA AND FUZZY LOGIC

This section introduces FA which represents a mathematical model of computing used in the design of many computer hardware and software [91]. FA is used for implementing multiple EMSs within the integrated framework in Chapter 4. The application of FA in power systems application is also presented. Moreover, an introduction on FLC and its application in a microgrid is presented.

2.7.1 *Finite Automata and Discrete Event Systems*

Discrete Event Systems (DESs) are discrete-state, event-driven systems among a set of finite states, with an initial state and one or more of marked states [92, 93]. Traditionally, regular languages and finite automata have been used both for modelling and analysis of DESs in the supervisory control community [94].

The first application of DESs in the power system was in 1995, where Prosser et al. [95] modeled a 14-bus 40-line transmission network using DES. Two states were considered for each line: line in service and line out of service. While the events that triggered the system are: line restoring and line tripping. The Supervisory Control of Discrete Event Systems (SCDES) was designed to manage the restoring operation of tripping lines with a high level of security. In a similar fashion, Lee et al. applied SCDES to obtain the restoration strategies for the power distribution networks, while maintaining a high level of security and satisfaction of the demand [96]. Another work of utilising DES was done by Afzalian et al [97, 98]. The SCDES was applied for the operation of the tap-changing transformer, and dynamic flow controllers. The components were modeled using Automata and synthesized using TCT software [99]. In [100], Kharrazi et al. investigated the application of SCDES to a custom power park. The components in the CPP were modeled using Automata, synthesized using the TCT software and simulated using MATLAB/Simulink. Recently, Sadid et al. [101] presented the scheduling of thermal devices operation in the framework of DESs. Two algorithms were developed to reduce the peak demand, and the results showed a noticeable improvement in peak demand reduction. In this thesis, FA are used to implement an EMS. Modelling the EMSs using FA has many advantages in terms of reducing the complexity of the system, a better understanding of the microgrid. As well as, facilitate the adding or changing of the operating conditions (conditions responsible for the operation of a certain asset in the microgrid), and increasing the ability to accommodate new assets smoothly.

2.7.2 *Fuzzy Logic*

The FLC is a flexible tool with rules based on human knowledge and experience. The uncertainty in the input variables can be handled efficiently by the FLC. Moreover, FLC is very suitable for complex models, such as HES [102]. The success of FLC is due to their ability to deal with the knowledge represented in a linguistic form instead of the conventional mathematical method [103].

The FLC follows three basic steps [104, 103]; the first step is converting the inputs into fuzzy values as a degree of membership of fuzzy sets. This membership function is a curve that defines how each point in the input space is mapped to membership value or degree of membership between 0 and 1. This step is called *fuzzification*. The second step is to link the controller output to the inputs using a list of IF – THEN rules. A fuzzy IF – THEN rule represents an IF – THEN statement in which some words are characterized by membership functions. The IF part of a rule specifies the combination of inputs for which a rule holds. The THEN part of a rule refers to values of the output variable [105, 106]. Finally, converting the output fuzzy set into a particular value that can be used as an output, which called *defuzzification*.

The FLC has been extensively used by researchers for several applications in microgrids with RERs [107]. For example, implementing FLC-based EMS for both grid-connected and stand-alone microgrids. A FLC was employed by ArcosvAviles et al. [108] to implement an EMS in a grid-connected microgrid. The microgrid consists of PV, WT, and BESS. The objective of the FLC-based EMS was to achieve smooth power profile by minimising the fluctuations and power peaks during the energy exchange with the grid. The FLC-based EMS also proved to maintain the level of the BESS close to 75% leading to improvement in the lifetime of the BESS. A FLC-based EMS was also presented by Kyriakarakos et al. [109] for a stand-alone microgrid. The microgrid includes PV, WT, BESS, EL, FC, HT, and water tank. The objective of the EMS was to minimise the Net Present Cost (NPC) as well as the penalty cost on BESS, HT and water tank. The demand divides into three types; electrical. hydrogen and water. The decision

inputs for the FLC were the state of the charge for the BESS, water and system frequency.

Implementing a Maximum Power Point Tracking (MPPT) for a PV system based on FLC is also one of the applications of FLC in microgrids. Gheibi et al. [110] utilised FLC to obtain the maximum power from PV. The objective of the MPPT-based FLC was to minimise the uncertainties in the solar data. In addition to the abovementioned applications, Macedo et al. developed a FLC for the order of implementation of smart grid electrical systems [111]. The FLC calculates a priority index which evaluates the energy systems to achieve the best cost-benefit analysis.

2.8 MICROGRIDS SIZING METHODS

The key concept of system unit sizing is derived from the importance of optimally managing all available assets and achieving suitable cost and reliability levels. These mentioned objectives are commonly in conflict since sometimes over-sizing the system will increase the total cost and under-sizing could cause a system failure. Therefore, a reasonable trade-off is sometimes necessary to design a reliable system with minimum costs [112]. Additionally, increasing the number of components in the system to be optimised will increase the system complexity, causing an increase in the time and effort required. Accordingly, it is fundamentally significant to find an optimisation method to select optimum system configurations readily and precisely.

Sizing methods of microgrids can be either a single objective or multi-objective functions. Single objective function depends on determining the optimal size depending on the minimum or maximum of a defined parameter. In contrast, the multi-objective function uses more than one defined parameters to optimise the microgrid size [113].

Finding the optimal sizing of the assets in a microgrid is an active research area with extensive literature regarding this topic. It can be classified into seven approaches, each one demonstrating a different technique to achieve the main

objective of microgrid sizing. Figure 2.6 lists the sizing methods described in this section.

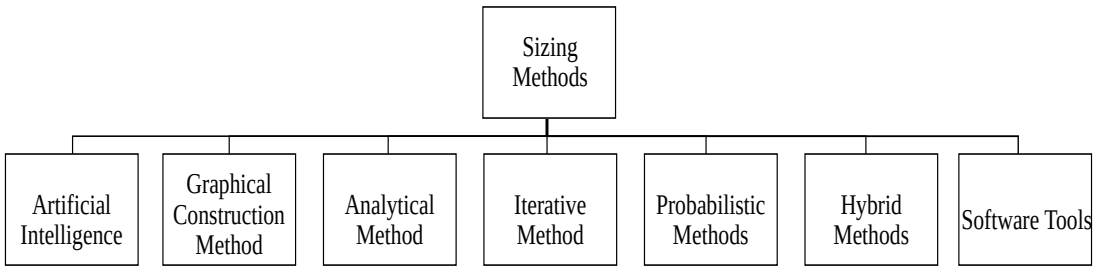

Figure 2.6: Methods used for sizing microgrids with RERs and classified into seven methods.

2.8.1 *Graphical Construction Methods*

A graphical construction technique is based on a seasonal analysis that is made for the variation in demand and resource availability during winter and summer months. Due to this analysis, a sizing curve is developed between the various sizes of wind turbines and PV generators available. If the data are collected for a longer period, then a more refined curve is obtained.

Markvart [114] used the graphical construction method to determine the size of a stand-alone HES consists of PV, WT, and BESS. The methodology based on the situation where the average value of demand must be satisfied by the average values of PV and wind power. Boroway et al. [115] developed a technique to find the optimum combination for a PV-WT system with a BESS for a stand-alone HES. The procedure based on long-term meteorological data of PV and wind profiles recorded each hour and each day for 30 years. These profiles were used to obtain the average power generated by PV and WT. The calculation of the optimum number of PV modules and BESS was based upon LPSP concept and minimum cost of the system. However, the main disadvantage of the graphical construction method is that only two parameters can be included in the optimisation process. For example, either PV and ESS or PV and WT can be optimised [8, 71]. Additionally, these methods require long-term meteorological

data to provide effective results. Basically, the graphical construction method does not require an EMS, since the sizing is done by implementing a fitting curve and based on the solution of the demand-supply criteria.

2.8.2 *Analytical Methods*

Analytical methods are computational methods that describe the system size as a function of its techno-economic feasibility. In these methods, a series of steps need to be followed in order to achieve the desired optimisation. Once the model is set, system performance can be evaluated according to certain criteria [113, 73].

Khatod et al. [116] presented an analytical approach for a small autonomous power system using WT and PV sources in Kandla, India. The objective of this approach was to minimize the cost of the production. The simulation was performed using the proposed analytical approach and Monte Carlo simulation, and the obtained results were compared in terms of accuracy and computational time. The analytical method showed less computational burden and time compared to the Monte Carlo simulation, as well as less meteorological data needed.

Bortolini et al. [117] proposed an analytical method to find the techno-economic sizing of a grid-connected PV-BESS. The analytical method determines the PV rated power and the BESS capacity based on the minimum LCOE. The authors employed the same analytical method to design a stand-alone HES with PV, BESS, and DSL installed in a remote village in Yakutsk, Russia. For the latter study, the analytical method used to calculate the carbon footprint of electricity.

The application of analytical methods is also presented by Kanase-Patil et al. [118]. A methodology is developed to select and size different system components, namely micro-hydropower, biomass, biogas, WT, PV, and BES. The stand-alone system is designed to meet the electrical and cooking energy needs of a cluster of villages in Uttarakhand state in India. The purpose of this study was to determine the optimal combination of energy subsystems to minimize the Cost of Energy (COE) generation and EENS.

Hung et al. [119] presented an analytical method to obtain the optimal power factor of each DG to reduce the energy losses. The analytical expression is based on a multi-objective function, then the optimal location, size, and the number of DGs are determined based on benefit-cost analysis.

In [120], Wissem et al. exploited mathematical models to determine the optimal configuration of a stand-alone PV-ESS. The objective was to satisfy the requirements of a typical residential home located in Sfax, Tunisia. The optimising step was performed based on lack of energy to generate probability, percentage of the surplus of energy produced and the cost of the kilowatt-hour produced.

The system performance can be assessed in an accurate way with the use of analytical methods. However, in case of multi-objective function optimisation, these methods do not always offer accurate solutions. The analytical methods perform well for small and simple systems; they are inappropriate for large and complex systems [121]. For this type of optimisation, iterative, artificial intelligence and hybrid methods provide better results for multi-objective functions [73]. As these approaches can deal with non-linear behavior of systems' components.

2.8.3 *Iterative Methods*

An iterative method represents a recursive process which stops when the best configuration is reached according to the design specifications [6, 9, 74]. Iterative methods have been extensively employed in the literature because of their ability to deal with multi-objective systems.

Akram et al. [122] presented an optimal sizing of a WT, PV, and BESS grid-connected HES. In this study, two iterative algorithms are implemented to find the optimal sizing of the HES. The first algorithm finds the size of RERs, while the second algorithm determines the size of the BESS. The optimisation of these algorithms is based on maximum reliability and minimum cost.

A methodology to determine the optimal sizing of an autonomous hybrid PV-WT system has also been suggested [123], in which accurate mathematical models for

characterizing the PV module, WT and BESS were proposed. Then the optimal sizing of the system was found according to minimising the LPSP and the LCOE.

Hosseinalizadeh et al. [124] presented an algorithm to optimise the size of a stand-alone HES. The HES consists of PV, WT, BESS, and hydrogen system where the fuel cell is treated as a backup system. The optimal size is based on minimizing the system's total cost for different four regions in Iran. The authors assessed the reliability of the HES using less of load expectation and loss of energy expectation. The study found HES is more economical and reliable without a fuel cell.

Smaoui et al. [125] developed an iterative algorithm to find the optimal sizing of a HES. The HES consists of PV, WT, and hydrogen system. The algorithm gives all possible configurations that can completely cover the freshwater requirements of isolated consumers in Kerkennah Island, South Tunisia. The optimal configuration is chosen based on the minimum initial costs. The proposed HES was able to satisfy the demand, and the complementary characteristics of PV and WT reduce the installation cost due to decreasing the storage capacity.

Bhuiyan et al. [126] proposed a single-objective iterative algorithm to determine the optimal size of a stand-alone microgrid. The microgrid composes of PV, WT,BESS, and DSL. The main optimisation function is minimizing the LCC while the LPSP is used to assess the HES reliability. Applying this algorithm provides lower LCC when comparing the results of the same system implemented in HOMER. Additionally, the study found the LCC is reduced when LPSP is decreased.

Iterative methods proved to provide efficient results since it is using multiple configurations, then choosing the best configuration based on the optimisation criteria. However, when the number of optimisation variables rises, the computation time increases exponentially.

2.8.4 *Probabilistic Methods*

These methods are among the simplest sizing methodologies, it can optimise one or more parameters for microgrid sizing. It can handle the problem of missing data in the solar radiation or wind speed by generating the data statistically. The selected parameters are chosen as random variables and the optimised results are obtained by the distribution function of these random variables [6, 127, 9, 8, 74].

The probabilistic approach employed by Tina et al. [75] based on the convolution technique to assess the long-term performance of PV and WT system for both stand-alone and grid-connected HES. The presented method allows for estimating the long-term average performance of the HES. To estimate the energy performance of the HES the reliability analysis is performed by the use of the energy index of reliability directly related to EENS. The same authors proposed a probabilistic model applied to a PV and WT hybrid system equipped with either a one-axis or two-axis solar tracking system [128]. The effect of the solar tracking systems on the annual energy gain was determined by performing a reliability analysis using EIR which is directly related to EENS.

The probabilistic methods are simple to implement and very helpful in cases of missing data. However, according to the amount of weather data considered and the probabilistic model used, results obtained may not be suitable for finding out the best possible solution [129].

2.8.5 *Artificial Intelligence Methods*

AI means the flexibility of a machine to mimic activities that characterize human minds. AI algorithms have the ability to learn from examples, handle noisy and incomplete data, address non-linear problems, and once trained can perform prediction and generalization at high speed. AI methods such as GA, Particle Swarm Optimisation (PSO) are widely used in sizing power systems, mainly because of their symbolic reasoning, flexibility and explanation capabilities [130].

GA considered is one of the most powerful optimisation algorithms, it produces solutions using techniques based on natural advancement eg. inheritance and mutual selection. GA is suitable for problems of multiple soulitions [113, 8]. Abbes et al. [131] applied GA to perform a multi-objective design of a HES to find the best compromise between three objectives; LCC, the system embodied energy and LPSP. The HES composes of PV, WT, and BESS. The optimal configuration was chosen from a set of solutions such that the HES is capable to supply the residential house with at least 95% of its energy requirements. Merei et al. [132] optimised a stand-alone PV, WT, DSL with various BESSs types using GA. The component sizes and model settings are varied while the system is re-examined to minimize overall costs. The results showed that integrating BESSs with DG is economical and ecological.

PSO is one of the most well-known AI algorithms in solving optimisation problems, because of its simplicity, ease of implementation and fast convergance [113]. A recent study on using PSO simulation-based approach has been carried out by Combe et al. [133]. The study determines the optimal size of an AC mini-grid HES in a remote area in Australia. Four different configurations are considered including PV, WT, DSL, and BESS. All the models are optimised using PSO and the aim is to minimize the system NPC whilst meeting the operational constraints. The results found there are some factors that lead to further cost reduction such as the increase in the wind turbine hub height and demand-side management. Finding the right values of these factors allows reducing the operating reserve requirements and hence further optimisation of the HES. Another application of the PSO algorithm in grid-connected HES is presented by Maleki et al. [134]. A grid-connected HES including PV, WT, and FC is optimised using two AI algorithms namely, PSO and GA. The optimisation objective is to minimize the operation and maintenance cost of the HES. The results showed GA appears to be more promising in performance evaluation while PSO proved to be more efficient regarding the computation time.

In general, AI methods can provide convenient results and are beneficial in system design. However, their implementation is complex and some algorithms

such as GA require a large number of iterations which increases the response time [129, 113].

2.8.6 *Hybrid Methods*

Hybrid methods are developed by combining two or more of the above sizing methods utilising the advantages of complementary characteristics of these methods to solve complex optimisation problems [42, 113].

Khatib et al. [135] applied a hybrid method to size a stand-alone HES consisting of PV, WT, and BESS for rural housing electrification in Kuala Terengganu, Malaysia. The optimisation is based on loss of load probability and system total cost and using hybrid iterative-GA. The iterative part of the proposed algorithm is applied to generate a set of possible configurations for the proposed system, while the genetic algorithm is applied to find the optimum configuration.

Zhou and Sun [136] presented a simulated annealing particle swarm optimisation algorithm to find the optimal size of a PV and WT HES and battery-supercapacitor hybrid storage system. The optimisation objective is to find the optimal size while minmizing system's LCC. The power balance between generation and demand is used to assess the reliability of the system. The new algorithm enhances the ability to escape from local optimum and improve the diversity of PSO and enhance the global searching ability of the algorithm. The results show the convergence of the new algorithm is faster than the traditional PSO and its cost optimisation is better.

A study proposed by Katsigiannis et al. [137] employed a hybrid method using the simulated annealing and Tabu Search algorithms to find the optimal sizing of a stand-alone HES. The parameters to be sized are the WT, PV system, DSL, biodiesel generator, FC, and BESS. The minimization of energy costs was the main aim of the study, and the results proved that SA-TS improved the solution obtained in terms of quality and convergence.

A hybrid method implemented to find the optimal size of a HES including RERs and ESSs. The aim was to match the demand with the RERs without the

need for additional conventional or grid-connected strategies [138]. A Pattern Search-based optimisation method was used in conjunction with a Sequential Monte Carlo simulation to minimize system costs and satisfy the reliability requirements. The results showed that the proposed PS-based SMCS provides improved efficiency compared to each algorithm separately.

Although the hybrid methods are considered the most efficient algorithm for microgrid optimisation in terms of reliability, accuracy and cost minimization. However, the main limitation of these methods is the complexity in designing the system [129].

2.8.7 *Software Tools*

Currently, there are many computer tools available for the unit sizing and optimisation for microgrids. Among these, the hybrid optimisation model for electric renewables (HOMER) is one of the most widely used for sizing hybrid systems. HOMER is considered user-friendly and easy to understand, as well as it provides an efficient graphical representation of the results [139].

Many research studies have been conducted using HOMER. For instance, Sen and Bhattacharyya [140] utilised HOMER to determine the most proper hybrid combination for electricity generation from a mix of RERs. The system is designed to satisfy the electrical needs of a stand-alone remote village in India. Four RERs, namely, small-scale hydropower, PV, WT, and bio-diesel generators, were considered. Using HOMER, it was noted that a system consisting of PV, small hydropower, biodiesel, and BESSs was the least-cost combination.

Ramli et al. [141] employed HOMER to determine the optimal size of a grid-connected PV system in Saudi Arabia. Unmet demand, surplus energy, fraction of renewable electricity, NPC and carbon dioxide emissions (CO_2) percentage were considered to obtain the optimal sizing. The results obtained by HOMER provided 100% utilisation of PV and minimized CO_2 and NPC.

Rajbongshi et al. [142] used HOMER to optimise a HES including biomass gasifier, PV, DSL, BESS and converters for different demand profiles. The cost

of energy is calculated for different peak demand, energy demand profiles, and grid availability. The results showed that the cost of energy for a grid-connected hybrid system is lower compared to an off-grid hybrid system for similar demand profiles.

Other unit sizing computer tools are HYBRID2, HYBRIDS, Hybrid Optimisation by Genetic Algorithm (HOGA), TRNSYS, HYDRO, and RETscreen, and explanation about these tools can be found in [112, 129, 139].

Although HOMER has been utilised in the literature on a wide-scale, there are some limitations of this software such as it performs only a single-objective optimisation by minimizing NPC. Moreover, HOMER does not consider the Depth of Discharge (DOD) of the BESS which plays a vital role in the optimisation process [113, 139].

Table 2.1 summarizes the key features and limitations of research efforts to date in the domain of sizing microgrids.

Table 2.1: Comparison of sizing methods available in the literature [6, 7, 8, 9].

Ref.	Sizing method	Highlights	Strength	Limitation
[114] [115]	Graphical Construction Methods	Provide graphical solutions for the optimisation problem	Easy to understand and use	Some important factors are neglected and require long-term meteorological data
[116] [117] [118] [120]	Analytical Methods	The system is represented by computational models	Easy to understand and use	Complexity because of large number of parameters, and impossible to apply to large systems
[122] [123] [124] [125] [126]	Iterative Methods	The optimisation problem is solved recursively until it reaches the optimum solution	Easy to understand and to find any defects at an early stage	Requires more computational time
[75] [128]	Probabilistic Methods	Multiple possible outcomes with varying degrees of certainty or uncertainty of occurrence	Easy to understand and use	Cannot represent the dynamic performance of the system
[131] [132] [133] [134]	Artificial Intelligence	The ability to train the machine to perform similar kinds of function that characterise human thought	Fast and robust system, ability to handle missing data	Large dimensionality of data
[140] [141] [142]	Hybrid Methods	Combination between two or more different techniques	More accurate, sometimes less computational time and more competitive than single method	Increasing complexity and difficult to code
[135] [136] [137] [138]	Software Tools HOMER	Carrying out quick pre-feasibility, optimisation and sensitivity analysis	User friendly easy to understand	Allows only single objective function and does not consider DOD.

2.9 CONCLUDING REMARKS AND DISCUSSIONS

This chapter provides background and literature review of microgrids, the integrated assets, criteria for microgrid optimisation, control and management, and sizing methods reported in the state-of-the-art. Finding both the appropriate size and EMS of a microgrid are fundamental to obtain the best performance of all the integrated assets. The efforts in sizing the assets in a microgrid have been distinguished in seven methods: graphical construction, analytical, iterative, probabilistic, artificial intelligence, hybrid and software tools. In addition, the EMS has been classified into two categories. The first category is the EMSs that use classical methods in implementation such as rule-based and linear programming. The second category uses AI techniques for the EMS implementation such as GA and PSO. The key principle of the sizing and EMS methods is to achieve optimal performance of the microgrid in terms of cost and reliability. Nevertheless, the existing methods for sizing face different challenges (see Table 2.1). For instance, AI methods offer efficient results in microgrid optimisation regarding the size and EMS. However, in these methods, the amount of data required to provide a reliable analysis grows exponentially. In addition, the time required for the optimisation is considerably high. The hybrid methods provide accurate optimisation results, however, implementing them is not simple and their complexity increase for complex microgrids. To this end, in this thesis, the analytical method is employed for finding the size of the assets in a microgrid. This method is coupled with the levelised cost of energy to increase the efficiency of the results. Moreover, finite automata have been combined with this analytical and economic sizing method to obtain the optimal size and EMS. Finally, a fuzzy logic controller is developed to maintain the performance of the microgrid regardless of the uncertainty in the meteorological datasets. The work done in this thesis aims to mitigate the above-mentioned challenges.

3

SIZING OF GRID-CONNECTED MICROGRID

3.1 INTRODUCTION

The previous chapter surveys the methods for determining the optimal size of power system with RERs/AERs and ESSs. The criteria used for microgrid assessment. Additionally, the importance of the EMS in the sizing optimisation is discussed.

This chapter is based on the author's published work on sizing a grid-connected microgrid using an AES approach [10]. The objective of the AES approach is to find the optimal size of the combination PV-BESS such that the cost of the system is minimised. This includes the cost of the involved assets, maximising the profit by increasing the energy exported to the grid and minimising the energy imported from the grid. The grid-connected system composed of PV, BESS, inverter, charge controller and the necessary connections to the demand and grid is presented. In the beginning, the proposed AES approach determines the BESS capacity, generate multiple combinations of PV-BESS over a defined range of PV rated power. Along with determining the optimal size, three types of BESS are examined to determine the best type to be combined with the PV. Moreover, a suitable EMS is proposed to control the energy flow through the system. This is followed by an economic model to accurately calculate the system LCOE for all possible PV-BESS combinations. Finally, the optimal PV size and best BESS coupled with the PV system is selected depending on the minimum LCOE. To achieve this, an improved formula of LCOE is proposed which includes new parameters reflecting the impact of surplus PV energy and the energy purchased from the grid. The proposed model uses the Levelised Cost of Delivery (LCOD) for BESS and compares it with system LCOE. Real datasets over one year of

hourly solar radiation, temperature, and demand are used for system sizing. The architecture of the grid-connected PV-BESS microgrid is explained in the following section.

3.2 GRID-CONNECTED PV-BESS ARCHITECTURE

The diagram in Figure 3.1 shows the grid-connected system under study which consists of PV, BESS, inverter, charge controller and the necessary connections to the load and grid. The DC/AC inverter is necessary to bring the DC output of the PV to the AC load or grid. While the charge controller preserves the BESS from over charging and discharging. Although the inverter efficiency is not constant in reality, in this study, it is assumed to be constant. The Isle of Wight is taken as a case study to validate the AES approach. The island is currently working on decarbonising the electricity system to make it self-sufficient in energy using RERs by 2020 [143]. Therefore, the hourly values of solar radiation and ambient temperature for the island are taken into consideration for the optimisation of the size of PV and BESS. While the demand profile was downloaded from OpenEI website (US Department of Energy) [3]. Since it was a challenge to obtain the demand data for the Isle of Wight.

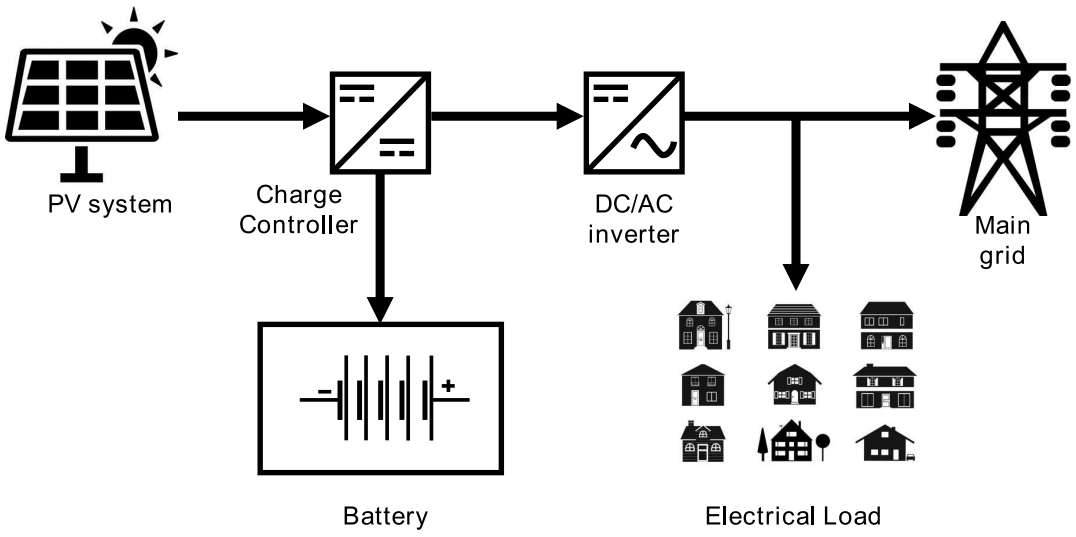

Figure 3.1: Grid-connected PV-BESS system consisting of PV, BESS, inverter, and charge controller.

The demand in the grid-connected system is mainly covered by the PV-BESS system, or by purchasing energy from the grid whenever the energy generated/stored by PV-BESS is insufficient. When solar energy is higher than the demand, then the generated PV energy covers the demand. In case there is a surplus PV energy, it will be used to charge the BESS. While any surplus after charging the BESS will be sold to the grid. In case that the PV energy is insufficient for the demand, the BESS is checked firstly, if the state of charge (soc) is higher than the allowed minimum (soc_{min}), then the BESS covers the rest of the demand. When there is not enough energy in the BESS, a decision to buy energy from the grid takes place.

The following section introduces the proposed AES approach and explains in detail the steps followed to obtain the optimal size of the PV-BESS.

3.3 SIZING METHODOLOGY OF PV-BESS GRID-CONNECTED

Determining the optimal size is crucial for many reasons (Section 2.8). In the first place, it maximises the utilisation of PV generated energy, secondly, it helps in obtaining minimum operating costs. Fundamentally, over-sizing the system increases the total cost and reduce profitability while under-sizing the system may cause a system failure since it can not supply the demand efficiently. To evaluate the PV-BESS system on an economic basis, LCOE is utilised as a metric to find the relative cost of PV systems and different BESSs [144].

To begin, for each hour in the year, a power balance calculation is conducted, such that the hourly power demand is primarily covered by the PV-BESS. An AES algorithm is developed and implemented in MATLAB to simulate different scenarios for three BESS technologies. These technologies are LAB, LIB, and RFB respectively. The LAB and LIB are conventional rechargeable batteries that offer a convenient and efficient way to store electricity. While RFB is a recent BESS technology with advantages of high efficiency and large scale ESS.

The AES approach determines the size of the PV system by iteratively changing the PV rated power ($P_{PV,rated}$) from 200 kW to 1400 kW with a step of 30 kW each

time. This approach is repeated for the three BESSs. This range is determined based on the maximum hourly demand which is equal to 417.7 kW, where the selected range covers all possible PV sizes. The combination that provides the lowest LCOE while covering the load demand will be selected as the optimal solution. The EMS is developed based on the analytical method, where its priority is to supply the demand from the energy generated from the PV-BESS system. When this energy is insufficient to supply the demand, the decision to purchase energy from the grid takes place. Alternatively, surplus energy generated from the PV system will be sold to the grid.

Figure 3.2 explains the methodology of the AES used to size the grid-connected PV-BESS system. P_{PV-min} and P_{PV-max} are the minimum and maximum values for PV rated power range respectively. P_{PV} is the power produced by the PV, soc represent the state of charge of the battery, and d indicates the BESS types involved in this study. In the beginning, the value of $P_{PV,rated}$ is set to P_{PV-min} which is equals to 200 kW. The BESS capacity is calculated for the first type, which is LAB using Equation 3.6 (explained in Section 3.4.2). For each hour in the year, the energy generated from the PV (P_{PV}) is calculated using Equation (3.1) (as explained in Section 3.4.1). $P_{PV}(n)$ is compared to the demand ($P_{load}(n)$) if the condition is true, $P_{PV}(n)$ is used to supply the demand. Any surplus $P_{PV}(n)$ is directed to the BESS until it is entirely charged, and then it is sold to the grid. On the contrary, when the solar radiation is low or during night time ($P_{PV}(n) < P_{load}(n)$), the BESS supplies the demand until deficit ($soc \leq soc_{min}$). In such case, the grid supplies the demand to cover the lack of energy.

The variable n, which represents the index of the hours in a year, is checked every iteration until it reaches 8760 hours. Then, the LCOE for the combination PV-LAB is computed using Equation (3.16). The AES approach is repeated where LAB is replaced by LIB with the same computations. The algorithm iterates until all the combinations of PV with the three types of BESSs are covered. The analytical and economic models for PV and BESS are explained in the following section.

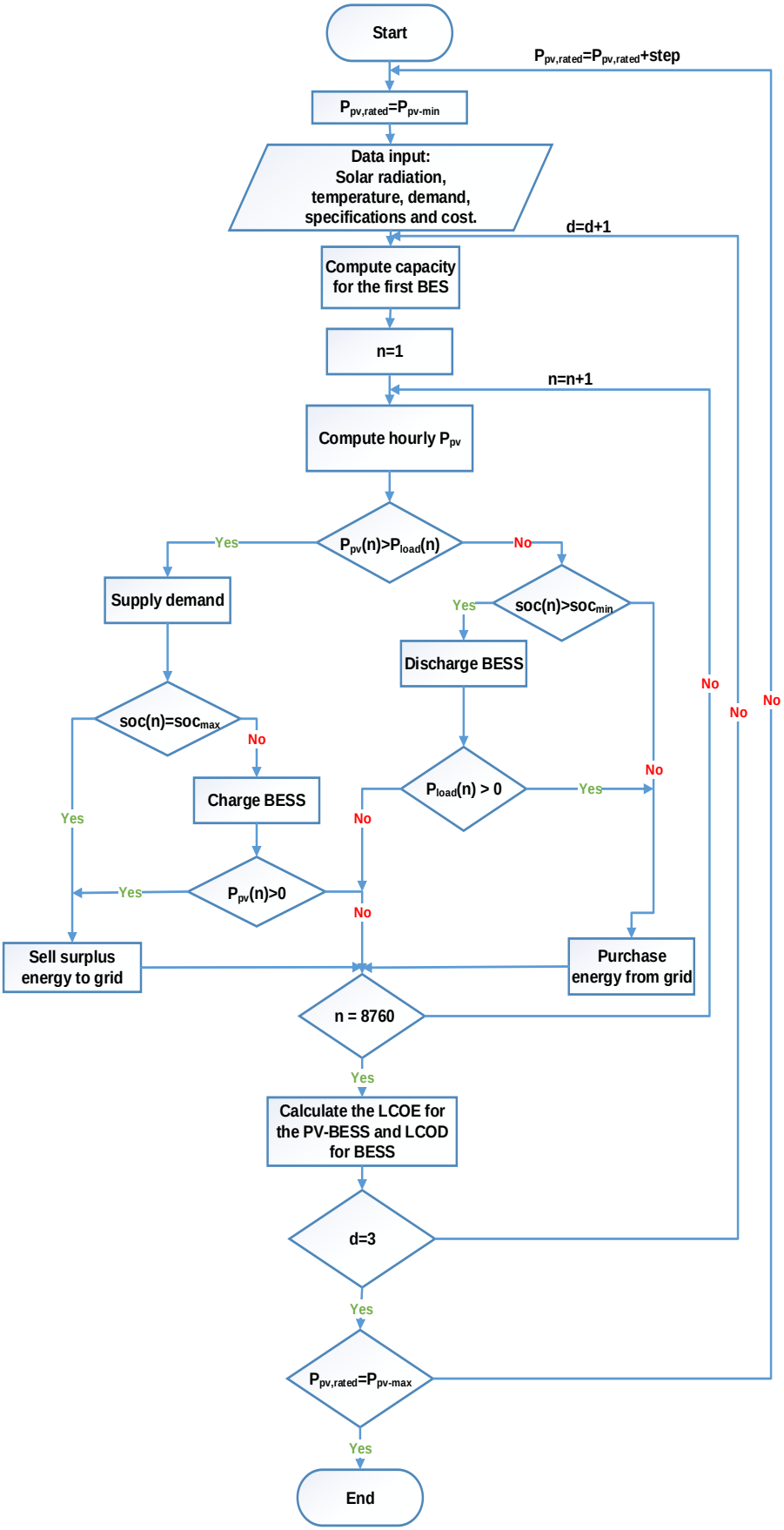

Figure 3.2: The flowchart of the proposed AES approach.

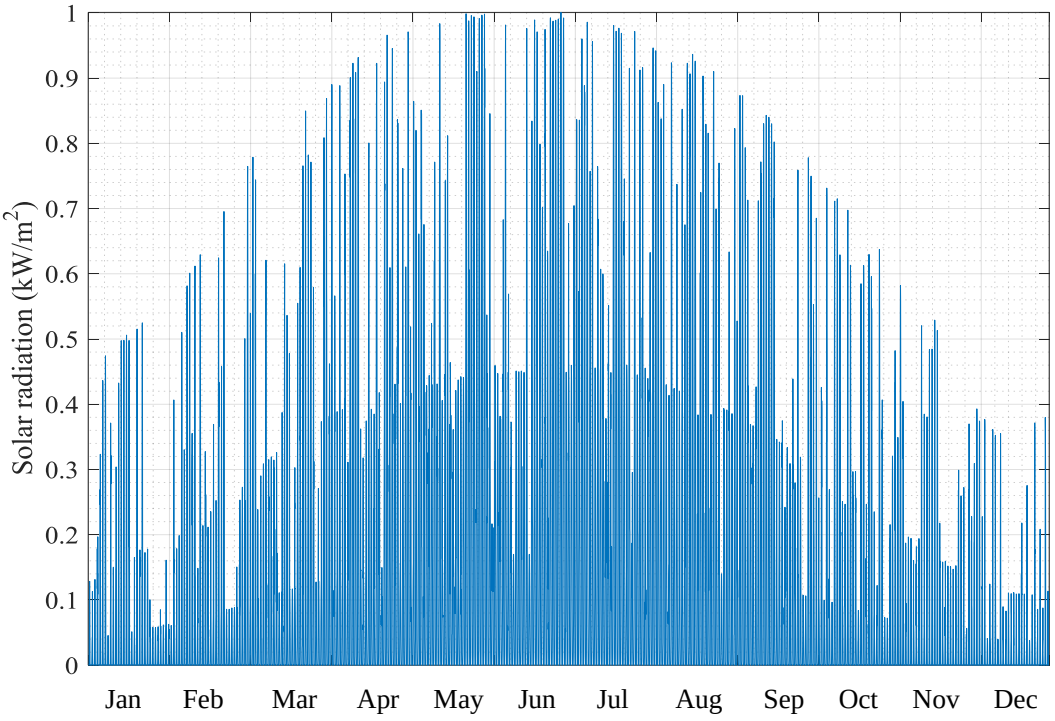

Figure 3.3: Solar radiation of the Isle of Wight for one calendar year [2].

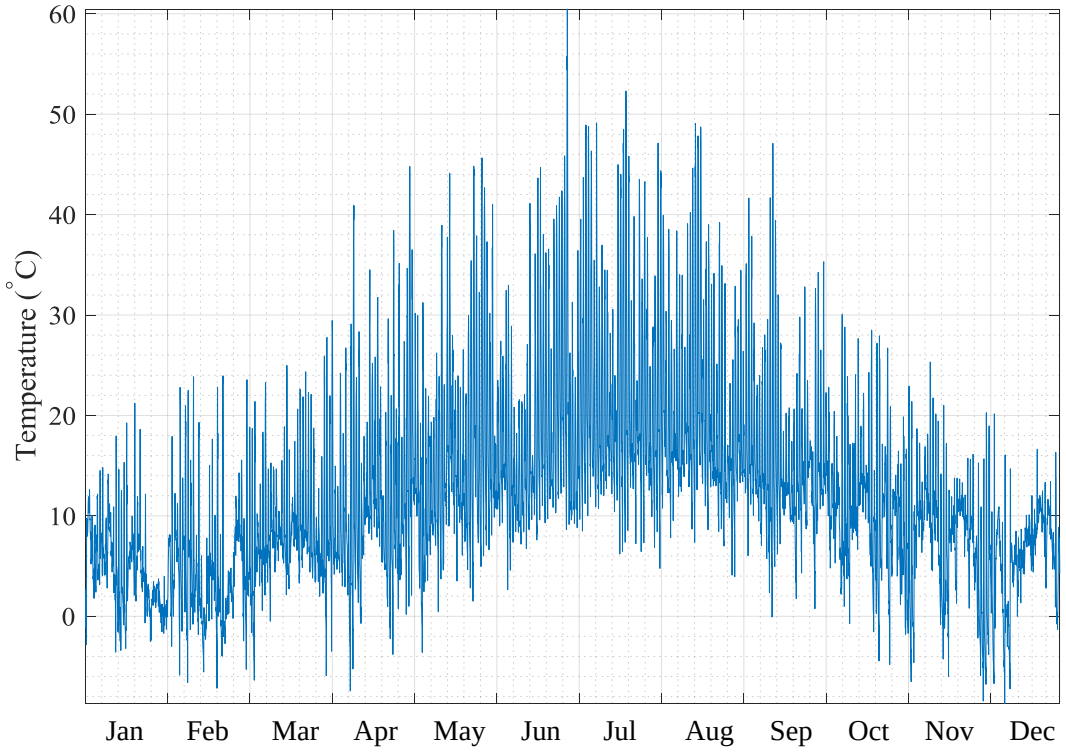

Figure 3.4: Hourly ambient temperature profile for the Isle of Wight for one calendar year [2]

The Solar radiation, temperature, and demand profiles, presented in Figures 3.3, 3.4, and 3.5 represent the input data. Figure 3.3 shows the solar radiation distribution for the Isle of Wight [2]. The temperature profile is presented in Figure 3.4, the highest temperatures are during the summer and spring and the lowest temperatures are during the winter and autumn months. Figure 3.5 illustrates the demand profile. On the contrary to solar radiation and temperature profiles, the demand is higher during the winter and the autumn months due to more electricity consumption during these seasons. Whereas during the remaining seasons, electricity consumption is minimal.

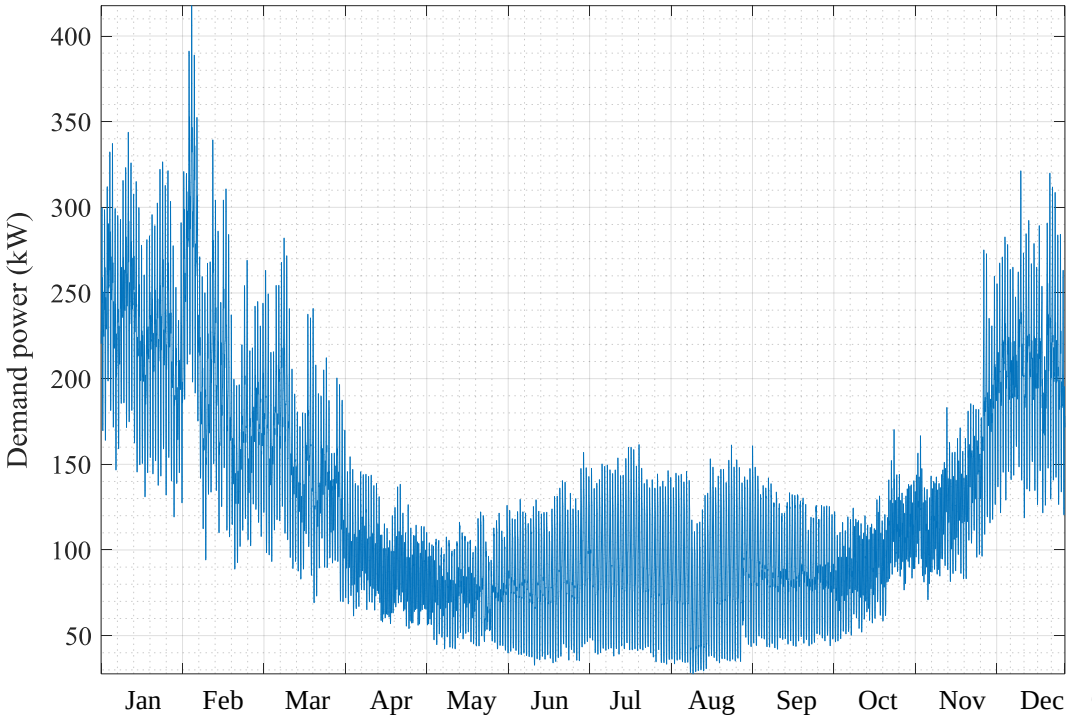

Figure 3.5: Demand distribution of one calendar year [3].

3.4 PV-BESS ANALYTICAL AND ECONOMIC MODEL

This section presents the analytical model for the PV-BESS system, as well as the economic model used to compute the LCOE. This metric is used for assessing the system's economic profitability in order to find the optimal size of the grid-connected PV-BESS.

3.4.1 *PV System Analytical Model*

The hourly output power produced by the PV arrays is given by Equation (3.1) [145]. This generated power strongly depends on the PV arrays area A_{PV}, the total solar radiation onto one square metre in one hour I_{PV}, and the overall PV efficiency η_{PV}. A_{PV} can be found using Equation 3.2 [145].

$$P_{PV}(n) = \begin{cases} I_{PV}(n) \cdot A_{PV} \cdot \eta_{PV}(n), & I_{PV}(n) \geq 0 \ . \\ 0, & I_{PV}(n) \leq 0 \ . \end{cases} \tag{3.1}$$

$$A_{PV} = \frac{P_{PV,rated}}{\eta_{module} \cdot H} \quad , \tag{3.2}$$

where $P_{PV,rated}$ is the PV rated power obtained by the AES approach. H is the yearly module reference in-plane radiation, usually assumed to be 1000 W/m^2 and η_{module} is the PV module efficiency.

The $\eta_{PV}(n)$ is not constant and vary every hour, Equation (3.3) shows how the overall PV efficiency is computed. η_{PV} depends on η_{module}, hourly temperatue efficiency $\eta_{temp}(n)$, inverter efficiency η_{inv}, the system lifetime N, and PV degradation DEG_{PV}. Among these variables, the η_{temp} is varying each hour and can be calculated using Equation (3.4). Equation (3.5) computes the PV cell temperature $T_{cell}(n)$ where their values depend on the hourly ambient temperature $T_{amb}(n)$ (see Figure 3.4).

$$\eta_{PV}(n) = \eta_{module} \cdot \eta_{temp}(n) \cdot \eta_{inv} \cdot (1 - (N-1) \cdot DEG_{PV}) \ , \tag{3.3}$$

$$\eta_{temp}(n) = [1 - \beta(T_{cell}(n) - T_{ref})] \quad , \tag{3.4}$$

$$T_{cell}(n) = T_{amb}(n) + [(NOCT - T_{amb,NOCT})/I_{NOCT}] \cdot I_{PV}(n) \ , \tag{3.5}$$

where β is the temperature coefficient of solar cell efficiency, T_{ref} is the PV cell reference temperature. $NOCT$ is the normal operating cell temperature and

I_{NOCT} is the solar radiation at $NOCT$. The values of the parameters used in the Equations (3.1) to (3.5) are presented in Table 3.1.

Table 3.1: Cost and technical specifications of PV system used for energy and cost calculations.

Parameter	Description	Value/range	Ref.
$P_{PV,rated}$	PV rated power	200-1400 kW, step 30 kW	-
η_{PV}	PV efficiency	14%	[117]
η_{inv}	Inverter efficiency	92%	[117]
DEG_{PV}	PV degredation rate	0.5%	[117]
β	Temperature coefficient of solar cell efficiency	0.005/° C	[117]
C_{PV}	Total cost of PV	$P_{PV,rated} \cdot 2828.7 \cdot P_{PV,rated}^{-0.128}$	[146]
C_{inv}	Total cost of inverter	$1.1 \cdot P_{PV,rated} \cdot Pr_{inv}$	[147]
Pr_{inv}	Unit cost of inverter	0.56 £/W	[147]
IC_{PV}	Inital cost of PV	C_{PV}+C_{inv}	-
$C_{PV,OM}$	O&M cost of PV	1% of IC_{PV}	[148]
RC_{inv}	Replacement cost of inverter	C_{inv}, for j=10 &20	[146]
Pr_{cc}	Unit cost of charge controller	4.62 £/amp	[147]
C_{cc}	Total cost of charge controller	$(P_{PV,rated}/V_b) \cdot Pr_{cc}$	[147]
NOCT	Normal operating cell temperature	45° C	[117]
I_{NOCT}	Solar radiation at NOCT	800 W/m^2	-
T_{ref}	PV cell reference temperature	25° C	-
H	Yearly module reference in-plane radiation	1 kWh/m^2	[146]
r	Discount rate	5%	-
$Pr_{e,purchase}$	Unit price of purchased energy	0.13822 £/kWh	[149]
$Pr_{e,sold}$	Unit price of sold energy	0.0485 £/kWh	[149]

3.4.2 *BESS Analytical Model*

The size of three types of the BESSs (LAB, LIB and RFB) can be obtained using Equation (3.6) [145]. The capacity of the BESS is expressed in terms of the hours of autonomy HA, $P_{load.avg}$, η_{inv}, η_{ch}, and DOD. HA represents how many hours a completely charged BESS is able to supply the demand continuously. The average hourly demand of the reference year $P_{load.avg}$ is equal to 124.8 kW. Where η_{inv} and η_{ch} are the inverter and charging efficiencies respectively. DOD is the depth of discharge which is chosen to be 80% for the three types of the BESSs. The capacities of the LAB, LIB and RFB are shown in Table 3.2.

$$Bat_C = \frac{HA \cdot P_{load.avg}}{\eta_{inv} \cdot \eta_{dch} \cdot DOD} \quad , \tag{3.6}$$

A fundamental parameter to represent the state of the BESS is the state of charge (soc), which is used to decide whether to charge or discharge the BESS. An energy balance is required every hour to obtain the soc of the BESS. If the PV-generated power is greater than demand, $P_{PV}(n) > P_{load}(n)$, then the demand is supplied firstly and the extra PV power is used to charge the BESS. The soc equation in the charging case can be expressed as follows [145]:

$$soc(n) = soc(n-1) + \frac{(P_{PV}(n) - P_{load}(n)) \cdot \eta_{ch} \cdot \Delta t}{\eta_{inv} \cdot Bat_C} \quad , \tag{3.7}$$

where $soc(n)$ and $soc(n-1)$ are the states of charge of the BESS at time n and $n-1$ respectively. While Δt represents the time step in the simulations and equals to one hour. On the other hand, if $P_{PV}(n) < P_{load}(n)$, the PV produced power is directed to the demand while the BESS covers the remaining demand. Equation (3.8) shows the BESS discharging expression [145], and at any time, the BESS soc is subject to the constraints in Equation 3.9:

$$soc(n) = soc(n-1) - \frac{(P_{load}(n) - P_{PV}(n)) \cdot \Delta t}{\eta_{inv} \cdot \eta_{dch} \cdot Bat_C} \quad , \tag{3.8}$$

$$soc_{min} \leq soc(n) \leq soc_{max} \quad , \tag{3.9}$$

Table 3.2: Cost and technical specifications of the three types of BESS.

Parameter	Description	LAB	LIB	RFB	Ref.
η_{rt}	Round trip efficiency	80%	90%	85%	[150]
DEG_{BESS}	BESS degredation rate	3.7%	2%	0.1%	[151]
η_{dch}, η_{ch}	BESS charging and discharging efficiency	85%	85%	80%	[52]
BESS lifetime	-	5-15	5-20	10-15	[152]
IC_{BESS} (£/kWh)	Initial cost of BESS	250	850	700	[52]
$C_{BESS,OM}(IC_{BESS})$	O&M cost of BESS	5%	1%	2%	[151]
Bat_C	BESS capacity	1 MWh			-
RC_{BESS}	Replacement cost of BESS	IC_{BESS} for j=10&20			[117]
soc_{max}	Maximum state of charge	100%			-
soc_{min}	Minimum state of charge	20%			-
DOD	Depth of discharge	80%			-

where soc_{min} and soc_{max} represent the minimum and maximum allowable soc respectively. Δt is the time step used in the simulations and equals to one hour.

3.4.3 *The Economic Model of the Grid-connected PV-BESS*

LCOE methods are widely used to evaluate the economic feasibility of PV systems and BESSs. The main principle of LCOE is to find the costs distributed over the project lifetime, and this provides a more-accurate economic picture of the project under analysis [77, 78, 79]. As reported by [79], the LCOE of a stand-alone PV-BESS system can be obtained by dividing the total cost of the system on the total energy generated. The energy generated from the PV is utilised to

supply the demand and to charge the battery. Accordingly, the cost of the PV is computed in terms of these two components. The proposed model modifies the above-mentioned LCOE method to be used in a grid-connected PV-BESS system.

The LCOE of the PV-BESS system ($LCOE_{system}$) employed in this study combines the LCOE of the PV ($LCOE_{PV}$) and LCOE of the output energy from the BESS, which is called LCOD. Equations (3.10) and (3.11) give the LCOE for the PV which consist of $C_{PV,Extra}$ and $C_{PV,load}$. $C_{PV,Extra}$ represents the cost of extra PV energy used to charge the BESS and sold to the grid. And $C_{PV,load}$ is the cost of energy used to supply the demand. Whereas, $E_{PV,Extra}$ and $E_{PV,load}$ are the extra PV energy and energy supplied to the demand by the PV respectively.

$$LCOE_{PV} = \frac{\sum_{j=0}^{j=N} \frac{(C_{PV,Extra} + C_{PV,load})_j}{(1+r)^j}}{\sum_{j=0}^{j=N} \frac{(E_{PV,Extra} + E_{PV,load})_j}{(1+r)^j}} \quad , \tag{3.10}$$

$$LCOE_{PV} = \frac{\sum_{j=0}^{j=N} \frac{C_{PV,Extraj}}{(1+r)^j}}{\sum_{j=0}^{j=N} \frac{(E_{PV,Extra} + E_{PV,load})_j}{(1+r)^j}} + \frac{\sum_{j=0}^{j=N} \frac{C_{PV,loadj}}{(1+r)^j}}{\sum_{j=0}^{j=N} \frac{(E_{PV,Extra} + E_{PV,load})_j}{(1+r)^j}} \; . \tag{3.11}$$

The formula for LCOD in Equation (3.12) has also been introduced in [79], which identifies the cost of the energy delivered by the BESS. LCOD modifies the LCOE of the storage by including the cost of the PV arrays that are responsible for generating energy to charge the BESS. This is indicated by Equation (3.13). Moreover, LCOD takes into consideration the round trip efficiency (η_{rt}) of each BESS and the Levelised Cost of Storage (LCOS). The LCOS is defined as the cost of the BESS C_{BESS} to the energy supplied by the BESS E_{BESS} computed during its lifetime and illustrated by Equation (3.14).

$$LCOD = LCOE_{E_{out}} = \frac{1}{\eta_{rt}} LCOE(E_{PV,charge}) + LCOS \quad , \tag{3.12}$$

$$LCOE(E_{PV,charge}) = \frac{\sum_{j=0}^{j=N} C_{PV,charge}}{\sum_{j=0}^{j=N} E_{PV,charge}} \quad , \tag{3.13}$$

$$LCOS = \frac{\sum_{j=0}^{j=N} C_{BESS}}{\sum_{j=0}^{j=N} E_{BESS}} \quad , \tag{3.14}$$

Combining the above Equations (3.11) and (3.12) with the difference between the cost of the energy sold and purchased to/from the grid produces $LCOE_{system}$ for the grid-connected PV-BESS system. The general form of LCOE is represented by Equation (3.15) while Equation (3.16) derives the $LCOE_{system}$ to obtain the optimal PV-BESS size and best combination. According to the latter Equation, the cost of the system is expressed by the cost of the PV system (C_{PV}), the cost of the BESS (C_{BESS}), and the difference between the cost of energy purchased and sold ($C_{E,purchase} - C_{E,sold}$). The C_{PV} is divided into three components: $C_{PV,charge}$, $C_{PV,load}$ and $C_{PV,Esold}$. $C_{PV,charge}$ represents the cost of PV arrays responsible for generating energy to charge the BESS. $C_{PV,load}$ is the cost of PV arrays responsible for generating energy to supply the demand. Whereas, $C_{PV,Esold}$ represents the cost of PV arrays that generate surplus energy sold to the grid. Meanwhile, the total energy in the system represents the summation of energy stored in the BESS, energy supplied to the load, energy sold and energy purchased.

$$LCOE_{system} = \frac{\sum_{j=0}^{j=N} \frac{C_{system_j}}{(1+r)^j}}{\sum_{j=0}^{j=N} \frac{E_{system_j}}{(1+r)^j}} \tag{3.15}$$

$$LCOE_{system} =$$

$$\frac{C_{PV,charge} + C_{BESS} + C_{PV,load} + C_{PV,Esold} + C_{E,purchase} - C_{E,sold}}{E_{BESS,j} + E_{PV,load,j} + E_{sold,j} + E_{purchase,j}}. \tag{3.16}$$

The cost of the energy purchased from the grid $C_{E,purchase}$ is calculated by multiplying the energy purchased from the grid $E_{purchase}$ by its unit price $Pr_{e,purchase}$, as shown in Equation (3.17). On the other hand, the cost of the surplus PV energy sold to the grid $C_{E,sold}$ is computed using Equation (3.18). This is achieved by

multiplying the PV energy sold to the grid E_{sold} by the unit price of energy sold to the grid $Pr_{e,sold}$. $Pr_{e,purchase}$ and $Pr_{e,sold}$ are obtained from ScottishPower Standard Domestic Tariff [149] and given in Table 3.1.

$$C_{E,purchase} = E_{purchase} \cdot Pr_{e,purchase} \quad . \tag{3.17}$$

$$C_{E,sold} = E_{sold} \cdot Pr_{e,sold} \quad . \tag{3.18}$$

Equations (3.19)-(3.22) clarify how to find the first four terms in the numerator of Equation (3.16). The PV-BESS system lifetime N is considered 30 years and the discount rate r equals 5%. Table 3.1 shows all the parameters values and costs of the PV that is used for PV cost and energy calculations. Whereas Table 3.2 presents the parameters used for LAB, LIB and RFB cost and energy calculation. The four terms in the denominator of the $LCOE_{system}$ equation are calculated using the Equations (3.23)-(3.25).

$$C_{BESS} = IC_{BESS} + \sum_{j=0}^{j=N} \frac{C_{BESS,OM}}{(1+r)^j} \quad . \tag{3.19}$$

$$C_{PV,charge} = (IC_{PV} + \sum_{j=0}^{j=n} \frac{C_{PV,OM}}{(1+r)^j}) \cdot N_{PVextra_T} \quad . \tag{3.20}$$

$$C_{PV,load} = (IC_{PV} + \sum_{j=0}^{j=N} \frac{C_{PV,OM}}{(1+r)^j}) \cdot N_{PVload_T} \quad . \tag{3.21}$$

$$C_{PV,Esold} = (IC_{PV} + \sum_{j=0}^{j=N} \frac{C_{PV,OM}}{(1+r)^j}) \cdot N_{PVEsold_T} \quad . \tag{3.22}$$

$$E_{BESS} = \eta_{rt} \sum_{j=0}^{j=N} \frac{E_{PV,Extra} \cdot (1 - DEG_{BESS})^j}{(1+r)^j} \quad . \tag{3.23}$$

$$E_{PV,load,j} = \sum_{j=0}^{j=N} \frac{E_{PV,load} \cdot (1 - DEG_{PV})^j}{(1+r)^j} \quad . \tag{3.24}$$

$$E_{sold,j} = \sum_{j=0}^{j=N} \frac{E_{sold} \cdot (1 - DEG_{PV})^j}{(1+r)^j} \,. \tag{3.25}$$

The terms N_{PVload_T}, $N_{PVEsold_T}$, and $N_{PVextra_T}$ represent the fractions of PV arrays that generate energy to supply demand, sell to the grid and to charge the BESS respectively. These terms are calculated using Equations (3.26)-(3.28).

$$N_{PVcharge_T} = \frac{\sum_{i=0}^{i=Y} P_{PV,charge,i}}{\eta_{PV} \sum_{i=0}^{i=Y} I_{PV,i}} \,. \tag{3.26}$$

$$N_{PVload_T} = \frac{\sum_{i=0}^{i=Y} P_{PV,load}(n)}{\eta_{PV} \sum_{i=0}^{i=Y} I_{PV}(n)} \,. \tag{3.27}$$

$$N_{PVEsold_T} = \frac{\sum_{i=0}^{i=Y} P_{PV,Esold,i}}{\eta_{PV} \sum_{i=0}^{i=Y} I_{PV}(n)} \,, \tag{3.28}$$

where Y is is the total number of hours in a year (Y=8760 hour), η_{PV} is the PV efficiency. Tables 3.1 and 3.2 shows the description and values of all parameters used in the proposed technical and economic models for the grid-connected PV-BESS system.

The optimal sizing of the grid-connected PV-BESS system obtained by the AES is presented in the following section. Moreover, a comparison between the three combinations; PV-LAB, PV-LIB, and PV-RFB is conducted to evaluate the performance of these combinations.

3.5 RESULTS AND DISCUSSION

The aim of the proposed approach is to find the optimal size of the combination PV-BESS for a grid-connected system using AES approach. Three types of batteries are considered in this research, LAB, LIB, and RFB. The solar radiation and temperature profiles used in these simulations are for the Isle of Wight and adopted from National Laboratory of the US Department of Energy (NREL) [2].

Since it was challenging to get the actual demand profiles for the Isle of Wight, the profiles used in these simulations were obtained from OpenEI (US Department of Energy) [3].

In this research, the lifetime of the system is 30 years, where the BESSs, inverter and charge controller are replaced twice during the system lifetime at 10 and 20 years. Using Equation (3.6), the capacities of the BESSs are calculated for 5 HA. As illustrated in Table 3.2, the variations in capacities were around 1 MWh, and so all of the three types of the BESSs are assumed to have the capacity of 1 MWh.

The simulations are performed in MATLAB, and the relationship between various sizes of PV with the three BESS are illustrated in Figure 3.6. Each line represents the LCOE of the three combinations: PV-LAB, PV-LIB, and PV-RFB. To determine the optimal PV-BESS combination in terms of minimum cost, the obtained LCOE values for each combination should be less than the unit price of the energy purchased from the grid (0.13822 £/kWh). Referring to Figure 3.6, the minmum LCOE across the three combinations occurs when $P_{PV,rated} = 710\ kW$ for the combination PV-RFB and $LCOE_{system} = 0.1135$ £/kWh. The minimum LCOE for the combination PV-LAB happening for $P_{PV,rated} = 590\ kW$ and $LCOE_{system} = 0.1167$ £/kWh. Whereas the minimum LCOE for the combination PV-LIB founded at $P_{PV,rated} = 710\ kW$ and $LCOE_{system} = 0.1348$ £/kWh. These results presented in Table 3.3 besides the value LCOE for the three combinations at $P_{PV,rated} = 710\ kW$. As detailed in Table 3.3, it is observable that both combinations PV-LIB and PV-RFB have the same $P_{PV,rated}$, however, the $LCOE_{system}$ for PV-LIB is higher. That results in selecting the combination PV-RFB with $P_{PV,rated} = 710\ kW$ as the optimal size for the grid-connected system. In contrast, the PV rated power for PV-LAB combination is 590 kW but the $LCOE_{system}$ for this combination equals to 0.1167 £/kWh. Since the main objective for this study is to find the optimal combination of PV and BESS based on minimum LCOE, the best selection is PV-RFB system with $P_{PV,rated} = 710\ kW$.

Additionally, Table 3.3 shows the LCOE for the three combinations when PV rated power is 710 kW. The $LCOE_{system}$ is minimum at 710 kW PV rated power

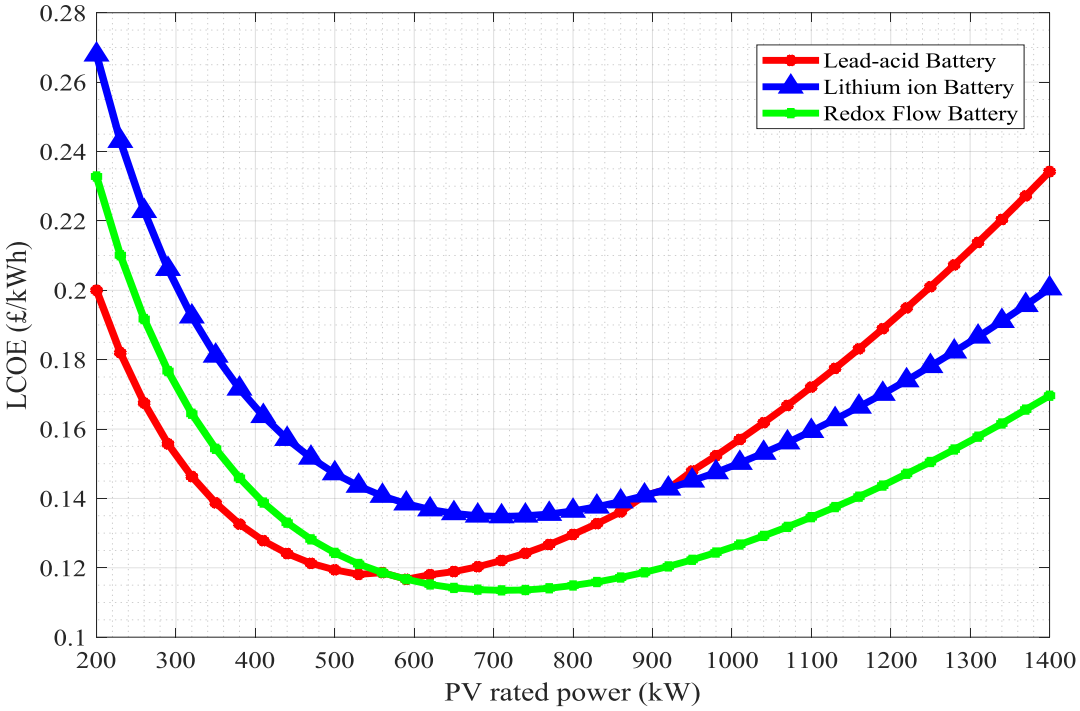

Figure 3.6: The relationship between different values $P_{PV,rated}$ and LCOE for the three combinations; PV-LAB, PV-LIB, and PV-RFB.

Table 3.3: Summary of the results obtained from Figure 3.6 regarding the minimum LCOE at $P_{PV,rated} = 710\ kW$ and the value of PV rated power at minimum $LCOE_{system}$ for the three PV-BESS systems.

PV-BESS	$LCOE_{system}$ at $P_{PV,rated} = 710\ kW$	Min $LCOE_{system}$	$P_{PV,rated}$ at min $LCOE_{system}$
PV-LAB	0.1211 £/kWh	0.1167 £/kWh	590 kW
PV-LIB	0.1348 £/kWh	0.1348 £/kWh	710 kW
PV-RFB	0.1135 £/kWh	0.1135 £/kWh	710 kW

Table 3.4: LCOD for the three BESSs; LAB, LIB and RFB when $P_{PV,rated} = 710\ kW$.

BESS	LCOD (£/KWh)
LAB	0.1670
LIB	0.1711
RFB	0.1394

for the combination PV-RFB. The reason behind having minimum LCOE for the combination PV-RFB can be clarified by referring to Table 3.2 that presents the

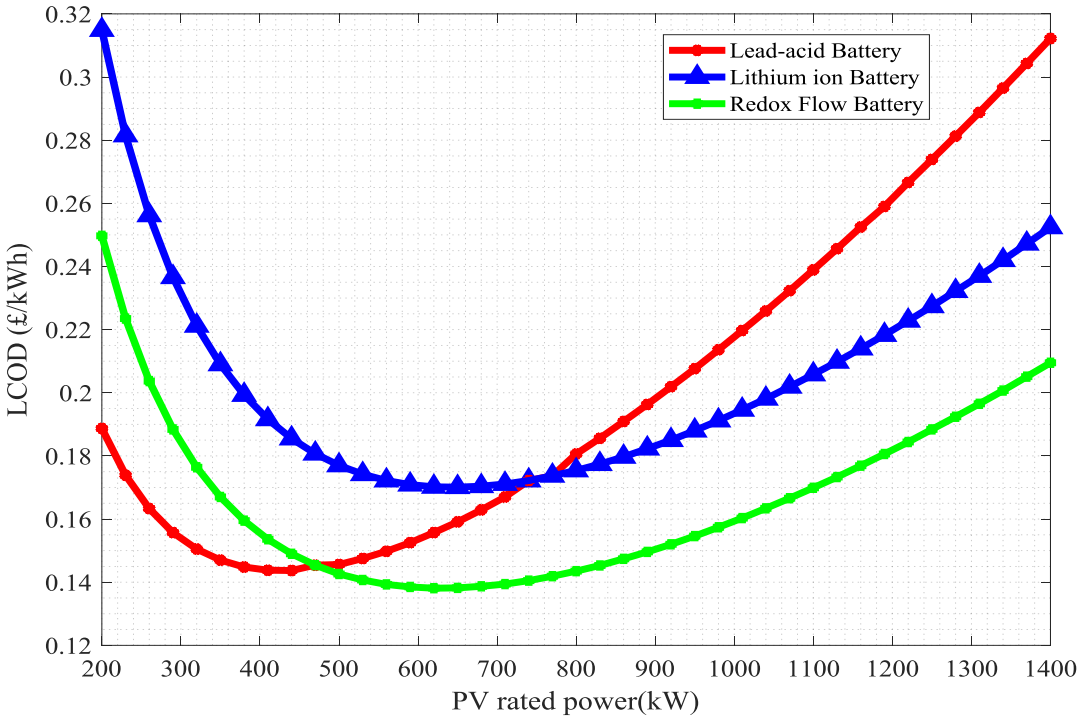

Figure 3.7: The relationship between different values $P_{PV,rated}$ and LCOD for the three BESSs; LAB, LIB, and RFB.

cost data for the three types of the BESSs. The table shows that the lifetime for RFB generally ranges between 10-15 years and is chosen to be 10 years in this study. This implies that the BESS changed twice during the project lifetime at 10 and 20 years. This equally applied to the other two BESSs. Therefore, to compare the three BESSs, their costs and degradation rates are considered. The initial cost IC_{BESS} is less for LAB and higher for LIB, while the operation and maintenance cost $C_{BESS,OM}$ is higher for LAB and less for LIB. Observing these data, it is found that the RFB costs are intermediate between LAB and LIB. Considering that DEG_{BESS} causes a direct effect on finding the energy supplied by the BESS (Equation (3.23)), this value plays a significant role in determining the $LCOE_{system}$. The DEG_{BESS} for RFB is the lowest between the three types of the BESSs which 0.1% compared to 2% and 3.7% for LIB and LAB respectively.

Figure 3.7 shows the LCOD for the three types of the BESSs, LAB, LIB and RFB. As can be seen from this figure, the RFB has the minimum LCOD compared to LAB and LIB. Referring to Table 3.4, the values of LCOD for the three types of the BESSs are presented for $P_{PV,rated} = 710\ kW$. This also confirms why the

RFB is the best option to be combined with the PV for the grid-connected system. Furthermore, the LCOD values are higher than LCOE values for the three PV-BESS combinations. This is due to the high cost of BESS and the energy stored in it is small compared to the energy produced by the whole system. The ratio of the BESS cost to its energy is higher than the ratio of the total system cost to its produced energy. This is the reason why the LCOD values are shown in Figure 3.7 are higher than the system LCOE values.

Three case studies are selected which are the three PV-BESS combinations presented in Table 3.3. Each combination has the value of $P_{PV,rated}$ and $LCOE_{system}$ presented in the table. A comparison is performed between these studies to evaluate which combination has the optimal size and BESS type.

- **Case study 1: PV-LAB system at $\mathbf{P_{PV,rated}}$ = 590 kW and $\mathbf{LCOE_{system}}$ = 0.1167 £/kWh.**

  A comparison between PV-LAB system, the grid-connected PV system alone, and the case where there is no integration of the PV and BESS are presented in Table 3.5. The amount of yearly energy production, yearly energy demand and the energy purchased and sold from/to the grid for the three scenarios are presented in Table 3.5. The total energy demand for one year is 1093.4 MWh. For PV-LAB system the percentage of PV contribution is 83% which is more than the PV contribution for PV alone. Moreover, the energy purchased from the grid is 656.61 MWh, which is obviously less than the energy purchased in the other two scenarios. However, the energy production from the grid-connected PV-LAB system for one year is 437.79 MWh, this energy is used to supply the demand. The surplus PV energy sold to the grid is 88.76 MWh. While in case of PV only system the production is 525.76 MWh, almost half of the generated energy is directed to the demand. The remaining energy is sold to the grid, and an amount of 808.91 MWh is purchased from the grid which is higher than the same value in the PV-LAB scenario.

  Figure 3.8 demonstrates the energy purchased and sold for one year. It is observed that during winter the energy purchased from the grid is

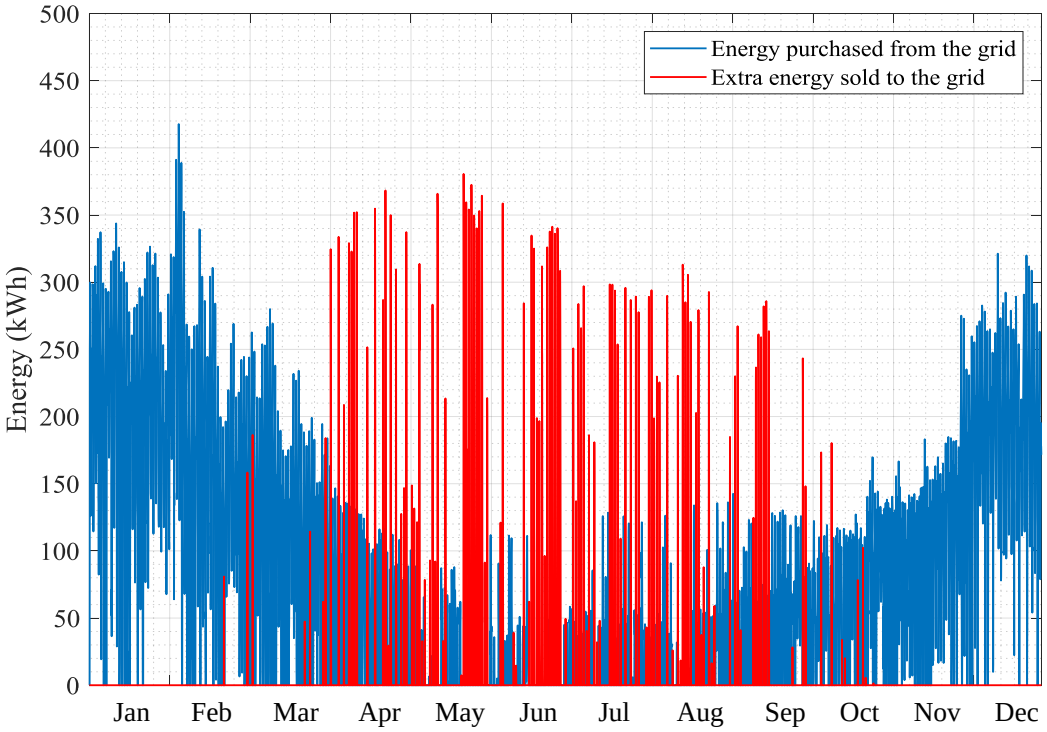

Figure 3.8: Energy purchased and extra PV energy sold to the grid for the combination PV-LAB and $P_{PV,rated} = 590\ kW$ and $Bat_C = 1\ MWh$.

considerably higher than in summer, this is because of the lower generation of PV energy in winter. The surplus PV energy sold to the grid is high in the summer period and is approximately zero during the rest of the year. Figure 3.9 displays the LAB state of charge during the corresponding year, the *soc* during summer days is higher due to the availability of solar radiation.

Table 3.5: PV-LAB system, PV system only and Grid only scenarios, where $P_{PV,rated}$=590 kW and LAB Bat_C=1 MWh

Parameter	PV-LAB	Grid only	PV only
Energy Produced	437.79 MWh	0 MWh	525.76 MWh
Energy Demand	1093.4 MWh	1093.4 MWh	1093.4 MWh
Energy Purchased	655.61 MWh	1093.4 MWh	808.91 MWh
Energy Sold	88.76 MWh	0 MWh	241.22 MWh
PV contribution	83%	0 %	54.1%

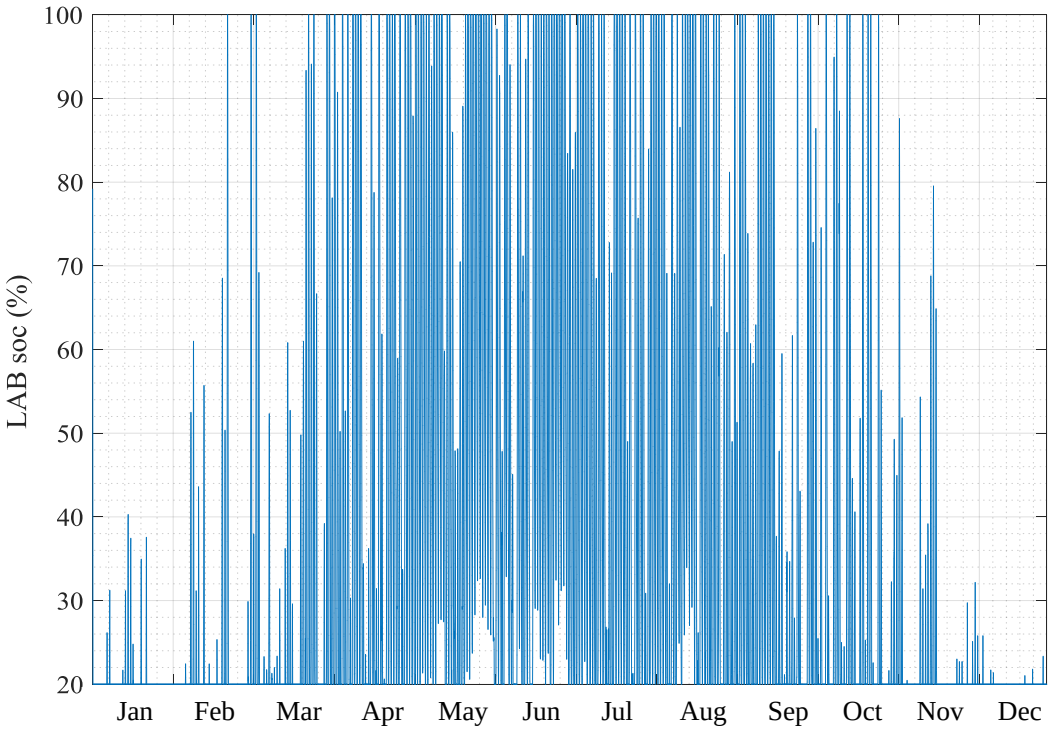

Figure 3.9: State of charge for lead-acid BESS for one calendar year.

- **Case study 2: PV-LIB system at $P_{PV,rated}$ = 710 kW and $LCOE_{system}$ = 0.1348 £/kWh.**

  The amount of yearly energy production, yearly energy demand and the energy purchased and sold from/to the grid are presented in Table 3.6. The table shows these values for the three scenarios same as case study 1. Compared to the previous case study, PV-LIB energy production is higher since the PV rated power is higher. The energy purchased from the grid for the PV-LIB is less than in case study 1, whereas the energy sold to the grid is more. However, the LCOE of this system is higher than the previous case study the highest between all the three case studies as it is seen in the next case study.

  The summary of the comparison between PV-LIB and the other two scenarios in Table 3.6 yields that the integration of LIB is more beneficial than using PV alone or completely depending on the grid. Figure 3.10 provides

Table 3.6: PV-LIB system, PV system only and Grid only scenarios where $P_{PV,rated}$=710 kW and LIB Bat_C=1 MWh

Parameter	PV-LIB	Grid only	PV only
Energy Produced	477.18 MWh	0 MWh	632.69 MWh
Energy Demand	1093.4 MWh	1093.4 MWh	1093.4 MWh
Energy Purchased	616.22 MWh	1093.4 MWh	789.14 MWh
Energy Sold	156.3 MWh	0 MWh	328.38 MWh
PV contribution	75.3%	0 %	48.1%

the distribution of the energy purchased from the grid during winter and surplus energy sold to the grid during summer. While Figure 3.11 shows LIB soc for one year of the study.

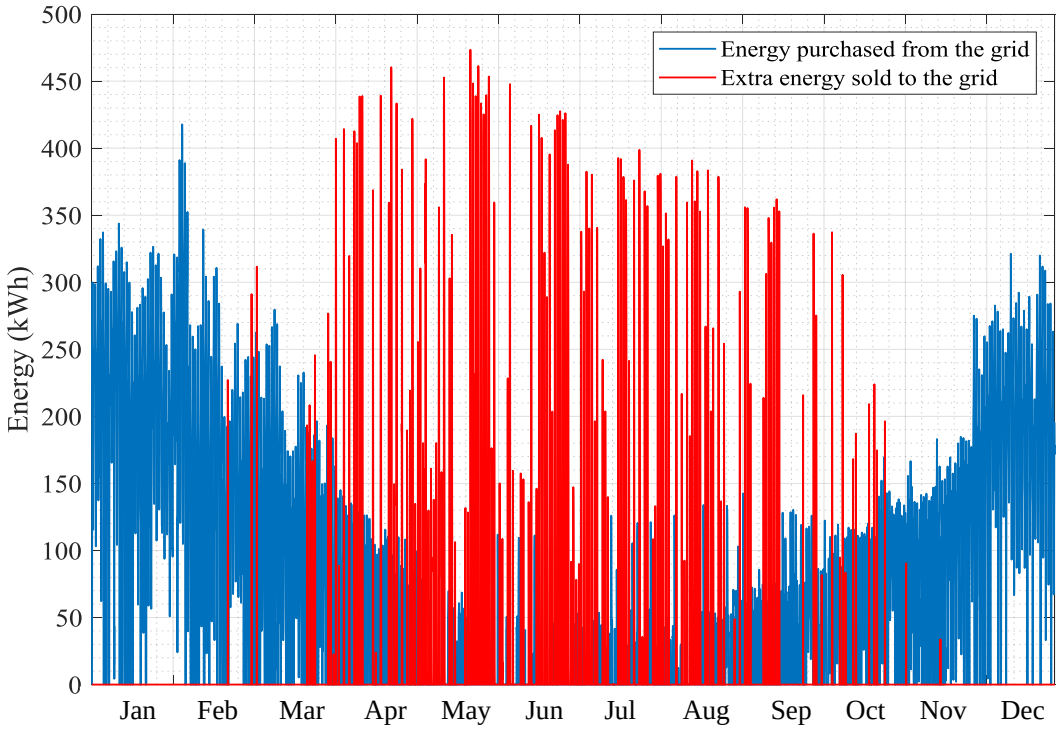

Figure 3.10: Energy purchased and extra PV energy sold to the gridfor the combination PV-LIB and $P_{PV,rated} = 710\ kW$ and $Bat_C = 1\ MWh$.

- **Case study 3: PV-RFB system at $P_{PV,rated} = 710$ kW and $LCOE_{system} = 0.1135$ £/kWh.**

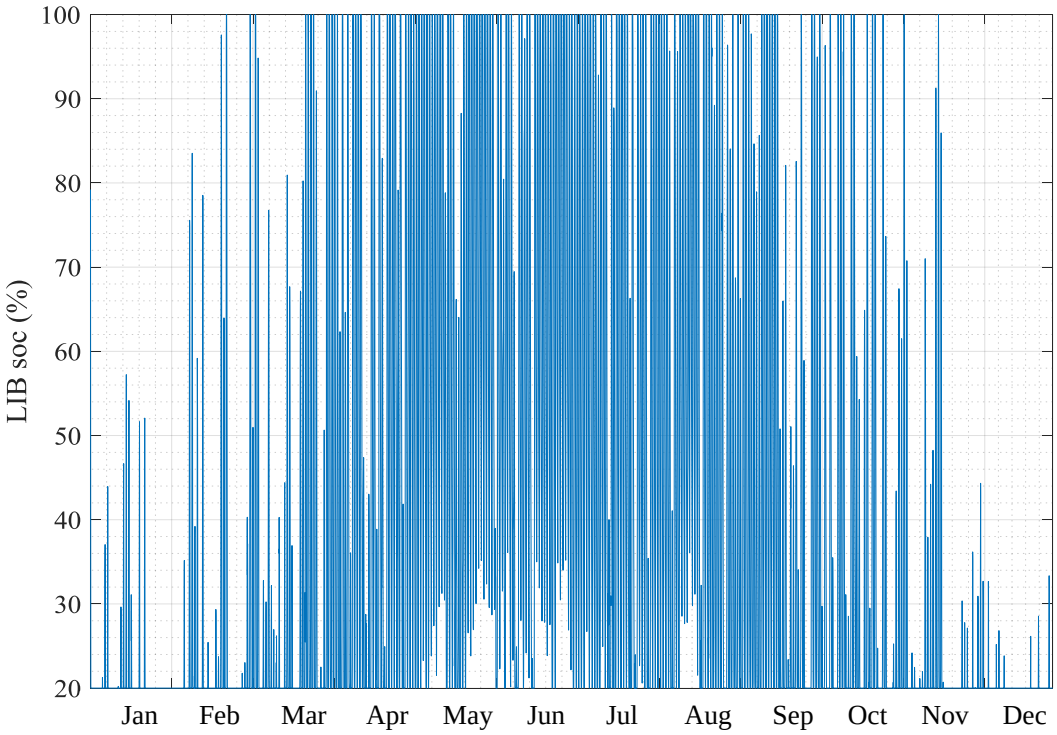

Figure 3.11: State of charge for lithium-ion BESS for one calendar year.

In this case study, the results obtained from the simulations are presented in Table 3.7. Since all the three BESSs in all the case studies have the same capacity, and the $P_{PV,rated} = 710\ kW$ similar to case study 2, the results obtained are the same as the previous case study. The obvious difference between this case study and case study 2 is that the $LCOE_{system} = 0.1135\ £/kWh$, indicating a significant reduction in LCOE compared to the previous study. From the data in Tables 3.5 , 3.6 and 3.7,

Table 3.7: PV-RFB system, PV system only and Grid only scenarios. $P_{PV,rated}$=710 kW and RFB Bat_C=1 MWh

Parameter	PV-RFB	Grid only	PV only
Energy Produced	476.38 MWh	0 MWh	632.69 MWh
Energy Purchased	616.22 MWh	1093.4 MWh	789.14 MWh
Energy Sold	156.3 MWh	0 MWh	328.38 MWh
PV contribution	75.3%	0 %	48.1%

it is obvious that the system PV-RFB has the minimum LCOE across the three case studies and PV-LIB has the maximum LCOE. Regarding to these

findings, the system PV-RFB is considered the best combination for the grid-connected PV-BESS for the Isle of Wight. Although the performance of PV-LIB and PV-RFB are the same, the economic metric plays an important role in deciding the optimal combination for the grid-connected PV-BESS. As previously mentioned the performance of the system in case study 3 is simillar to case study 2, this is indicated in Figures 3.12 and 3.13 that represent the energy exchanged from/to the grid for PV-RFB and state of charge for RFB. These figures are also similar to Figure 3.10 and Figure 3.11, but when refering to Fig 3.6 it is clearly noticed that the PV-RFB is the most economic option compared to the other systems.

According to the above case studies and the results obtained that the combination PV-RFB are the optimal combination, Table 3.8 displayes the sizes of te grid-connected system. The inverter size can be found by $P_{inv} = 1.1 \cdot P_{PV}$.

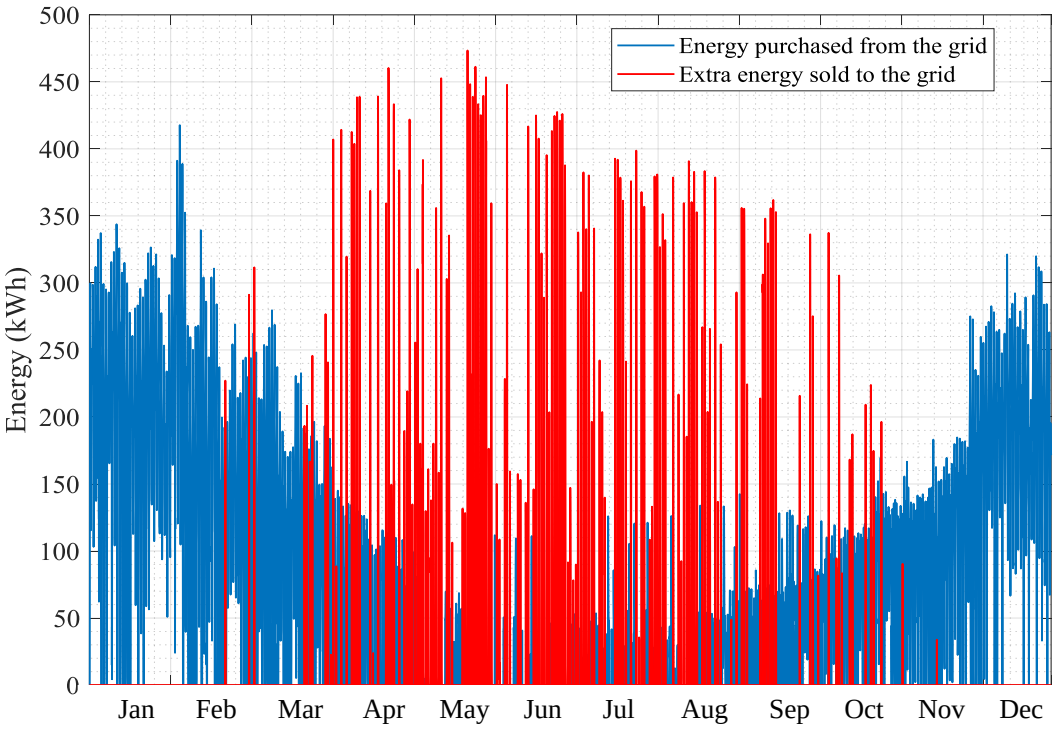

Figure 3.12: Energy purchased and extra PV energy sold to the gridfor the combination PV-LIB and $P_{PV,rated} = 710\ kW$ and $Bat_C = 1\ MWh$.

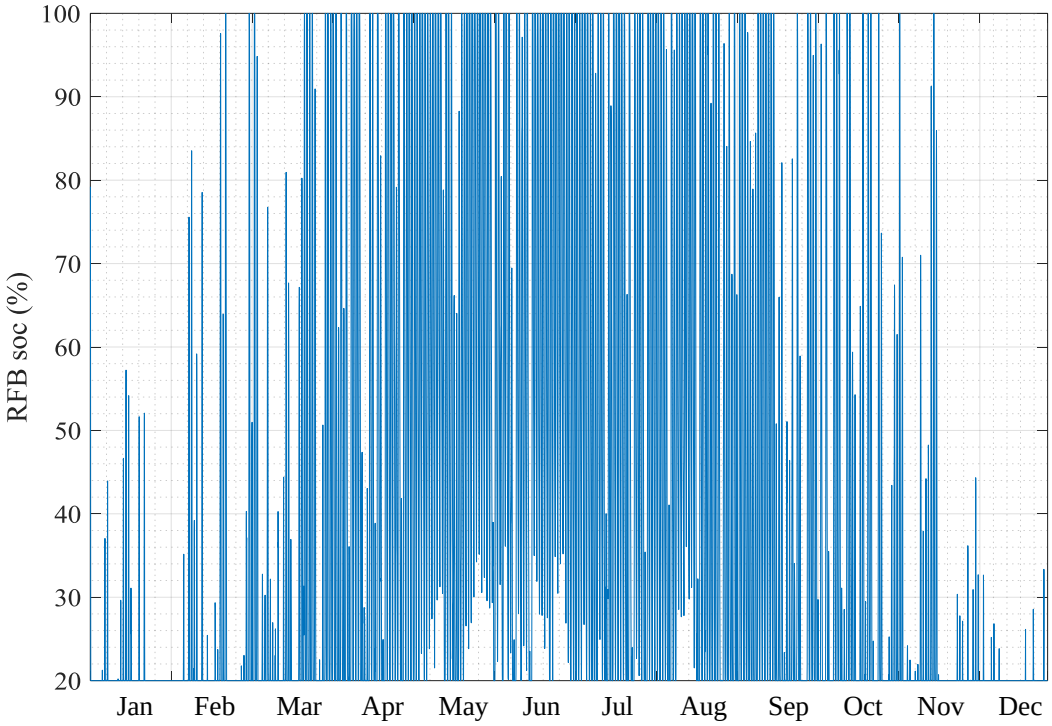

Figure 3.13: State of charge for redox flow BESS for one calendar year.

Table 3.8: PV-RFB components sizes.

Component	Size
PV	710 kW
RFB	1 MWh
Inverter	781 kW

3.6 CONCLUDING REMARKS

In this chapter, a technical and economic model for determining the optimal sizing of a grid-connected PV-BESS system for different battery technologies is proposed. An improved formula for LCOE is utilised to find the best PV-BESS combination at the optimal PV rated power. The LCOE calculation includes new parameters to reflect the impact of surplus PV output and the energy purchased from the grid, as well as looking at the PV system cost in a different way by dividing it into three parts: i) the cost of the part generating energy to supply the load; ii) the cost of the part generating energy to charge the battery; and iii) the

cost of the part generating surplus energy. The obtained results show that the best type of BESS to be integrated with the PV is RFB. After examining three combinations of PV-BESS, it is found the minimum system LCOE (0.1135 £/kW) is for the RFB with a capacity of 1 MWh, and PV size of 710 kW. A reduction of 18% of electricity cost with respect to the grid electricity price is obtained. Moreover, the proposed model allows for 75% of the PV contribution of the PV-RFB system compared to 48% when using the PV alone. After investigating the AES approach for finding the optimal size for a PV-BESS, the following chapter employs this approach in an integrated framework. The key objective of the framework is to find the optimal size-EMS combination for a stand-alone HES.

4

THE INTEGRATED FRAMEWORK

4.1 INTRODUCTION

Chapter 3 showed the AES approach for sizing grid-connected PV-BESS system. The optimal size and PV-BESS combination are obtained based on minimum LCOE. An improved formula of LCOE is introduced to determine the optimal size of the grid-connected microgrid. However, in remote areas, the grid extension is very costly and the expense of fuel increases drastically. As a result, the development of stand-alone HESs becomes necessary as an alternative solution to the grid-connected systems.

In this chapter, the integrated framework for determining the best size-EMS combination for a HES is introduced. Figure 4.1 illustrates the integrated framework presented in this chapter. Fundamental to this framework is utilising FA to implement and instantiate multiple EMSs. The proposed integrated framework consists of three main steps. First, an AES approach is performed to find the initial sizes of the HES assets based on an initial EMS. Second, using FA to implement the initial EMS and instantiate different EMSs. Third, an evaluation model is developed to assess the instantiated EMSs and select the featured conditions to develop an improved EMS. This improved EMS is used to re-exercise the AES approach to obtain the best size-EMS combination. This chapter further explores the significance of maximising the use of PV generated energy to reduce the total LCOE.

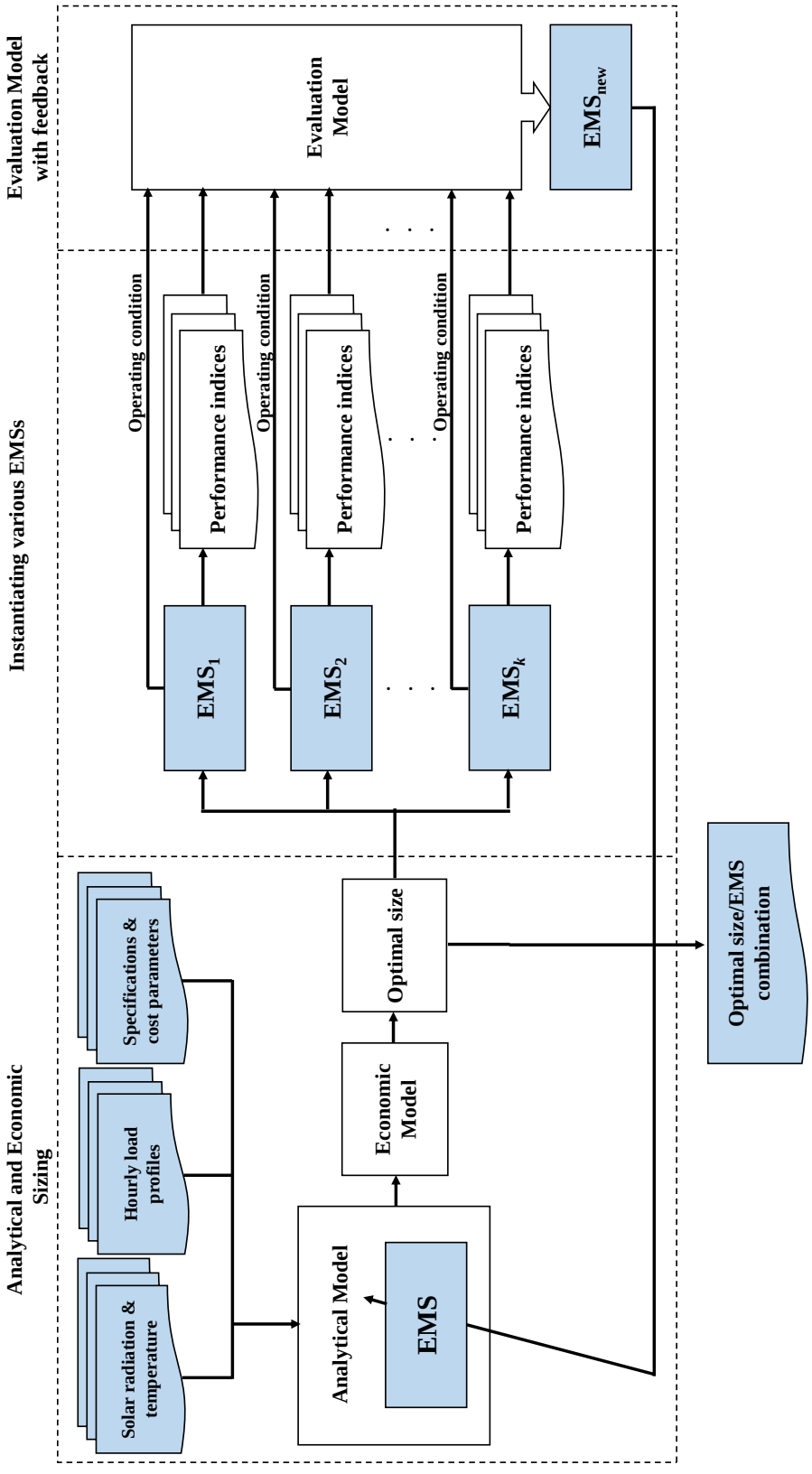

Figure 4.1: Stylized demonstration of three-step proposed framework: (1) analytical and economic sizing; (2) using FA to generate various EMS; and 3) evaluation model and feedback.

4.2 HES STRUCTURE AND MODELLING IN FINITE AUTOMATA

This section introduces the architecture of the HES, a brief background of FA with an illustration example. Then it describes the implementation of the initial EMS in FA in detail.

4.2.1 *HES Architecture*

A simplified scheme of stand-alone HES is reported in Figure 4.2. The HES consists of PV, BESS, EL, FC, HT, and DSL. The energy generated from the PV used to supply the demand and the surplus energy is stored in the BESS. Any further surplus PV energy is directed to the EL to produce hydrogen which is stored in the HT. The *soc* of the BESS is checked continuously, there are two *soc* predefined levels that determine the operating point of the FC and DSL. The first level is soc_{FC} when the BESS *soc* reaches this level, the FC starts operating after checking if there is available H_2 in the HT. The second level is soc_{DSL} when *soc* of the BESS reaches or goes below this level, the DSL starts operating. All the energy sources use DC/AC power inverters for the connection to a common AC bus. Although, in reality, the inverter efficiency is not constant, it is assumed to be constant in this research.

The next section explains what is FA showing an example of how a single asset in the HES can be implemented in the FA. Following that, the implementation of EMS_{initia} in FA is clarified.

4.2.2 *Modelling the BESS in Finite Automata*

Modelling the HES using FA has many advantages: (i) reducing the complexity of the HES by dividing it into smaller subsystems, (ii) making the control of each subsystem simpler, (iii) providing a graphical representation of the system for better understanding of the HES, (iv) reducing the computation time since

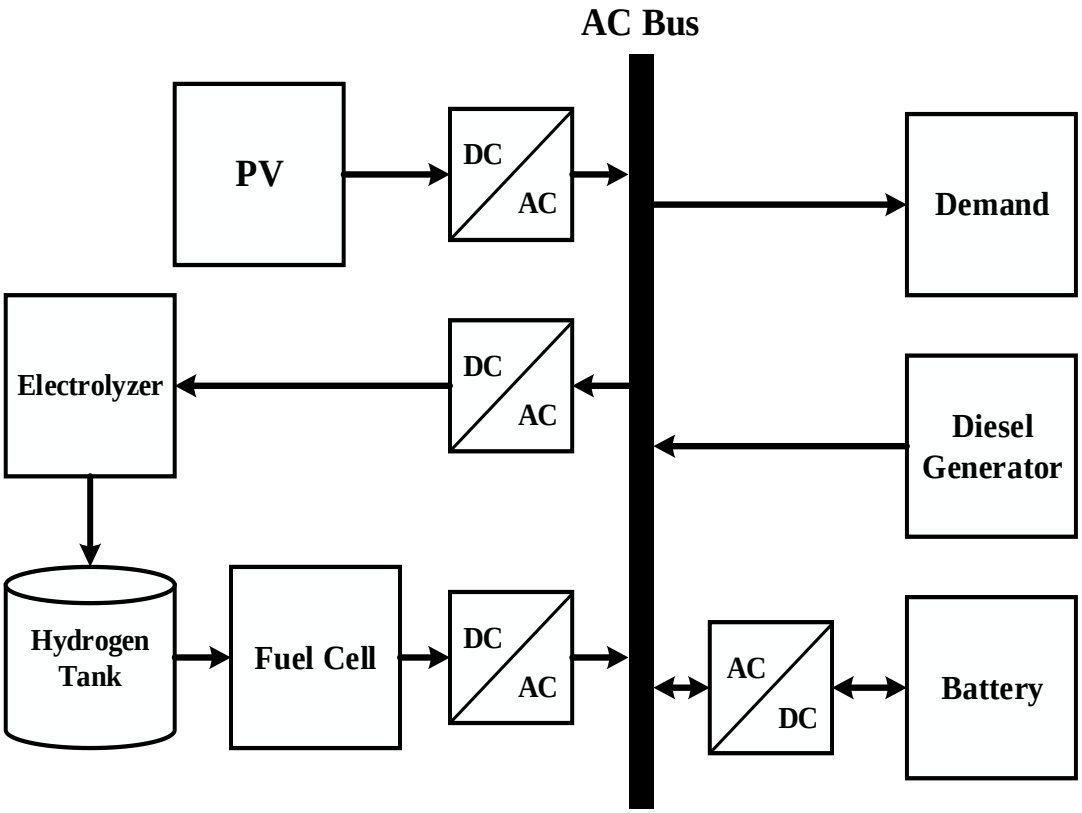

Figure 4.2: The network diagram of a stand-alone HES which consists of PV, BESS, FC, EL, HT, DSL, and multiple inverters.

the state transition for each subsystem is done in parallel, (v) providing more convenient way to modify the predefined conditions or adding new conditions to the HES, and (vi) increasing the ability to accommodate new subsystems.

To illustrate how a subsystem in HES can be treated as a DES and modeled in FA, an example of a BESS is presented in Figure 4.3. The BESS in HES has four states: charging, discharging, idle and OFF. The circles in the figure represent the states, while the transitions are the events or the operating conditions. The state with double circles symbolizes the marked state. This state is the final state that indicates the completion of the operation of any subsystem. In this context, the marked state occurs when the system reaches to the final hour in the year. The states and the events are labelled by numbers; the numbers from 0-9 represent the states and any number from 10 and above are used for events. The description of the conditions is provided in Table 4.1. The states of the BESS can be explained as follows:

- State 0 represent the OFF state which is the initial state, OFF state indicates that BESS is either full (reaches soc_{max}) or empty (reaches soc_{min}). The BESS is OFF because it is fully charged when the condition 11 is satisfied "$soc \geq soc_{max}$". While the BESS is OFF because it is empty when condition 13 is satisfied "$soc \leq soc_{min}$". From state 0, the BESS can move either to state 1 or 2 depending on the occurred condition 10 or 12.

- State 1 denotes that BESS is in charging state which the desired state (the state that the system is preferred to in). The condition related to entering this state is 10, "$P_{input}(n) \geq P_{load}(n)$ & $soc(n) < soc_{max}$". While condition 11 returns the BESS to state 0.

- State 2 is the discharging state, condition 12 "$P_{input}(n) < P_{load}(n)$ & $soc(n) > soc_{DSL}$" is responsible to transfer the BESS from the states 0, 1, and 3 to state 2. Condition 13 "$soc \leq soc_{min}$" changes the state of BESS from state 2 to state 0.

- State 3 represents the idle state, where the $P_{input}(n)$ at that instance equals to the demand, leading to entering the BESS in idle state (no charging or discharging). Conditions 14 or 19, which are responsible to operate the DSL or FC, move the BESS to state 3. There is no condition that transfers BESS from state 3 to 0 directly, since the BESS can not move from the idle state

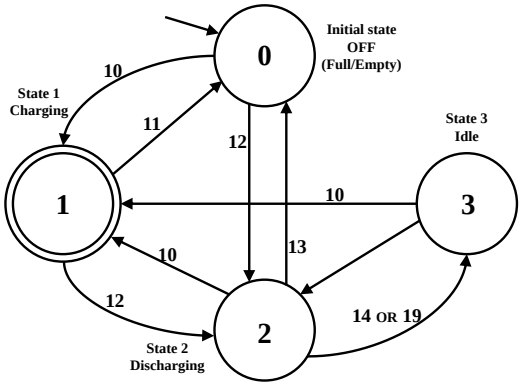

Figure 4.3: Modelling BESS in finite automata.

Table 4.1: Conditions for BESS operation.

Conditions	Subsystem states	Description
10	BESS charging	$P_{input}(n) \geq P_{load}(n)$ & $soc(n) < soc_{max}$
11	BESS OFF	$soc(n) \geq soc_{max}$
12	BESS discharging	$P_{input}(n) < P_{load}(n)$ & $soc(n) > soc_{DSL}$
13	BESS OFF	$soc(n) \leq soc_{min}$
14	DSL ON	$P_{input}(n) < P_{load}(n)$ & $soc(n) \leq soc_{DSL}$ & $B_{FC}(n) = 0$
19	FC ON	$P_{input}(n) < P_{load}(n)$ & $soc(n) \leq soc_{FC}$ & $socHT(n) > socHT_{min}$

to OFF state without passing the charging or discharging state. Condition 12 transfers BESS from state 3 to 2 and condition 10 makes the BESS move from states 3 or 2 to 1.

The behavior of any system modeled using FA is usually described by a regular language and can be found in [153, 154, 155].

4.2.3 *Implementing EMS using Finite Automata*

The EMS is a group of steps the system follows to manage the energy generated by all the assets in the HES. The objective of EMS is to guarantee the energy balance under system constraints and constantly supply the demand. Since the HES consists of multiple subsystems, a number of states can be assigned to each subsystem, combining all these states form the total states of the EMS. Thus, the HES switches between these states according to predefined operating conditions. This section describes how the $EMS_{initial}$ used in the initial sizing of the HES is implemented in FA.

In the previous section, the four states of BESS have been described. In this section, the states of the rest of the assets in the HES are explained. Each of the DSL, FC and EL has two states ON and OFF. The HT has three state: OFF (full or empty), charge and discharge. The state of the PV and the demand are considered always ON even if the solar radiation is zero or there is no demand. Every state of the HES combines the sub-states of subsystems and identifies the status of the HES at each instant in the year. Figure 4.4 shows all the possible states that the HES can endure. The HES has nine states and each state contains the sub-states of all assets in the HES. Additionally, each state of the HES identifies the status of HES at each instant in the year. Meaning which asset is ON/OFF and whether the BESS and HT are charging or discharging.

TTable 4.2 and Figures 4.4 and 4.5 provide a complete description of the $EMS_{initial}$. Table 4.2 introduces the operating condition that determines the following state of the HES. Such that the occurrence of one of the operating conditions in the table decides the state of the HES in the next hour. Figure 4.4

State 0	
PV:	ON
demand:	ON
BESS:	discharge
DSL:	OFF
EL:	OFF
FC:	OFF
HT:	OFF (empty)

State 1	
PV:	ON
demand:	ON
BESS:	idle
DSL:	ON
EL:	OFF
FC:	OFF
HT:	OFF (empty)

State 2	
PV:	ON
demand:	ON
BESS:	charge
DSL:	OFF
EL:	ON
FC:	OFF
HT:	charge

State 3	
PV:	ON
demand:	ON
BESS:	OFF (empty)
DSL:	ON
EL:	OFF
FC:	OFF
HT:	OFF (empty)

State 4	
PV:	ON
demand:	ON
BESS:	idle
DSL:	OFF
EL:	OFF
FC:	ON
HT:	discharge

State 5	
PV:	ON
demand:	ON
BESS:	OFF (full)
DSL:	OFF
EL:	ON
FC:	OFF
HT:	charge

State 6	
PV:	ON
demand:	ON
BESS:	charge
DSL:	OFF
EL:	OFF
FC:	OFF
HT:	OFF (full)

State 7	
PV:	ON
demand:	ON
BESS:	discharge
DSL:	OFF
EL:	OFF
FC:	OFF
HT:	OFF (full)

State 8	
PV:	ON
Load:	ON
BESS:	charge
DSL:	OFF
EL:	OFF
FC:	OFF
HT:	OFF (empty)

Figure 4.4: Nine states describing $EMS_{initial}$ based on finite automata. Each state illustrates which asset is operating and whether the BESS and HT are charging or discharging. The PV and demand are considered always as ON state

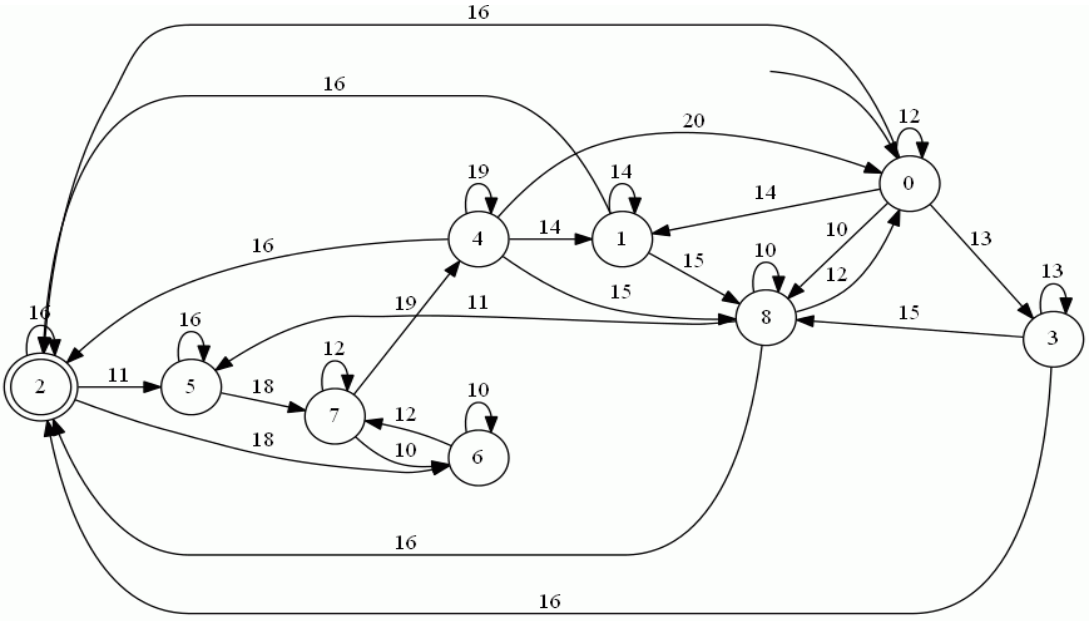

Figure 4.5: Finite automata model for $EMS_{initial}$.

Table 4.2: Conditions for $EMS_{initial}$.

Conditions	Subsystem states	Description
10	BESS charging	$P_{input}(n) \geq P_{load}(n)$ & $soc(n) < soc_{max}$
11	BESS OFF	$soc(n) \geq soc_{max}$
12	BESS discharging	$P_{input}(n) < P_{load}(n)$ & $soc(n) > soc_{DSL}$
13	BESS OFF	$soc(n) \leq soc_{min}$
14	DSL ON	$P_{input}(n) < P_{load}(n)$ & $soc(n) \leq soc_{DSL}$ & $B_{FC} = 0$
15	DSL OFF	$P_{input}(n) > P_{load}(n)$
16	EL ON	$P_{EL,min} \leq P_{PV,surplus}(n) \leq P_{EL,rated}$ & $socHT(n) < socHT_{max}$
17	EL OFF	$P_{PV,surplus}(n) < P_{EL,min}$
18	EL OFF	$socHT(n) \geq socHT_{max}$
19	FC ON	$P_{input}(n) < P_{load}(n)$ & $soc(n) \leq soc_{FC}$ & $socHT(n) > socHT_{min}$
20	FC OFF	$socHT(n) \leq socHT_{min}$

describes the nine states of the HES. While Figure 4.5 presents the graphical representation of $EMS_{initial}$ using FA. $EMS_{initial}$ has nine states which are all the possible states that the HES can experience. State 0 is the initial state and state 2 represent the marked state. The marked state can be defined as the state at which the HES achieves the desired behavior at the end of the year. In the first hour of the year, all the subsystems are OFF (the BESS is assumed to be fully charged at the beginning). During each hour, the power generated from the PV, DSL, and FC is calculated to find the hourly input power to the BESS (P_{input}). The soc of the BESS and $socHT$ of the HT are computed hourly as well. All these values are used to find the binary values of DSL, FC, and EL (described in Section 4.3). These binary values identify the state of each asset in the HES. $EMS_{initial}$ starts with state 0, where all the assets are OFF, the BESS in the

discharging mode, and the PV is ON. The rest of the states and events can be explained as follows:

1. From state 0, the HES can move to one of the following states 1, 2, 3 or 8 through the following conditions:
    a) Condition 14 leads a movement to state 1, where the DSL is ON, the BESS is idle and the assets EL, FC, and HT are OFF.
    b) Condition 16 moves the HES from state 0 to state 2. This condition relates to EL operation to generate H_2 and consequently the HT is in charging state. While the BESS is fully charged (*i.e.* OFF), the FC and DSL are OFF.
    c) Condition 13 moves the HES from state 0 to state 3, in state 3 the DSL is ON, the BESS is empty (*i.e.* OFF). The EL, FC, and HT are OFF.
    d) Condition 10 transfers the HES from state 0 to state 8, where there are surplus power from the PV to charge the BESS. The EL, FC, and HT are OFF.
    e) Condition 12 keeps the HES in state 0.
2. In state 1, the BESS is idle since the DSL is ON. The EL, FC, and HT are OFF. From state 1, there aretwo destinations the HES can move to, either state 2 or state 8 and the conditions responsible fo the movemonet are:
    a) Condition 16 moves the HES from state 1 to state 2, that relates to EL operation (see point 1.b).
    b) Condition 15 moves the HES from state 1 to state 8. In state 8, the DSL becomes OFF, since there is surplus power to charge the BESS. The EL, FC, and HT are OFF.
    c) Condition 10 keeps the HES in state 1.
3. In state 2, the BESS is charging and the surplus power is used to operate the EL. The HT is charging to store H_2. The DSL and FC are OFF. From

state 2, the HES can move to state 5 or 6 depending on the operating conditions:

a) Condition 11 moves the HES from state 2 to state 5, the BESS is fully charged, the EL is still ON and the HT is charging. The DSL and FC are OFF.

b) Condition 18 transfers the HES from state 2 to state 6, where in this state the HT is fully charged (*i.e.* OFF) and the EL is OFF. The DSL and FC are OFF, while the BESS is charging.

c) The occurrence of condition 16 causes the HES to stay in state 2.

4. In state 3, the BESS is empty and therefore, the DSL is ON. The EL, FC and HT are OFF. After state 3, the state of HES can be either 2 or 8. The following conditions can determine the HES destination:

   a) Condition 16 moves the HES to state 2 (see point 1.b).

   b) Condition 15 transfers the HES to state 8 (see point 2.b).

   c) The occurrence of condition 13 causes the HES to stay in state 3.

5. In state 4, the FC is ON and the HT is discharging. When FC is ON this means the BESS is idle, while the DSL and EL are OFF. From state 4. the HES has four choices for states 0, 1, 2 or 8 depending on the following conditions:

   a) Condition 20 causes the HES to move to state 0. The FC, HT, and DSL are OFF. The *soc* of the BESS is enough to supply the demand so the BESS is discharging.

   b) Condition 14 moves the HES to state 1 (see point 1.a).

   c) Condition 16 leads the HES to move to state 2 (see point 1.b).

   d) Condition 15 causes the HES to move to state 8 (see point 2.b).

   e) Condition 19 Keeps the HES in state 4.

6. In state 5, the BESS is fully charged, the surplus power directed to the EL and the HT is charging. The DSL and EL are OFF. The only option for the next state is state 7 and happens when condition 18 is satisfied:
   a) Condition 18 moves the HES to state 7 (see point 3.b).
   b) Condition 16 Keeps the HES in state 5.
7. In state 6, there is surplus power generated by the PV to charge the BESS, the HT is fully charged. The EL, FC, and the DSL are OFF. From state 6, the HES can move to state 7 through the following condition:
   a) Condition 12 causes the HES to move to state 7, there is no surplus PV power so the BESS discharges to supply the demand. The DSL, FC, EL, and HT are OFF.
   b) Condition 10 keeps the HES in state 6.
8. In state 7, there is no surplus PV power to supply the demand or charge the BESS, so the demand is supplied by the BESS. The DSL, FC, and EL are OFF and HT are fully charged. The next state of the HES is state 4 and can be achieved through the following condition:
   a) Condition 19 moves the HES to state 4, the *soc* of the BESS reaches to a level where it is required to operate the FC. The HT discharges to supply the FC with H_2, whereas the EL and DSL are OFF. The BESS is in idle mode.
   b) Condition 12 Keeps the HES in state 7.
9. In state 8, the BESS is charging, while the HT is empty. The EL, FC, and the DSL are OFF. The next state of the HES is state 2 and can be achieved through condition 16:
   a) Condition 16 leads the HES to move to state 0 (see point 1.b).
   b) Condition 10 keeps the HES in state 8.

To this end, all the states and conditions of $EMS_{initial}$ are explained and the relationship between conditions and states are clarified. Depending on this FA model

of $EMS_{initial}$, three different EMSs are instantiated. The process is explained in Section 4.6.1.

The following section demonstrates the analytical and economic approach AES. The AES is the initial step in the integrated framework that utilises $EMS_{initial}$ to find the initial size of the HES assets.

4.3 ANALYTICAL MODELLING OF HES

The AES performed in this chapter follows the same calculation steps as in Chapter 3. The AES in Chapter 3 is developed for a grid-connected PV-BESS microgrid. Whereas the AES utilised in this chapter is for stand-alone HES composing of multiple assets. Accordingly, the AES approach presented in the previous chapter needs to be modified.

The AES approach is used to determine the size of the PV and BESS by iteratively changing the PV rated power from (0 - $\alpha \cdot P_{load,max}$) kW with a step of 10 kW each time. α is a constant equal to 10 and chosen to ensure the selected range covers all possible PV sizes. $P_{load,max}$ in this chapter is 26.7 kW [5] see Figure 4.9), and therefore, the range of PV rated power is selected (0 - 267) kW. A factor that determines the BESS size is the Hours of Autonomy (HA), which means for how many hours a completely charged BESS is able to supply the demand continuously. Since the HES in this study is stand-alone, it is essential to select a high value for HA to ensure demand satisfaction. Thereby, HA is iteratively considered as 12, 24, 36, 48, and 60 hours. The size of the FC and DSL depend mainly on $P_{load,max}$ with some factor and this explained in the following sections. The size of the EL and HT are considered constant.

The EMS utilised by AES approach is the $EMS_{initial}$ explained in Section 4.2.3. This EMS guarantees the demand is continuously supplied with energy and at the same time ensures the other assets of the HES operate efficiently. The main idea is to generate multiple scenarios with different PV sizes and BESS capacities. Following that, the LCOE is calculated for each scenario. The combination that provides the lowest LCOE while covering the demand is selected as the optimal

solution. To ensure demand satisfaction, a power balance is conducted every time interval. As such, the total power generated by the PV, DSL, FC, BESS are equal to the demand and EL. This is represented by Equation (4.1).

$$P_{load}(n) + P_{EL}(n) = P_{PV}(n) + P_{FC}(n) + P_{DSL}(n) + P_{BESS}(n) \quad , \tag{4.1}$$

where $P_{load}(n)$ and P_{EL} the power needed by the demand and the power consumed by the EL. $P_{PV}(n)$, $P_{FC}(n)$, $P_{DSL}(n)$ are the hourly power generated by PV, FC and DSL, respectively. P_{BESS} is the power supplied by the BESS.

The flowchart in Figure 4.6 summarizes the management rules for the AES. P_{PV-min} and P_{PV-max} are the minimum and maximum values in PV rated power range. soc is the state of charge of the BESS, and k indicates the number of HA involved. B_{FC}, B_{DSL}, B_{EL} are binary logic values for the FC, DSL and EL. These binary values are computed hourly to identify which device is operating at that time.

The analytical model used for PV in this chapter is the same as the model explained in details in Chapter 3 (see Section 3.4.1). Newcastle upon Tyne is considered as a case study to validate this approach. The solar radiation and temperature data for the city of Newcastle upon Tyne [4] are used to find the optimal size-EMS of the HES. The demand profile are for 40 houses of the Customer-Led Network Revolution project [5]. Figures 4.7 and 4.8 illustrate the profiles of the solar radiation and temperature. Whereas, the data used for PV analytical model is presented in Table 4.3. The demand profile considered in this chapter is presented in Figure 4.9. The analytical model for BESS is the same concept as in Section 3.4.2 with a difference in the input and output power to the BESS, so it is explained in the next section. Furthermore, the analytical models for DSL, FC, EL, and HT are demonstrated in Sections 4.3.2 to 4.3.5.

4.3.1 *Battery Energy Storage System*

The values of the power generated from the PV and the demand power at each time step, determine whether to charge or discharge the BESS. In the case that

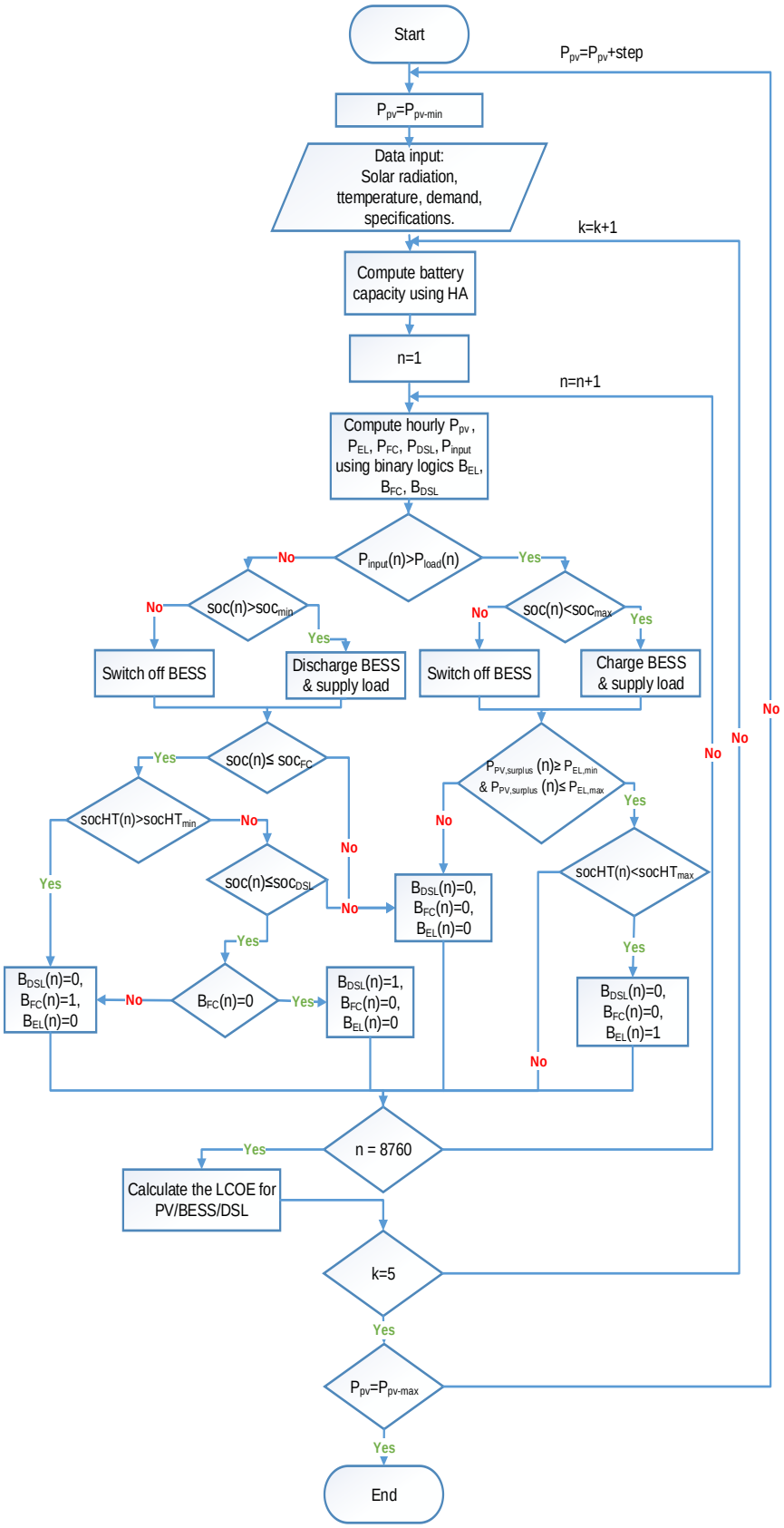

Figure 4.6: The flowchart of AES approach showing the steps of the EMS to find the initial size of the HES.

Table 4.3: Data used for PV analytical modele [10, 11].

Parameter	Value
PV module efficiency, η_{module}	14%
PV degradation, DEG_{PV}	0.5%
PV cell reference temperature, T_{ref}	20 °C
Normal operating cell temperature, NOCT	45°C
Ambient temperature of NOCT, $T_{amb,NOCT}$	20°C
Solar radiation at NOCT, I_{NOCT}	800 W/m^2
Temperature coefficient of solar cell efficiency, β	0.005 1/°C
Yearly module reference in-plane radiation, H	1000W/m^2
PV lifetime, N	20 years

the soc reaches the predefined level, then the decision to operate the FC or the DSL takes place. The BESS capacity Bat_C is calculated using Equation (4.2) [10]. The capacity of the BESS is expressed in terms of HA and the average hourly

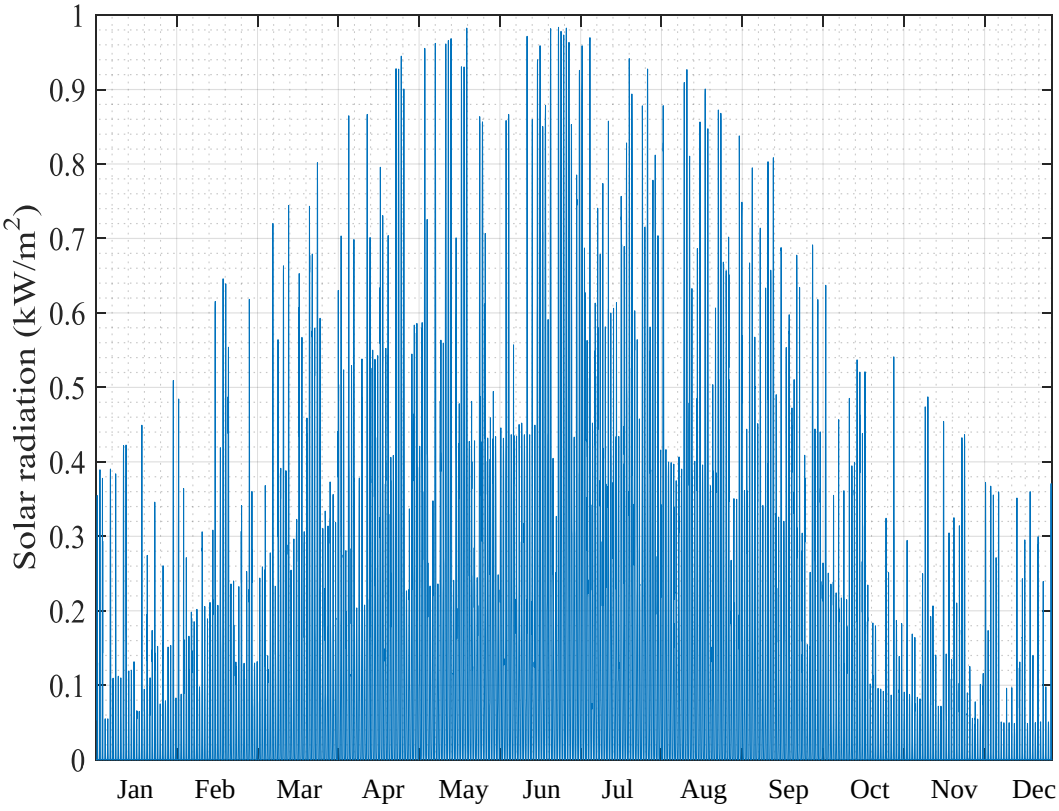

Figure 4.7: Hourly solar radiation profile for Newcastle upon Tyne city for one calendar year [4].

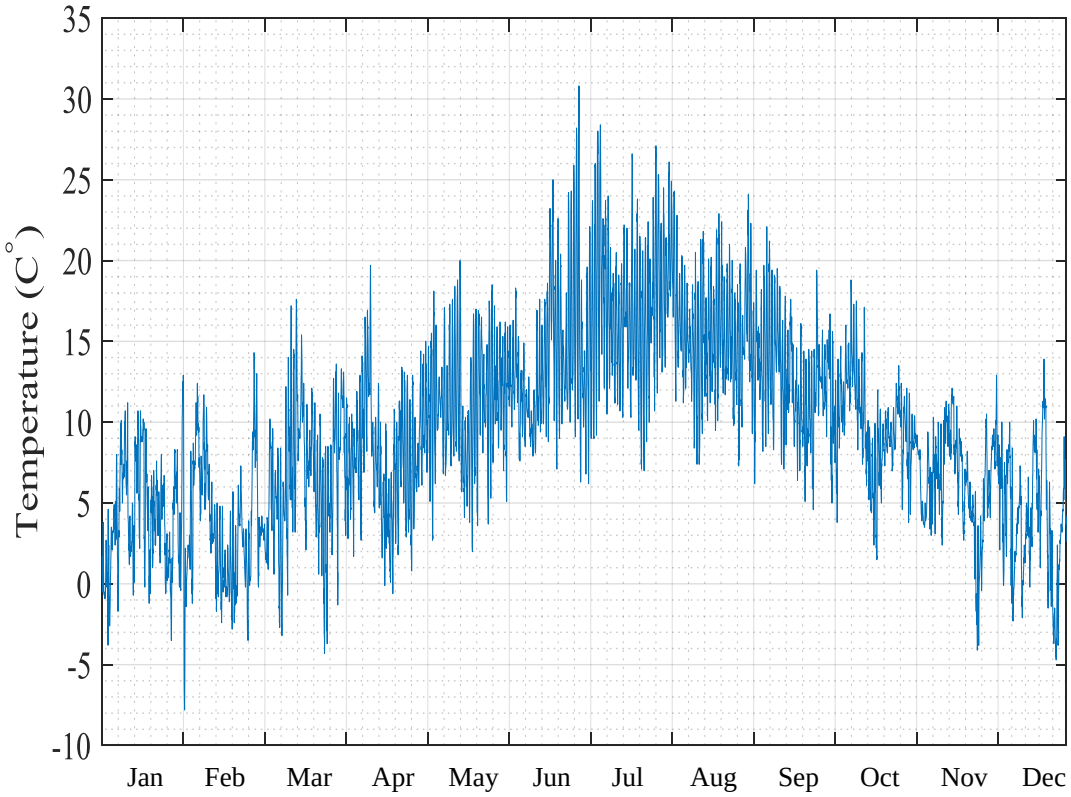

Figure 4.8: Hourly ambient temperature profile for Newcastle upon Tyne city for one calendar year [4].

demand $P_{load,avg}$. $P_{load,avg}$ is equal to 10.7 kW, whereas HA ranges between five values, 12, 24, 36, 48, 60 hours.

$$Bat_C = \frac{HA \cdot P_{load,avg}}{\eta_{inv} \cdot \eta_{ch} \cdot DOD} \quad , \tag{4.2}$$

where η_{inv} and η_{ch} are the inverter and BESS charge efficiencies, and DOD represent the depth of discharge. A fundamental parameter to represent the available capacity in the BESS is the state of charge (soc), which is used to decide whether to charge or discharge the BESS. Depending on the power generated by the HES assets and the demand requirements, the hourly BESS soc for charging

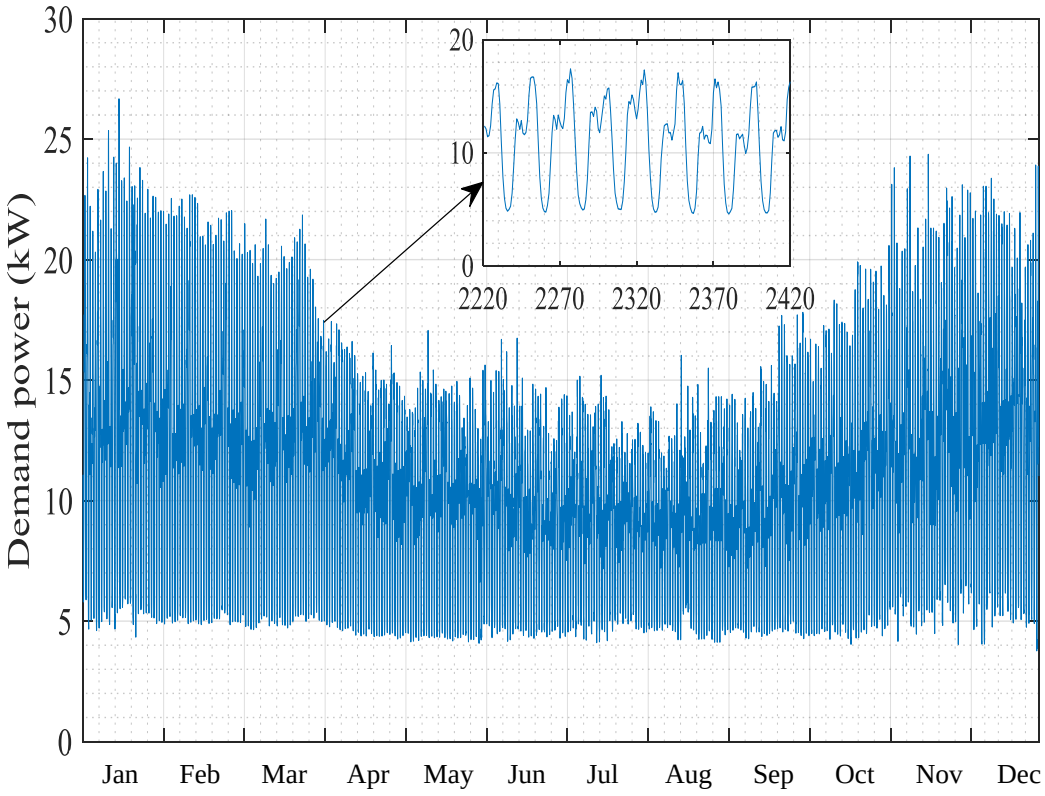

Figure 4.9: Hourly demand profile for Newcastle upon Tyne citry for one calendar year [5].

and discharging states can be calculated using Equation (4.3).

$soc(n)$=

$$\begin{cases} soc(n-1)+\dfrac{[P_{input}(n)-P_{load}(n)]\cdot\eta_{ch}\cdot\Delta t}{\eta_{inv}\cdot Bat_C}, & P_{input}(n)>P_{load}(n)\,, \\ \\ soc(n-1)-\dfrac{[P_{load}(n)-P_{input}(n)]\cdot\Delta t}{\eta_{inv}\cdot\eta_{dch}\cdot Bat_C}, & P_{input}(n)\leq P_{load}(n), \end{cases} \tag{4.3}$$

where $soc(n)$ and $soc(n-1)$ represent the states of charge of the BESS at n and $n-1$, respectively. η_{dch} is the discharging efficiency and Δt is the time step. In this thesis, the value of Δt is considered to be equal one hour. $P_{input}(n)$ is the sum of input power to the BESS at a specific hour and found using Equation (4.4). If BESS input power is greater than demand, $P_{input}(n) > P_{load}(n)$, then the demand is supplied firstly and the surplus poweris used to charge the BESS. On

the other hand, if $P_{input}(n) \leq P_{load}(n)$, the power generated is used to supply the demand and any deficiency is covered by the BESS.

$$P_{input}(n) = P_{PV}(n) + P_{DSL}(n) + P_{FC}(n) \quad . \tag{4.4}$$

To protect the BESS from overcharging or under-discharging, the BESS *soc* should be maintained at a reasonable level. The *soc* should be maintained between two limit levels, soc_{max} and soc_{min} subject to the following constraint:

$$soc_{min} \leq soc(n) \leq soc_{max} \tag{4.5}$$

The parameters used in the BESS analytical model are presented in Table. 4.4.

Table 4.4: Data used for battery energy system modelling [10].

Parameter	Value
Depth of discharge, DOD	80%
Charge efficiency, η_{ch}	80%
Discharge efficiency, η_{dch}	80%
Minimum state of charge, soc_{min}	20%
Maximum state of charge, soc_{max}	90%
Round trip efficiency, RT_{eff}	90%
Degradation rate of battery, DEG_{BESS}	0.1%
Hours of autonomy, HA	12, 24, 36, 48, 60 hrs

4.3.2 *Diesel Generator*

The power generated from RER is variable and therefore, to ensure the demand is constantly supplied, the existence of the DSL is necessary. When the integrated RERs/AER and BESS are unable to supply the demand, the DSL operated to supply the demand. Any surplus power generated by the DSL is used to charge the BESS. Since the first priority is to ensure the satisfaction of demand, the

rated power of the DSL depends on $P_{load,max}$ (see Figure 4.9) and expressed by the following equation:

$$P_{DSL,rated} = M_{DSL} \cdot P_{load,max} \quad , \tag{4.6}$$

where M_{DSL} is the DSL margin coefficient. In this thesis, M_{DSL} is considered to be 1.2 for safety purposes. According to this equation, $P_{DSL,rated}$=32 kW. The hourly output of DSL is found using Equation (4.7), and subjected to the constraint in Equation (4.8):

$$P_{DSL}(n) = \begin{cases} B_{DSL}(n) \cdot P_{load}(n), & B_{DSL}(n) = 1 \ , \\ 0, & B_{DSL}(n) = 0 \ , \end{cases} \tag{4.7}$$

$$0 \leq P_{DSL}(n) \leq P_{DSL,rated} \ , \tag{4.8}$$

where $B_{DSL}(n)$ represents a binary variable that describes the state of the DSL at a specific hour in the year [156, 157]. The key objective for using B_{DSL} is to decide whether to activate the DSL or not based on the soc level. Condition 14 in Table 4.2 describes the operating condition for DSL operation.

4.3.3 *Fuel Cell*

The FC is used as a backup power generator. The FC is activated when the solar power is insufficient to supply the demand and soc reaches soc_{FC}. Any surplus in the power generated by the FC is used to charge the BESS. The size of the FC is determined using the following equation:

$$P_{FC,rated} = M_{FC} \cdot P_{load,max} \quad , \tag{4.9}$$

where the FC margin coefficient M_{FC} and equals to 1.2 to leave some safe margin [158]. According to this equation, $P_{FC,rated}$= 32 kW. The hourly output power

generated from the FC can be identified by Equation (4.10) and its constraint in Equation (4.11):

$$P_{FC}(n) = \begin{cases} B_{FC}(n) \cdot P_{load}(n), & B_{FC}(n) = 1 \ , \\ 0, & B_{FC}(n) = 0 \ , \end{cases} \tag{4.10}$$

$$0 \leq P_{FC}(n) \leq P_{FC,rated} \quad , \tag{4.11}$$

where $B_{FC}(n)$ is a binary variable that describes the state of the FC at any hour in the year [156, 157]. Condition 19 in Table 4.2 shows the operationg condition for FC operation. The input hydrogen to the FC is consumed from the hydrogen tank. The FC consumption of hydrogen for 1 kW rated power in one hour can be calculated by [29]:

$$\begin{aligned} H_{2,cons,1kW} &= \frac{1kW}{2 \cdot V_{FC} \cdot F} \cdot 3600 \\ &= \frac{1000}{2 \cdot 0.7 \cdot 96487} \cdot 3600 = 26.8 \ mol/h \quad , \end{aligned} \tag{4.12}$$

where $H_{2,cons,1kW}$ represent the amount of hydrogen consumed by the FC at 1 kW which depends on the FC voltage V_{FC}, and Faraday constant F (see Table 4.5). The hourly amount of hydrogen consumed by the FC $H_{2,cons}(n)$ can be determined by multiplying the value of $H_{2,cons,1kW}$ by $P_{FC}(n)$. Equation (4.13) illustrates the hourly H_2 consumed by the FC.

$$H_{2,cons}(n) = \begin{cases} P_{FC}(n) \cdot H_{2,cons,1kW}, & P_{FC}(n) > 0 \ . \\ 0, & P_{FC}(n) \leq 0 \ . \end{cases} \tag{4.13}$$

4.3.4 *Electrolyser*

The purpose of using the EL is to produce hydrogen through the electrolysis of water. The produced hydrogen is stored in the HT and used as needed to operate the FC. The output pressure of hydrogen is considered 20 bar [159] in

this thesis. The hourly input power to the EL and its constraints can be identified by Equations (4.14) and (4.15):

$$P_{EL}(n) = \begin{cases} B_{EL}(n) \cdot P_{PV,surplus}(n), & B_{EL}(n) = 1 \ , \\ 0, & B_{EL}(n) = 0 \ , \end{cases} \tag{4.14}$$

$$P_{EL,min} \leq P_{EL}(n) \leq P_{EL,rated} \ , \tag{4.15}$$

where $P_{EL,min} = 20\% \cdot P_{EL,rated}$. While $B_{EL}(n)$ represents a binary variable that describes the state of the EL at any hour in the year [156, 157]. The value of $B_{EL}(n)$ decides whether to operate the EL or not. Condition 16 in Table 4.2 defines the EL operation. If the value of $P_{PV,surplus}(n)$ is sufficient to operate the EL and the state of charge of HT is less than the maximum, $B_{EL}(n)$ is set to one and the EL generates hydrogen. To operate the EL, the value of the working voltage between its electrodes V_{el} needs to be 2 $volts$ [29]. According to Faraday's law, the amount of hydrogen produced by the EL for 1 kW rated power in one hour, $H_{2,prod,1kW}$, can be calculated by [29]:

$$\begin{aligned} H_{2,prod,1kW} &= \frac{1kW}{2 \cdot V_{el} \cdot F} \cdot 3600 \\ &= \frac{1000}{2 \cdot 2 \cdot 96487} \cdot 3600 = 9.33 \ mol/h \quad . \end{aligned} \tag{4.16}$$

All the values used in calculations can be found in Table 4.5. The hourly amount of hydrogen produced by the EL, $H_{2,prod}(n)$ is determined by multiplying the value of $H_{2,prod,1kW}$ by $P_{EL}(n)$. This is illustrated in following equation:

$$H_{2,prod}(n) = \begin{cases} P_{EL}(n) \cdot H_{2,prod,1KW}, & P_{EL}(n) > 0 \ . \\ 0, & P_{EL}(n) \leq 0 \ . \end{cases} \tag{4.17}$$

$P_{EL,rated}$ is chosen to be 100 kW in this study. The reason for this is to guarantee that all the surplus power generated by the PV is utilised by the EL to generate hydrogen. Any surplus PV power between 20% and 100% of the $P_{EL,rated}$ is used to generate H_2.

4.3.5 *Hydrogen Tank*

The HT is required to store the hydrogen produced from the EL for later use by the FC. The HT analytical model assumes during the process of adding hydrogen to the tank, no energy is used and the tank experiences no leakage. The hydrogen produced by the EL provides another option for storing the surplus PV power. The size of the HT S_{HT} in kgs is determined by Equation (4.18), where the HT capacity depends strongly on the H_2 produced by the EL. E_{HT} is the tank size in kWh and given by Equation (4.19) [160]:

$$S_{HT} = HA_{HT_2} \cdot H_{2,prod,1kW} \cdot P_{rated,EL} \cdot H_2mass \ , \tag{4.18}$$

$$E_{HT} = HA_{HT_2} \cdot H_{2,prod,1kW} \cdot P_{EL,rated} \cdot H_2mass \cdot LHV \ , \tag{4.19}$$

HA_{HT_2} represents the hours of autonomy for the HT and considered 48 hours in this thesis. H_2mass is the molar mass of hydrogen gas, and LHV is hydrogen low heating value and presented in Table 4.5. According to Equations (4.18) and (4.19), the size of HT is 89.5 kg and 2955 kWh.

The level of hydrogen in the tank increases if the EL is operating, however, it decreases when the FC is generating power. Equation (4.20) determines the hourly state of charge of the HT $socHT(n)$ in both cases.

$socHT(n) =$

$$\begin{cases} socHT(n-1) + \dfrac{H_{2,prod}(n) \cdot H_2mass \cdot LHV \cdot \Delta t}{E_{HT}}, & P_{EL}(n) > 0, \\ \\ socHT(n-1) - \dfrac{H_{2,cons}(n) \cdot H_2mass \cdot LHV \cdot \Delta t}{E_{HT}}, & P_{FC}(n) > 0, \end{cases} \tag{4.20}$$

where $socHT(n-1)$ is the hydrogen level in the tank at time $n-1$. At any time the $socHT(n)$ is subjected to the following constraint:

$$socHT_{min} \leq socHT(n) \leq socHT_{max} \tag{4.21}$$

Table 4.5 presents all the values that is needed by the analytical models of the FC, EL, and HT.

Table 4.5: Data used for hydrogen system modelling (FC, EL, and HT).

Parameter	Value	Ref.
$socHT_{min}$	10%	-
$socHT_{max}$	90%	-
Pressure, P_{FC}	20 bar	[159]
Faraday constant, F	96487 C/mol	[29]
FC voltage, V_{FC}	0.7 volts	[29]
EL voltage, V_{el}	2 volts	[29]
H_2 low heating value, LHV	33 kWh/kg	[29]
Mole mass of H_2 gas, H_2mass	0.002 kg/mol	[29]
FC margin coefficient, M_{FC}	1.2	[158]
HT hours of autonomy, HA_{H_2}	48 hrs	-

4.4 THE ECONOMIC MODELLING

The LCOE methods are widely used to evaluate the economic feasibility of RERs. The costs distributed over the project lifetime are considered, and this provides a more accurate economic picture of the project under analysis [10]. In general, the LCOE is the total system cost computed across the lifetime of the system divided by the energy generated from that system also across the lifetime. It is noted here the FC, EL, and HT are not included in the calculation of the LCOE since this increases the complexity of the system. Equation (4.22) represents the general form of the LCOE.

$$LCOE = \frac{Total\ System\ Costs}{Total\ Energy\ Production}\ (£/kWh) = \sum_{j=0}^{N} \frac{\frac{Cost_{system}}{(1+r)^j}}{\frac{E_{system}}{(1+r)^j}}\ , \tag{4.22}$$

where the total system cost $Cost_{system}$ represents the sum of the total costs of the PV, BESS, DSL and the inverters and presented by the following equation:

$$Cost_{system} = C_{PV} + C_{BESS} + C_{DSL} + C_{Inv}\ , \tag{4.23}$$

where C_{PV} is the total cost of PV, C_{BESS} is the total cost of BESS, C_{DSL} is the total cost of the DSL, and C_{Inv} is the cost of the inverters for the PV and BESS. The total cost of any asset in the HES, C_{system} is presented in Equation (4.24).

$$C_{system} = IC_{system} + OM_{system} + RC_{system} \quad . \tag{4.24}$$

where IC_{system} represents the initial cost of all the assets in the HES. The OM_{system} is the operation and maintenance cost of all the assets and RC_{system} is the replacement costs of the assets that need to be replaced. All these costs are described in detail in the following sections. The denominator of Equation 4.22 is the E_{system} and represents the total energy generated by the PV/BESS/DSL. Equation 4.25 shows how to find E_{system}.

$$E_{system} = E_{PV,T} + E_{BESS,T} + E_{DSL,T} \quad , \tag{4.25}$$

4.4.1 *Photovoltaic*

The total cost of the PV is the sum of the initial costs, maintenance costs, and replacement costs. The lifetime for PV is 20 years which the same as the HES lifetime, so there are no replacement costs. Equation (4.26) illustrates the total costs for PV.

$$C_{PV} = IC_{PV} + \frac{\sum_{j=0}^{j=N} C_{PV,OM}}{(1+r)^j} \quad , \tag{4.26}$$

where N is the HES lifetime and equals to 20 years, r is the discount rate and considered to be 5% in this thesis. The total energy generated from the PV discounted during its lifetime $E_{PV,T}$, can be found using the following equation:

$$E_{PV,T} = \sum_{j=0}^{j=N} \frac{\sum_{n=0}^{n=8760} E_{PV} \cdot (1 - DEG_{PV})^j}{(1+r)^j} \quad , \tag{4.27}$$

DEG_{PV} is the degradation rate of the PV and equals to 0.5%. All the costs related to PV can be found in Table 4.7.

4.4.2 *Battery Energy Storage System*

The BESS is replaced once during the HES lifetime. The replacement cost of the BESS is equal to the initial cost. The total cost of the BESS is calculated using the following equation:

$$C_{BESS} = IC_{BESS} + \frac{\sum_{j=0}^{j=N} C_{BESS,OM}}{(1+r)^j} + \frac{\sum_{j=10} RC_{BESS}}{(1+r)^j} \quad , \tag{4.28}$$

The energy produced by the BESS can be found using Equation (4.29).

$$E_{BESS,T} = \eta_{rt} \cdot \sum_{j=0}^{j=N} \frac{\sum_{n=0}^{n=8760} E_{PV,charge} \cdot (1 - DEG_{BESS})^j}{(1+r)^j} \quad , \tag{4.29}$$

where $E_{PV,charge}$ is the PV energy used to charge the BESS. η_{rt} is the round trip efficiency for the BESS and DEG_{BESS} is the degradation rate for the BESS.

4.4.3 *Diesel Generator*

The total cost of DSL include the following four parts: (i) the initial cost of the DSL (IC_{DSL}), (ii) the operating and maintenance cost (OM_{DSL}), (iii) the replacement cost (RC_{DSL}), and (iv) the cost of the fuel consumed by the DSL ($C_{DSL,fuel}$).

The total fuel can be calculated by Equation (4.30) and the total cost of the fuel found by Equation (4.31).

$$F_{consume}(n) = \begin{cases} A \cdot P_{DSL,rated} + B \cdot P_{DSL}(n), & P_{DSL}(n) > 0. \\ 0, & P_{DSL}(n) = 0. \end{cases} \tag{4.30}$$

$$C_{DSL,fuel}(n) = \begin{cases} F_{consume}(n) \cdot f_p, & F_{consume}(n) > 0. \\ 0, & F_{consume}(n) = 0. \end{cases} \tag{4.31}$$

where A and B are DSL consumption curve coefficients ($Liter/kWh$), f_p is the DSL fuel unit cost (£/$Liter$).

The DSL lifetime is given in hours, $Life_{DSL,h}$, and can be found in years using Equation (4.32). $Life_{DSL,y}$ is essential to calculate the replacement cost for the DSL.

$$Life_{DSL,y} = \frac{Life_{DSL,h}}{WH_{DSL}} \quad . \tag{4.32}$$

The total cost of the DSL can be found using the following equation:

$$\begin{aligned} C_{DSL} = & IC_{DSL} + \frac{\sum_{j=0}^{j=N} C_{DSL,OM}}{(1+r)^j} + \\ & \frac{\sum_{j=Life_{DSL,y}} RC_{DSL}}{(1+r)^j} + \frac{\sum_{j=0}^{j=N} C_{DSL,fuel}}{(1+r)^j} \quad , \end{aligned} \tag{4.33}$$

and the total energy generated by the DSL is calculated using Equation (4.34).

$$E_{DSL,T} = \sum_{j=0}^{j=N} \frac{\sum_{n=0}^{n=8760} E_{DSL}}{(1+r)^j} \quad . \tag{4.34}$$

Tables 4.6 presents the costs for the PV, DSL, inverters, and BESS. The costs in the table are divided into initial, operating and maintenance, and replacement costs. Table 4.7 shows the data required for the economic models for the above-mentioned assets.

Table 4.6: The cost and lifetime of the HES assets [10, 12].

Component	IC	Yearly OM	RC	Lifetime
PV	2508 £/kW	33 £/kW	0	20 years
DSL	374 £/kW	0.1 £/kW	356 £/kW	15,000 hrs
Inverter	560 £/kW	5.6 £/kW	560 £/kW	10 years
BESS	700 £/kWh	14 £/kWh	700 £/kWh	10 years

4.4.4 *Objective Function and Constraints*

For any optimisation model, the definition of an objective function is a requirement. The objective function usually takes into account maximising/minimising one or more from the following aspects; reliability, economic and environmental. Simultaneously, the objective function is constrained by predefined limits to

Table 4.7: Data used for the economic models of the PV, BESS, and DSL.

Parameter	Value	Ref.
Project lifetime, N	20 years	-
Discount rate, r	5%	[10]
Fuel unit cost, f_p	1.2 £/L	[161]
Round trip efficiency, η_{rt}	90%	[10]
PV degradation rate, DEG_{PV}	0.5%	[10]
BESS degradation rate, DEG_{BESS}	0.1%	[10]
Fuel curve intercept coefficient, A	0.246 L/kWh	[162]
Fuel curve slope, B	0.08145 L/kWh	[162]

achieve the desired optimisation. For example, the reliability and environmental aspects of a HES is subjected to maximising. While the economic aspect is preferred to be minimised [25]. The objective function of the optimum design problem in this thesis is the minimization of the LCOE of the PV, BESS, and DSL while satisfying the operational constraints. PV rated power, HA of the BESS and fuel cost are the state variables of the optimisation study. When these values are optimised, the objective function is expected to get the lowest value. The objective function is defined by Equation (4.35).

$$min\ LCOE = min \sum_{j=0}^{N} \frac{\frac{Cost_{system}}{(1+r)^j}}{\frac{E_{system}}{(1+r)^j}} \quad , \tag{4.35}$$

where $Cost_{system}$ is expressed by Equation (4.23), and E_{system} is expressed by Equation (4.25).

For the assets PV, BESS, and DSL, the following operational constraints should be satisfied.

$$0 \leq P_{PV,rated} \leq \alpha P_{load,max} \quad , \tag{4.36}$$

$$12 \ \leq \ HA \ \leq \ 60 \quad , \tag{4.37}$$

$$0 \leq P_{DSL}(n) \leq P_{DSL,rated} \quad , \tag{4.38}$$

4.5 INITIAL SIZING

The AES constitutes the first step in the integrated framework (see Figure 4.1). The output of this step is the initial size of the HES using $EMS_{initial}$. Figure 4.10 presents the output results of the AES approach. Each colored line represents the LCOE values for a specific BESS hours of autonomy, and over the $P_{PV,rated}$ range from 0 to 267 kW. The results are compared to the cost of a DSL assuming that the DSL is the only source for supplying the demand (represented by the blue straight line in Figure 4.10). Such unitary energy cost, corresponding to the LCOE with no RERs/AERs integrated, is calculated by Equation (4.39) [163].

$$U_{DSL} = \frac{SFC \cdot f_p}{E_{load,total}} \quad , \tag{4.39}$$

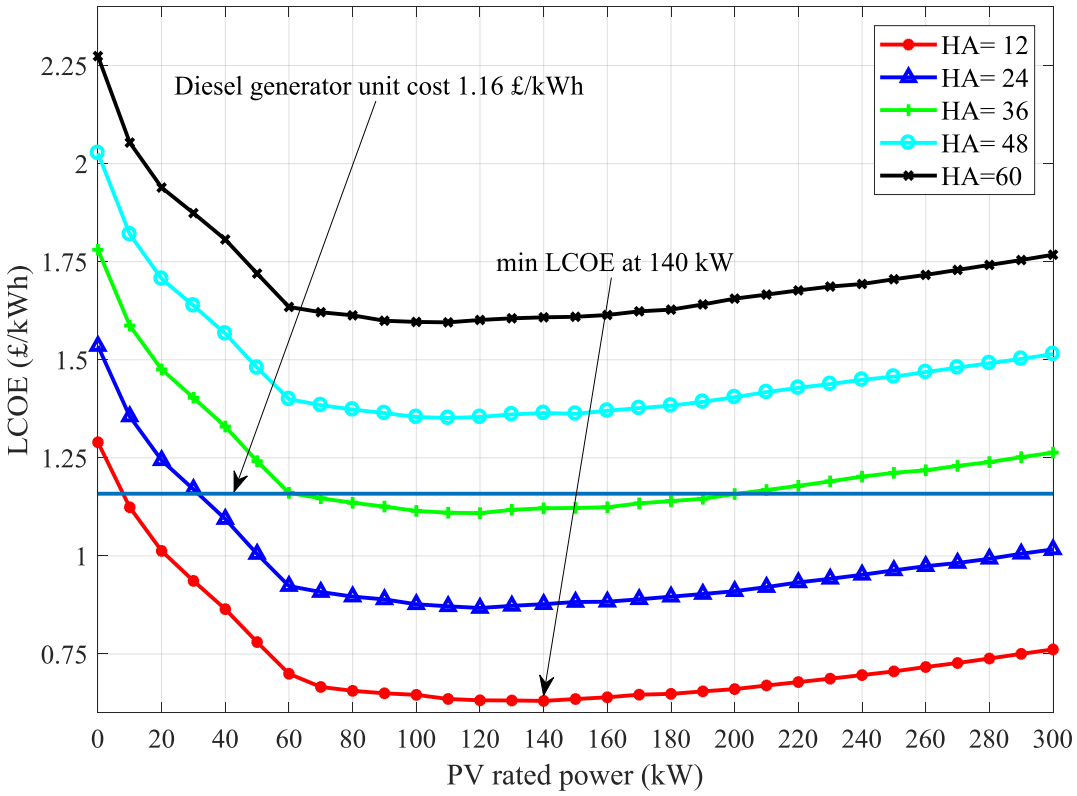

Figure 4.10: Levelised cost of energy for the HES when using AES approach.

where f_p is the fuel cost, $E_{load,total}$ is the total energy of the demand for one year, SFC is the specific fuel consumption for the DSL and calculated using the following equation [163]:

$$SFC = A \cdot P_{load,max} \cdot n + B \cdot E_{load,total} \quad , \tag{4.40}$$

where n is the number of hours in one year, and $P_{load,max}$ is the maximum demand.

The objective of the first step of the integrated framework is to optimise the size of PV, BESS to ensure achieving the minimum LCOE at the same time. As mentioned earlier, the size of the DSL and FC depend on the maximum demand. While the size of the EL is assumed to be 100 kW. However, the assets included in LCOE calculations are the PV, BESS, and DSL. According to Figure 4.10 the minimum LCOE is obtained when $P_{PV,rated}$ is equal to 140 kW, and 12 hours of HA for the BESS. The BESS capacity at 12 hours of HA is 218 kWh using Equation (4.2). The obtained size for the HES assets are presented in Table 4.8.

Table 4.8: The size of HES based on $EMS_{initial}$.

Subsystem	Size
PV / inverter	140 kW / 154 kW
BESS / inverter	218 kWh / 29.4 kW
DSL	32 kW
EL / inverter	100 kW / 110 kW
FC / inverter	32 kW / 35.2 kW
HT	89.5 kg

4.6 INTEGRATED FRAMEWORK

The proposed frame introduced in Figure 4.1 consists of three steps. The first step is applying AES approach (described in Section 4.5) to find the initial sizes of HES components based on $EMS_{initial}$. Once the sizes are obtained, they are exercised by three different EMSs instantiated from $EMS_{initial}$ using. These EMSs are generated using FA and this is the second step.

In addition, the second step includes the calculation of a number of performance indices for each EMS to be used by the following step. In the third step, an evaluation model is proposed to compare the performance indices of each EMS and track the conditions related to each performance index. Afterward, the selected conditions are used to obtain EMS_{new} which replaces $EMS_{initial}$ in the first step. Finally, the optimal size-EMS combination is achieved based on EMS_{new}. The next sections describe the integrated framework second and third steps in detail.

4.6.1 *Instantiation of EMSs using Finite Automata*

Finite automata is utilised to implement $EMS_{initial}$ and instantiate three EMSs. Employing FA to implement $EMS_{initial}$ has been described in detail in Section 4.2.3. The instantiation process is done by generating three models of $EMS_{initial}$. Then, by adjusting the operating conditions related to the activation of the DSL, FC, and EL, three different EMSs with different operation are generated. The initial sizes obtained in Section 4.5 are applied using these EMSs and an assessment between them is described by the performance indices, as explained in the next section.

All the instantiated EMSs have the same states as in $EMS_{initial}$ (see Figure 4.4). Figure 4.11 presents EMS_1 modeled in FA. The operating conditions of EMS_1 are illustrated in Table 4.9. Conditions from 10 to 13, which related to BESS operation have not been changed from $EMS_{initial}$. Conditions from 14 and 15 controls the DSL operation, while the conditions 17 and 18 related to EL operation. Conditions 19 to 21 decide when to operate the FC. The changes in operating condition occurred for the DSL, FC, and EL operation either in the generated power or the operation time. These changes can be summarised as follows:

- The operation of the DSL in EMS_1 provides the full rated power, and any surplus energy after satisfying the demand is used to charge the BESS.

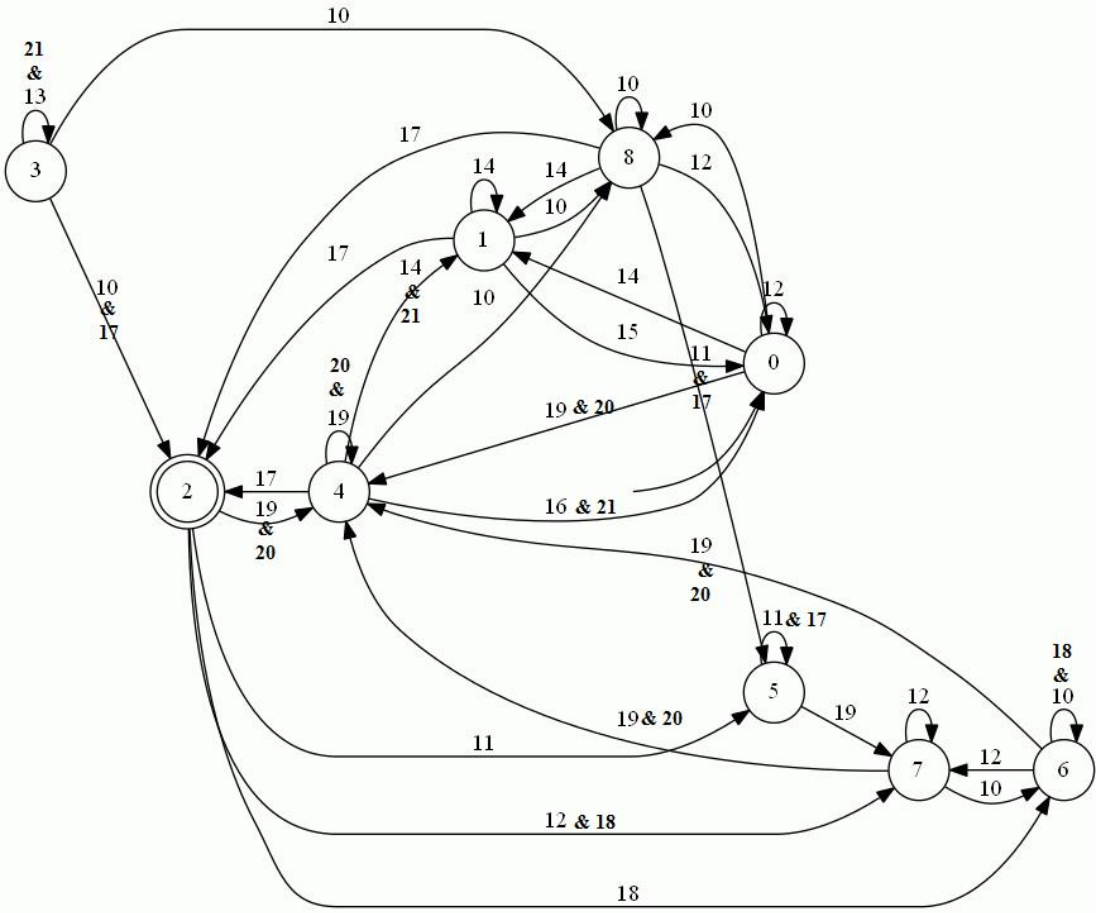

Figure 4.11: Finite automata model for EMS_1.

- The EL exploits any surplus PV power to produce hydrogen without any constraints.
- The FC is set to operate during a specified period in the year, from January to June and from October to December. Since the period from July to September, the power generation from the PV is the highest, so no need to operate the FC. The output power of the FC is equal to the demand at the time of operation.

The next instantiated EMS is EMS_2 and described by FA in Figure 4.12. The operating conditions of EMS_2 are given in Table 4.10. Conditions from 10 to 13 (BESS operation) have been unchanged from $EMS_{initial}$ (see Table 4.2). The conditions that describe the DSL operation are 14 to 16. The EL operation is characterised by conditions 17 to 19, which are also unchanged from $EMS_{initial}$. Finally, conditions 20 to 22 control the FC operation. Compared to $EMS_{initial}$,

Table 4.9: Operating conditions for EMS_1.

Condition	Subsystem states	Description
10-13	BESS	same as in Table 4.2
14	DSL ON	$P_{input}(n) < P_{load}(n)$ & $soc(n) \leq soc_{DSL}$ & $B_{FC}(n) = 0$
15	DSL OFF	$soc(n) > soc_{DSL}$
16	DSL OFF	$P_{input} > P_{load}$
17	EL ON	$P_{PV,surplus}(n) > 0$ & $socHT(n) < socHT_{max}$
18	EL OFF	$socHT(n) \geq socHT_{max}$
19	FC ON	$P_{input}(n) < P_{load}(n)$ & $Jan < n < Jun$ & $soc(n) \leq soc_{FC}$ & $socHT(n) > socHT_{min}$
20	FC ON	$P_{input}(n) < P_{load}(n)$ & $Oct < n < Dec$ & $soc(n) \leq soc_{FC}$ & $socHT(n) > socHT_{min}$
21	FC OFF	$socHT(n) \leq socHT_{min}$

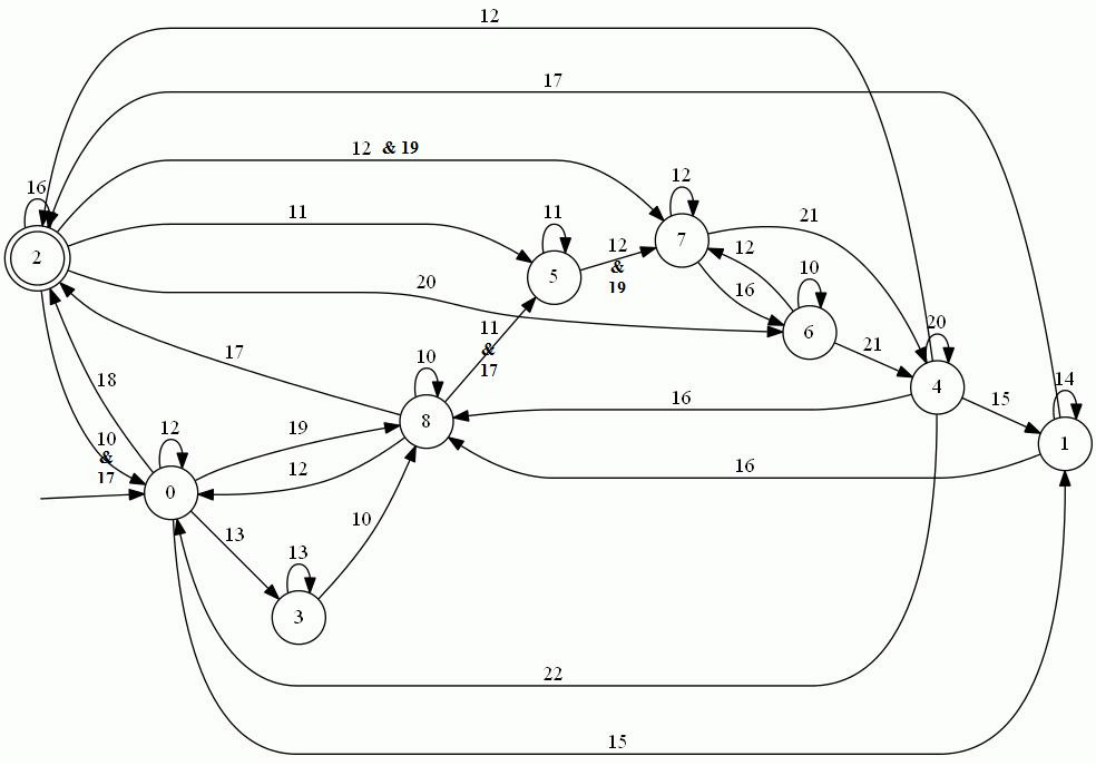

Figure 4.12: Finite automata model for EMS_2.

the changes can be described as:

- Two operating conditions for DSL operation; the ordinary operating condition (condition 15), and adding hysteresis zone to minimize the frequency of

Table 4.10: Operating conditions for EMS_2.

Conditions	Subsystem states	Description
10-13	BESS	same as in Table 4.2
14	DSL ON	$P_{input}(n) < P_{load}(n)$ & $soc_{DSL} < soc(n) < 30\%$ & $B_{DSL}(n-1) = 1$ & $B_{FC}(n) = 0$
15	DSL ON	$P_{input}(n) < P_{load}(n)$ & $soc(n) \leq soc_{DSL}$ & $B_{FC}(n) = 0$
16	DSL OFF	$P_{input}(n) > P_{load}(n)$
17	EL ON	$P_{EL,min} \leq P_{PV,surplus}(n) \leq P_{EL,rated}$ & $socHT(n) < socHT_{max}$
18	EL OFF	$P_{PV,surplus}(n) < P_{EL,min}$
19	EL OFF	$socHT(n) \geq socHT_{max}$
20	FC ON	$soc_{FC} \leq soc(n) \leq 40\%$ & $socHT(n) > socHT_{min}$ & $B_{FC}(n-1) = 1$
21	FC OFF	$soc(n) \leq soc_{FC}$ & $socHT(n) > socHT_{min}$
22	FC OFF	$socHT(n) \leq socHT_{min}$

switching. In both cases, the generated power is equal to 30% of $P_{DSL,rated}$, when $P_{load}(n) \leq 30\% \cdot P_{DSL,rated}$, otherwise $P_{DSL}(n) = P_{load}(n)$.

- The FC operation is also controlled by hysteresis zones as in condition 20. Condition 21 is for the normal operation of the FC. The output power of the FC is equal to the demand.

Figure 4.13 illustrates the third instantiated EMS using FA. The difference between EMS_3 and $EMS_{initial}$ is the status of BESS in state 1 changed from idle to charge. The reason for this is the generated power from the DSL and FC are their rated power at each time they are activated. Therefore, after supplying the demand, surplus power is used to charge BESS. The operating conditions for EMS_3 are the same as in Table 4.2 with a change in the EL operating condition 16 and 17 as following:

- Condition 16 in EMS_3: $0 < P_{PV,surplus}(n) \leq P_{EL,min}$ & $socHT(n) < socHT_{max}$ & $soc(n) > soc_{min}$

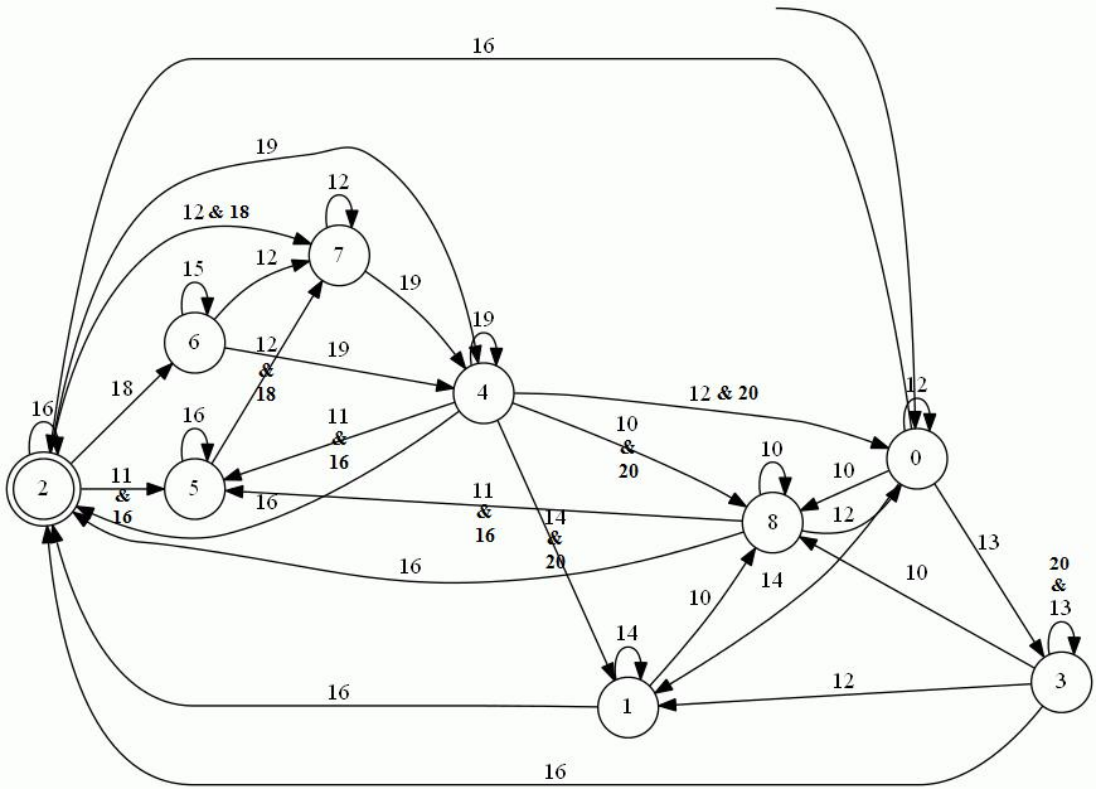

Figure 4.13: Finite automata model for EMS_3.

- Condition 17 in EMS_3: $P_{PV,surplus}(n) = 0$

The EL in EMS_3 is linked to the surplus PV power and the *soc* of the BESS. Such the EL expliots the surplus power and the remaining power is covered by the BESS until it reaches the $P_{EL,min}$.

The three instantiated EMSs along with $EMS_{initial}$ are simulated with the initial sizes and a number of performance indices are computed. These indices are the input to the third step in the integrated framework, the evaluation model and $EMS_{initial}$ replacement.

4.6.2 *Performance Indices*

There are multiple performance indices that have been adopted to asses the instantiated EMSs. Working hours for the DSL, FC and EL WH_{DSL}, WH_{FC}, and WH_{EL}, respectively, are among these indices. Table 4.11 shows the performance indices used in the evaluation model. Along with the working hours of the above-

Table 4.11: Performance indices for the generated EMSs using finite automata.

Index	$EMS_{initial}$	EMS_1	EMS_2	EMS_3	EMS_{new}
$WH_{DSL}(hrs)$	1994	800	1975	2276	793
$WH_{FC}(hrs)$	525	487	470	136	162
$WH_{EL}(hrs)$	224	322	213	337	396
$LCOE_{system}$ (£/kWh)	0.6306	0.4337	0.5846	0.6041	0.4141
Fuel cost (£)	21,037	10,061	21,197	24,030	9,973.2
PV contribution	57%	57%	57%	59%	57%
η_{sys}	89%	88%	88%	88%	89%

mentioned assets, the LCOE, fuel cost, PV contribution, and system overall efficiency are also selected for the evaluation. The most important index between all the indices is the WH_{DSL} since one of the desired properties in the optimal EMS is to reduce the working hours of the DSL. Moreover, the objective function of this study (see Section 4.4.4) is to minimize the LCOE. The PV contribution is also an important index that represents the percentage of utilised PV energy in charging the BESS, supplying the demand and activating the EL. Finding the PV contribution can help in obtaining an EMS that exploits higher PV energy and reduces PV energy losses.

4.6.3 *Evaluation Model and $EMS_{initial}$ Replacement*

To carry out the needed analysis, an evaluation model is introduced to compare the selected performance indices for all the instantiated EMSs and $EMS_{initial}$. The performance indices are illustrated in Table 4.11. The purpose of the evaluation model is to track and select the operating conditions that lead to the most reliable performance of the HES. After determining the most reliable indices for each EMS, the selected operating conditions are employed in the new EMS. The following gives an illustration regarding the evaluation process:

- It can be observed from Table 4.11 that WH_{DSL} is minimum for EMS_1, because the generated power from the DSL is the rated power. So the

condition that controls the operation of the DSL in EMS_1 is selected to be used in EMS_{new}.

- It is preferable to minimize WH_{FC} because of the high cost of the FC operation. In Table 4.11 it can be noticed that WH_{FC} is minimum for EMS_3. Therefore, this condition is elected to be in EMS_{new}.
- WH_{EL} is maximum for EMS_3, higher WH_{EL} means more H_2 generation. Similarly, the condition of the EL in EMS_3 is chosen to be used in EMS_{new}.
- The LCOE and fuel cost calculated for all the EMSs are minimum for EMS_1, this because the WH_{DSL} is also minimum which leads to decreasing in the fuel cost.
- The PV contribution for EMS_3 is the highest, this explains the highest WH_{EL}.
- The η_{sys} for all EMSs is almost the same, which means η_{sys} has no effect on choosing the operating conditions.

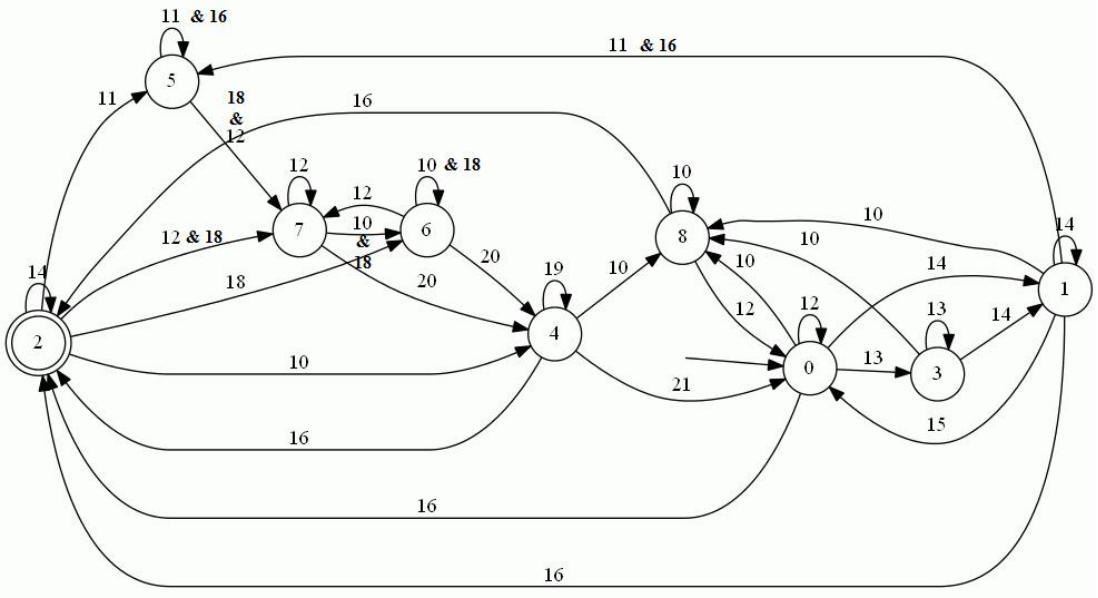

Figure 4.14: Finite automata model for EMS_{new}.

The values of $EMS_{initial}$ and EMS_2 performance indices in Table 4.11 are always intermediate between EMS_1 and EMS_3. As previously mentioned, the preferable performance indices are minimum for the WH_{DSL} and hence the fuel cost from one hand. On the other hand, maximising the PV contribution and WH_{EL}. Therefore none of the operating conditions of these EMSs are used in EMS_{new} generation.

Table 4.12: Operating conditions for EMS_{new}.

Conditions	Subsystem states	Description
10	BESS charging	$P_{input}(n) \geq P_{load}(n)$ & $soc(n) < soc_{max}$
11	BESS OFF	$soc(n) \geq soc_{max}$
12	BESS discharging	$P_{input}(n) < P_{load}(n)$ & $soc(n) > soc_{DSL}$
13	BESS OFF	$soc(n) \leq soc_{min}$
14	DSL ON	$P_{input}(n) < P_{load}(n)$ & $soc(n) \leq soc_{DSL}$ & $B_{FC} = 0$
15	DSL OFF	$P_{input}(n) > P_{load}(n)$
16	EL ON	$0 < P_{PV,surplus}(n) < P_{EL,min}$ & $socHT(n) < socHT_{max}$ & $soc(n) > soc_{min}$
17	EL OFF	$P_{PV,surplus}(n) = 0$
18	EL OFF	$socHT(n) \geq socHT_{max}$
19	FC ON	$P_{input}(n) < P_{load}(n)$ & $soc_{FC} < soc(n) \leq 40\%$ & $socHT(n) > socHT_{min}$ & $B_{FC}(n-1) = 1$
20	FC ON	$P_{input}(n) < P_{load}(n)$ & $soc(n) \leq soc_{FC}$ & $socHT(n) > socHT_{min}$
21	FC OFF	$soc(n) > soc_{FC}$
22	FC OFF	$socHT(n) \leq socHT_{min}$

To this end the EMS_{new} is generated by the evaluation model, the associated FA representation is described in Figure 4.14 and the featured operating conditions can be found in Table 4.12. The performance indices for EMS_{new} are introduced in Table 4.11. The new EMS has better performance indices when compared to all the indices of EMSs in terms of WH_{DSL}, WH_{FC}, LCOE, fuel cost and PV utilisation. Thus, the $EMS_{initial}$ is then replaced by EMS_{new}. Following that, the AES approach is re-exercised to generate an enhanced size of the HES based on EMS_{new}. The results of the integrated framework are discussed in the following section.

4.7 RESULTS AND DISCUSSION

The simulations are done using real data profiles for both PV and demand Figures 4.7, 4.8, and 4.9. Firstly, a PV/DSL/BESS/Hydrogen system HES having

an initial EMS is examined using AES approach and the results are analysed. Then, the same HES is examined using the proposed integrated framework, and the obtained sizing results are then compared to the results of the initial sizing.

Table 4.13 shows the sizing results of HES assets using the AES approach and integrated framework. The size of the PV reduced to almost half. The BESS, DSL and FC remained the same sizing for both sizing. The DSL and FC sizes depend only on the maximum demand. While the size of BESS is calculated from Equation (4.2) which also depends on the average demand and HA. Since the demand profile is the same, the size of the BESS, DSL and FC have been unchanged.

It can be observed from Figures 4.10 and 4.15, the PV and BESS sizes are determined based on the minimum LCOE for the PV/BESS/DSL system. The minimum LCOE obtained from the AES approach and integrated framework is when $HA = 12\ hrs$. This explains why BESS remains the same capacity. $P_{PV,rated} = 140\ kW$ when using AES approach and $P_{PV,rated} = 60\ kW$ when applying the integrated framework. There is a 42% increase in PV contribution, and therefore, a decrease in PV energy losses. The $P_{EL,rated}$ in AES approach is assumed to be 100 kW (see Section 4.3.4). However, the LCOE, WH_{DSL} and the fuel cost are substantially reduced. The EL rated power is assumed to be 50 kW as a tesult of the reduction in the size of the PV. The $P_{FC,rated}$ remains the same. The HT size depends on the EL size and is calculated to be 45 kg. The integrated framework leads to a significant reduction in PV size. However, although the sizes of BESS and DSL remained the same, the performance indices

Table 4.13: The size of HES using the AES approach and integrated framework.

Subsystem	AES	Integrated framework
PV / inverter	140 kW / 154 kW	60 kW / 66 kW
BESS / inverter	218 kWh / 29.4 kW	218 kWh / 29.4 kW
EL / inverter	100 kW / 110 kW	50 kW / 55 kW
FC / inverter	32 kW / 35.2 kW	32 kW / 35.2 kW
DSL	32 kW	32 kW
HT	89.5 kg	45 kg

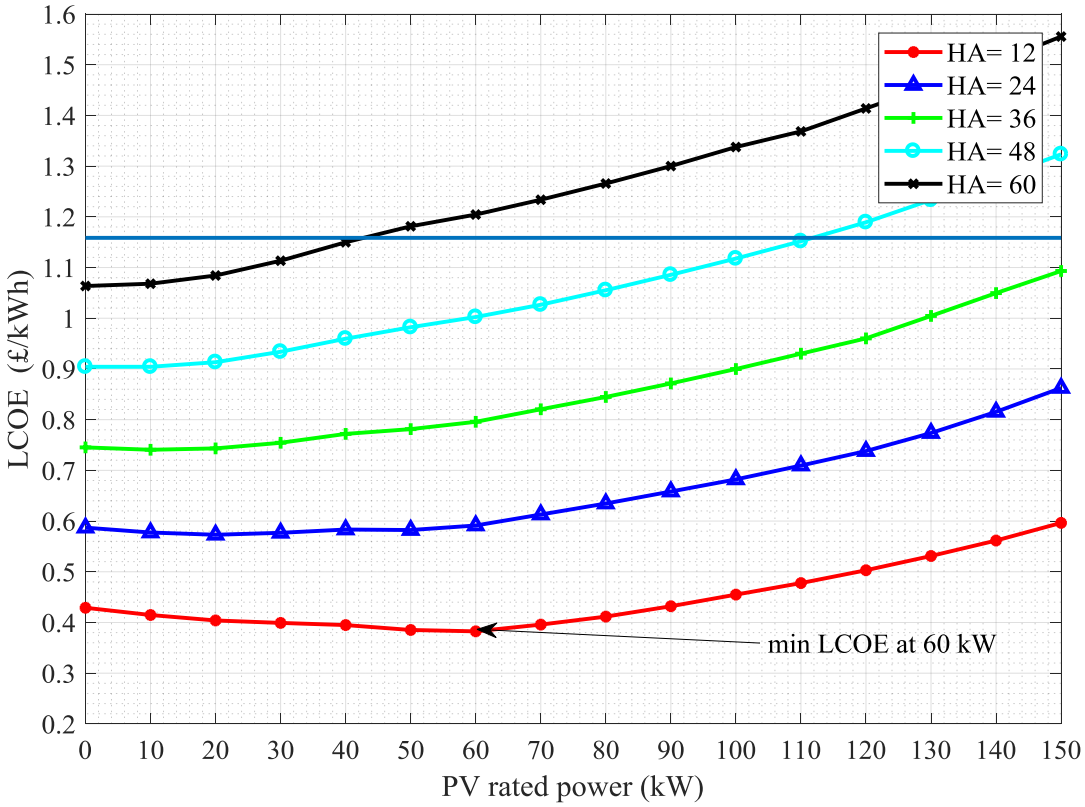

Figure 4.15: Levelised cost of energy for the HES when using integrated framework.

related to them show an improvement in performance. For example, as presented in Table 4.14, the operation hours of DSL and FC decreased by 35% and 83%, respectively. The LCOE is reduced by 40% and the fuel cost is decreased by 23%. In addition, more utilisation of PV energy is obtained by using the framework as the PV contribution increased to 98%. This indicates that PV energy is exploited effectively. Applying the integrated framework also yielded a reduction in the replacement cost of the DSL to the half. As the DSL is replaced twice during the HES lifetime compared to three times when using AES approach.

Figure 4.16 demonstrates the values of soc, P_{load}, P_{PV} and P_{FC} for 48 hours in June when applying the integrated framework. The DSL output power is zero during that period since there is available PV energy and soc is between 30% and 90%. The demand ranges between 5-15 kW during daylight, the BESS and PV power can cover the demand. During night hours, BESS goes below 35% and there is available H_2 in the HT, then, the FC is activated. The FC operated four times, generating power equal to the rated power each time. The extra generated

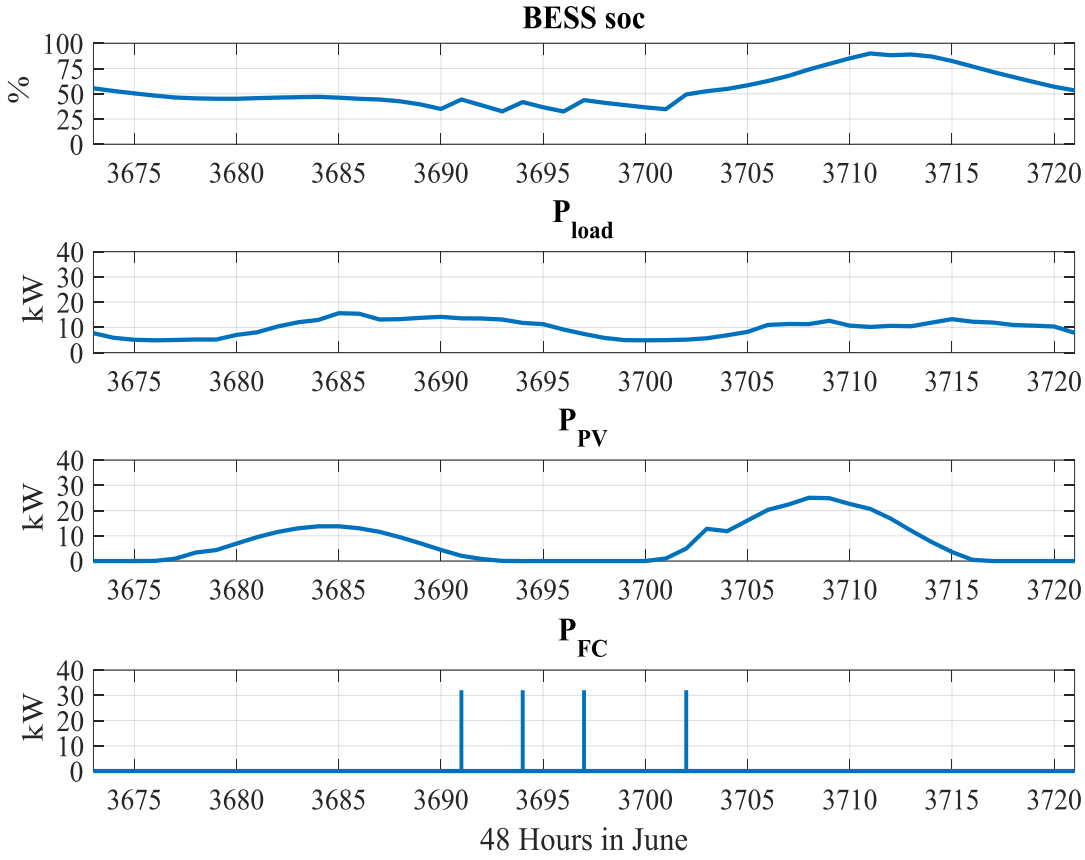

Figure 4.16: BESS soc, FC and PV power values during 48 hours in June, the DSL output is zero during these hours.

Table 4.14: Comparison between the results obtained using AES approach and the integrated framework.

Index	AES	Framework	Improvements
WH_{DSL} (hrs)	1994	1293	35% reduction
WH_{FC} (hrs)	525	88	83% reduction
WH_{EL} (hrs)	224	356	37% increase
$LCOE$ $(£/kWh)$	0.6300	0.3809	40% reduction
Fuel cost (£)	21037	16262	23% reduction
PV contribution	57%	98%	41.8% increase
$life_{DSL}$ $(years)$	8	12	50% reduction in RC_{DSL}
η_{sys}	90	93	7% increase

from the DSL is used to charge BESS. This also can be observed in Figure 4.18, which represents HT levels, P_{EL} and P_{FC} power values during the same 48 hours

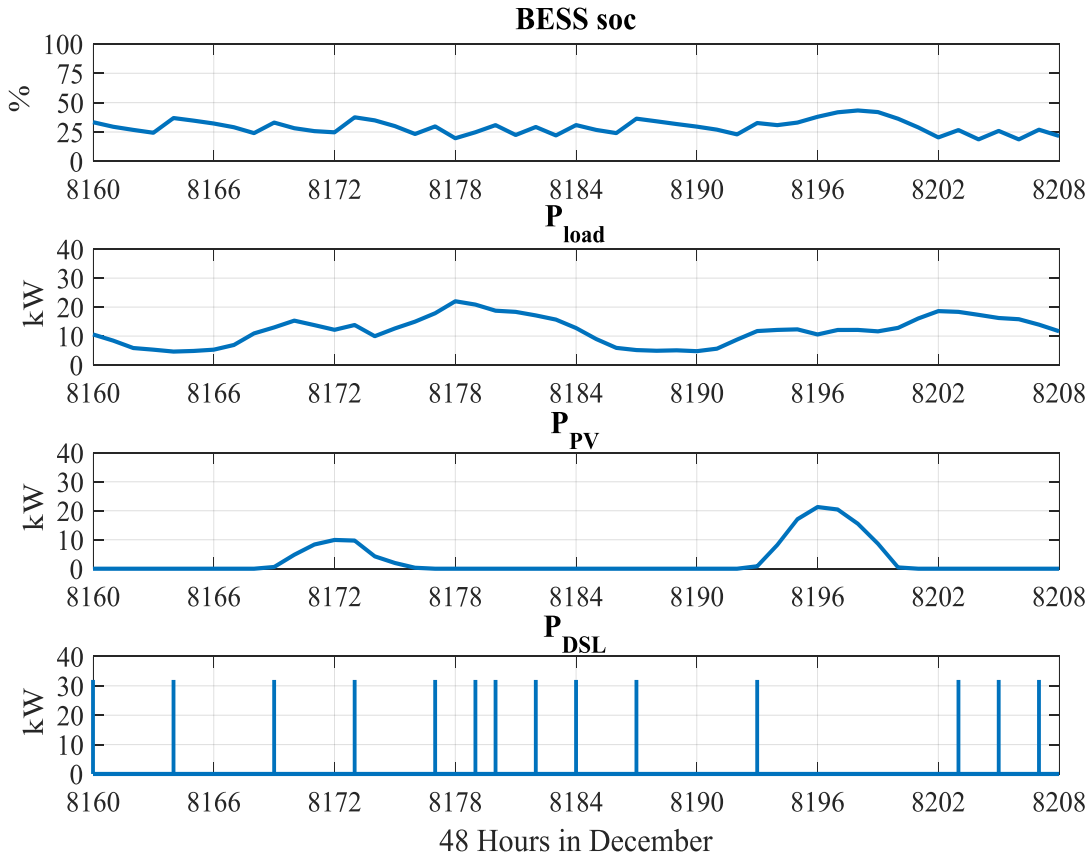

Figure 4.17: BESS soc, FC, PV, DSL power and demand values during 48 hours in December.

in June. The figure shows that $socHT$ starts to decrease when P_{FC} is on, and has a slight increase when P_{EL} is on due to the H_2 generation from the EL.

Since power generation, consumption and demand are varying throughout the year; it is important to display these changes during different times in the year. Figure 4.17 shows the values of BESS soc, P_{Load}, P_{PV} and P_{DSL} for 48 hours in December when applying the integrated framework. The FC output power is zero as there is not enough H_2 in the HT. The HES depends on the DSL to satisfy the demand because the PV output during winter is low while the demand is high. The EL operation relates to the surplus PV power since the PV generation is not enough to supply the load, the EL is not operating. The DSL operated 14 times during this period to supply the demand.

Figure 4.19 represents the $socHT$, P_{EL},P_{PV}, and P_{FC} values for 48 hours in September. $socHT$ ranges between 70% and 80%, this means the HT is almost

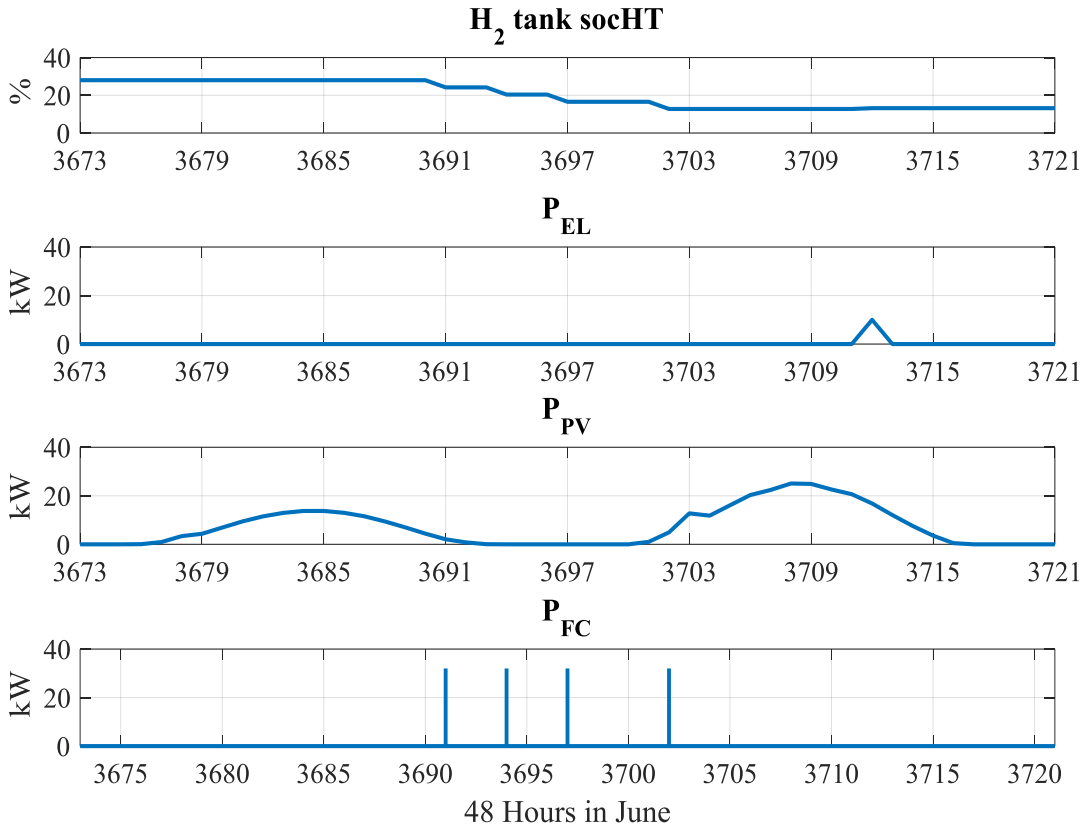

Figure 4.18: HT $socHT$, EL,PV, and FC power values during 48 hours in June.

full. The EL is operated when there is surplus PV energy while the FC is operated just once. The DSL working hours during the same period is zero, so it is not included in the figure.

Finally, to ensure that the generated EMS_{new} is the optimal among all the generated EMSs, a second iteration of the integrated framework is performed. This resulted in generating EMS_{1new}, EMS_{2new}, EMS_{3new} utilising the new sizes obtained from the first iteration of the integrated framework. Table 4.15 demonstrates the performance indices for EMS_{new}, EMS_{1new}, EMS_{2new}, and EMS_{3new}. Comparing these indices for the mentioned EMSs, it is concluded that EMS_{new} produces the best results and registers the minimum values in WH_{DSL}, LCOE and fuel cost.

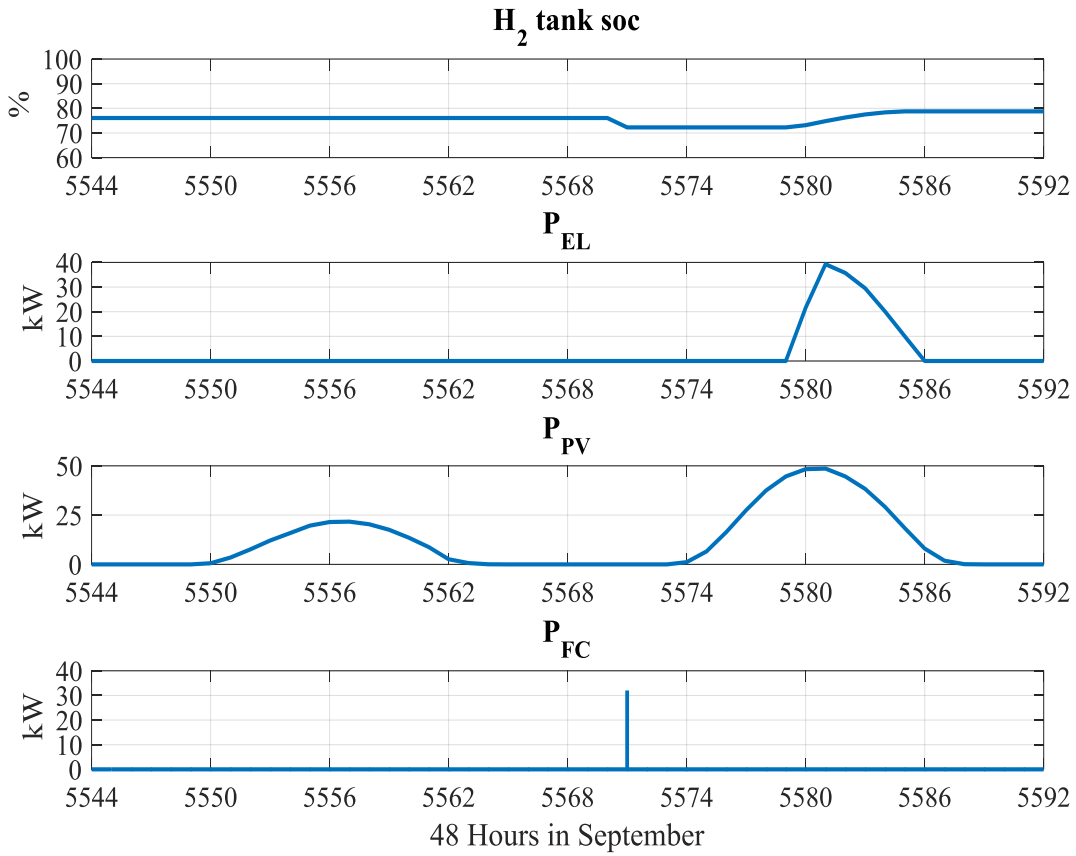

Figure 4.19: HT soc, EL,PV, and FC power values during 48 hours in September.

Table 4.15: Performance indices for EMS_{new} and the generated EMSs using the sizes obtained from the integrated framework.

Index	EMS_{new}	EMS_{1new}	EMS_{2new}	EMS_{3new}
$WH_{DSL}(hrs)$	1293	1327	3662	3663
$WH_{FC}(hrs)$	88	37	181	85
$WH_{EL}(hrs)$	356	174	176	352
$LCOE(£/kWh)$	0.3809	0.3911	0.6688	0.6808
Fuel cost (£)	16,262	16,689	39,256	38,640
PV contribution	98%	90%	98%	98%
η_{sys}	93%	96%	96%	93%

4.8 CONCLUDING REMARKS

A novel integrated framework is successfully developed to find the optimal size-EMS combination for a hybrid stand-alone PV/BESS/DSL/hydrogen system. The proposed framework consists of three consecutive steps; firstly, an analytical and

economic sizing is performed using an initial EMS to find the initial size of the HES. Secondly, Finite Automata is utilised to implement the initial EMS and instantiate various EMSs. A number of simulations are performed to exercise these EMSs using the initial sizes. A set of performance indices are also calculated for the instantiated EMSs which are used as entries to the next step. Thirdly, an evaluation model is implemented to compare the performance indices of the initial and instantiated EMSs. This evaluation is achieved to determine the best operating conditions to use them in generating a new EMS. Then, the new EMS replaces the initial EMS. The analytical and economical sizing is carried out again to find the new size based on the new EMS.

The integrated framework proved to produce better results in terms of assets sizing and HES performance when comparing to the AES approach. Such that, the PV, EL and HT sizes are reduced. The LCOE of the HES is reduced as well as increasing the PV contribution.

5

MODIFYING ENERGY MANAGEMENT USING FUZZY LOGIC

5.1 INTRODUCTION

Chapter 4 demonstrated an integrated framework to obtain the optimal size-EMS for stand-alone HES. The results obtained by the integrated framework showed minimising in the size of the PV, LCOE of the system, and maximising the PV contribution. Since the solar radiation and demand have unpredictable characteristics and they may change for the coming years, including the source and demand uncertainty in the HES optimization is necessary.

This chapter demonstrates the design of a FLC to detect the variabilities in the demand and solar radiation and accordingly modify the EMS of the HES. The work in this chapter is performed on three stages which are illustrated in Figure 5.1. The first stage is finding the size-EMS combination using the integrated framework (similar to that described in Chapter 4), and forecasted solar radiation and demand profiles. This step is vital in order to include any future changes in solar radiation and demand data. The second stage includes a sensitivity analysis, considering the new-obtained size of the HES and the real profiles for solar radiation and demand. The sensitivity analysis is conducted by changing the solar radiation and demand data for one year by ±5% and ±10% to generate 24 scenarios. In the third stage, the FLC is designed depending on the performance indices generated from the sensitivity analysis scenarios. The performance indices (see Section 4.6.2) used in the sensitivity analysis are the fuel cost, DSL working hours, PV contribution. The objective of the FLC is managing the uncertainty in demand and solar radiation and then modifying the operating conditions of the DSL, FC, and the EL in the original EMS. For example, the condition responsible

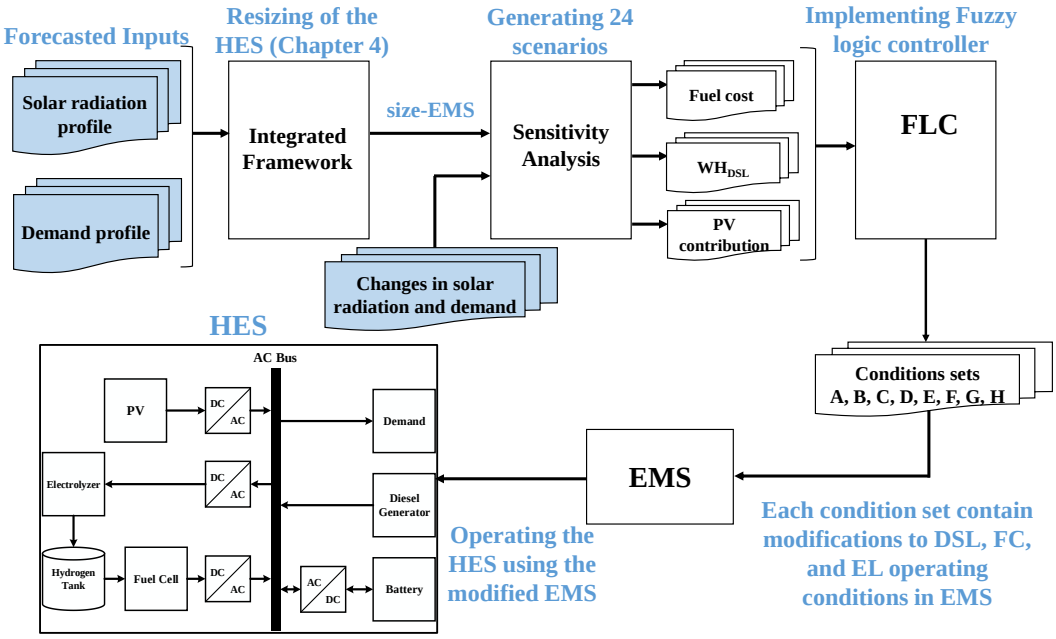

Figure 5.1: An illustrative diagram showing the three stages required to design a FLC. Starting from resizing the assets of the HES, conducting the sensitivity analysis, then implementing the FLC to modify the original EMS based on the output conditions set.

for operating the DSL is "$P_{input}(n) < P_{load}(n)$ & $soc(n) \leq soc_{DSL}$". One of the modifications to this condition is changing the part related to the soc of the BESS.

The following sections describe the three stages required for the FLC design in order to maintain the performance of the HES under uncertain demand and generation conditions.

5.2 RESIZING THE HYBRID ENERGY SYSTEM USING FORECASTED DATA

In this section, the HES is resized based on forecasted solar radiation and demand profiles. Figures 5.2 and 5.3 represent the original and forecasted solar radiation and demand profiles used in this chapter. The forecasted values of demand and solar radiation are generated by adding white Gaussian noise to the original values.

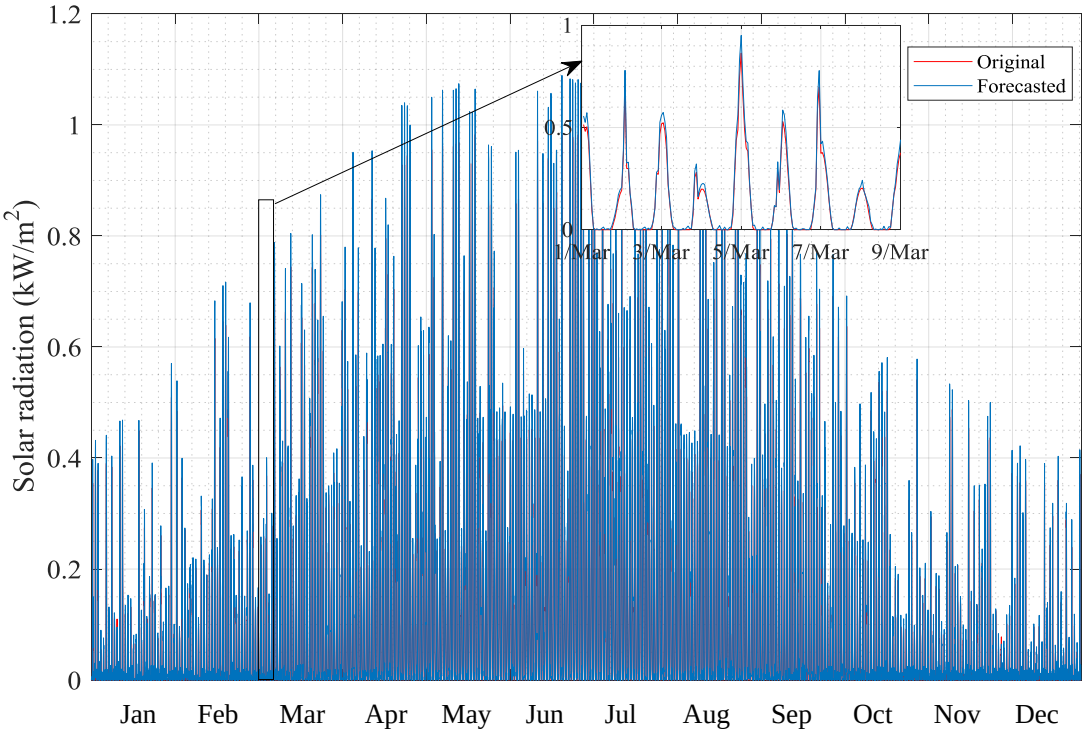

Figure 5.2: Original and forecasted solar radiation of one calendar year.

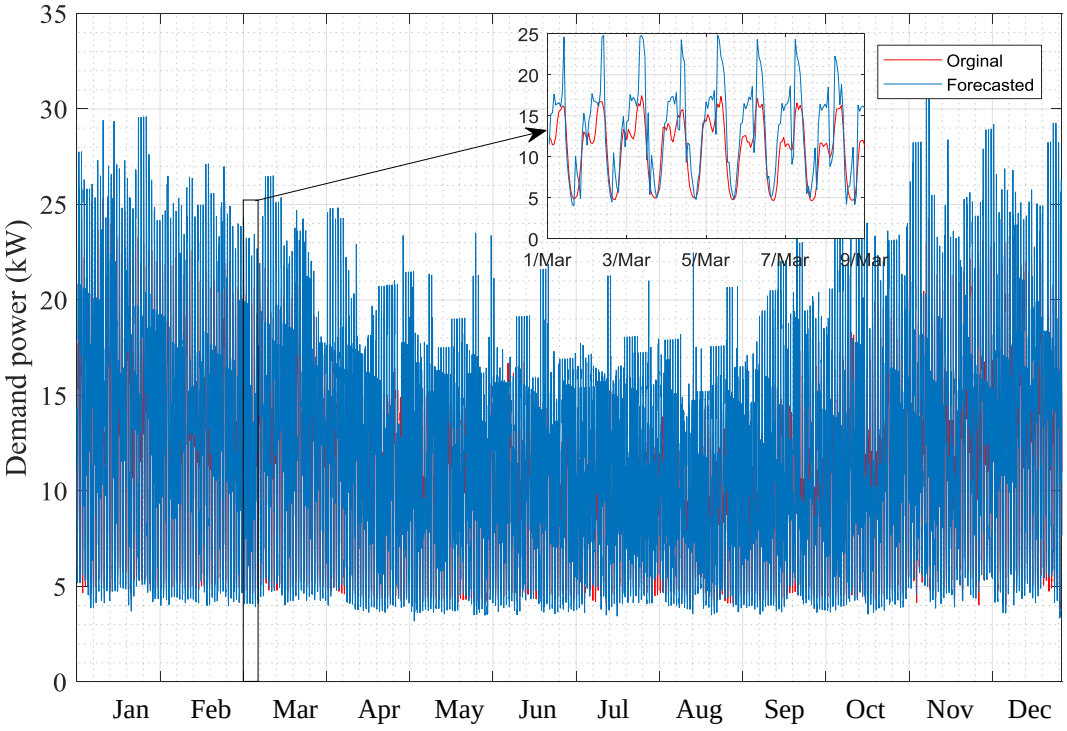

Figure 5.3: Original and forecasted demand distribution of one calendar year.

Table 5.1 illustrates the sizes of the HES resulting from the integrated framework using the forecasted profiles. Compared to the sizes obtained in Table 4.13

from Chapter 4, it can be noted that the PV size has not changed, while there is an increase in the DSL, FC and BESS sizes. The size of the EL and HT is fixed. The original solar radiation and demand profiles are called the base case in the sensitivity analysis and explained in the following section.

Table 5.1: The optimal size of HES using the integrated framework and forecasted demand and solar irradiance.

Subsystem in the HES	Obtained size
PV	60 kW
BESS	240.54 kWh
EL	50 kW
FC	38.55 kW
DSL	38.55 kW
HT	45 kg

5.3 SENSITIVITY ANALYSIS

A sensitivity analysis is conducted to measure the degree of uncertainty of demand and solar radiation data. It is performed by an annual change of ±5% and ±10% of demand and solar values. The performance indices that have been selected to be checked after carrying out the sensitivity analysis are fuel cost, WH_{DSL} and PV contribution. These performance indices are chosen since it is desirable to reduce the DSL working hours and the fuel cost while ensuring maximum utilisation of PV energy. The variations on demand and solar variation generate 24 scenarios, and these scenarios are displayed in Tables 5.2 - 5.7.

Table 5.2 presents the results of the sensitivity analysis performed by an annual change of ±5% and ±10% of the demand only. Scenario 1 shows an increase in the demand by 5%, causing an increase in the fuel cost, WH_{DSL}, and PV contribution as well. The increase in fuel cost and WH_{DSL} is expected as the increase in the demand is partly covered by the DSL. PV energy is also contributed to supply the demand and that explains the increase in PV contribution. However, increasing the annual demand by 10% leads to a further increase in those indices.

Table 5.2: Results of sensitivity analysis for an annual change of ±5% and ±10% of P_{load}.

Scenario No.	Description	Fuel Cost	WH_{DSL}	PV Contribution
Base case	-	£16071	1061	96%
Scenario **1**	+5% P_{load}	£17541	1158	98%
Scenario **2**	+10% P_{load}	£19131	1263	99%
Scenario **3**	-5% P_{load}	£14769	975	93%
Scenario **4**	-10% P_{load}	£13481	890	89%

Alternatively, the reduction in demand causes a reduction in the fuel cost, WH_{DSL} and PV contribution as the request for energy decreased.

In Table 5.3, scenarios 5 to 8 illustrate the performance indices resulted from changing the solar radiation by ±5% and ±10% of the base case. Increasing solar radiation causes a reduction in WH_{DSL} and fuel cost. This is due to the increase PV energy used to supply to the demand, generate H_2, and charging BESS. However, the increase in the PV energy has not been fully exploited leading to decrease in the PV contribution. On the other hand, the decrease in solar radiation leads to an increase in WH_{DSL} and hence the fuel cost. Whereas the PV contribution is increased since the demand has not changed and the generated PV energy is almost fully utilised.

Table 5.3: Results of sensitivity analysis for an annual change of ± 5% and ± 10% of I_{PV}.

Scenario No.	Description	Fuel Cost	WH_{DSL}	PV Contribution
Scenario **5**	+5% I_{PV}	£15617	1031	93%
Scenario **6**	+10% I_{PV}	£15147	1000	90%
Scenario **7**	-5% I_{PV}	£16682	1102	98%
Scenario **8**	-10% I_{PV}	£17420	1150	100%

Table 5.4 shows the performance indices for the scenarios 9, 10, 11 and 12. These scenarios are resulted from increasing the annual demand and solar radiation by 5% and 10%. It can be observed that the highest values of the fuel cost and PV contribution are for the scenarios where the annual increase in demand is 10%. While the values for the scenarios with an increase of 5% in the demand, range around the base case.

Table 5.4: Results of sensitivity analysis for an annual change of +5%, +10% of P_{load} and I_{PV}.

Scenario No.	Description	Fuel Cost	WH_{DSL}	PV Contribution
Scenario **9**	+5% P_{load}, +5% I_{PV}	£16950	1119	96%
Scenario **10**	+5% P_{load}, +10% I_{PV}	£16450	1086	93%
Scenario **11**	+10% P_{load}, +5% I_{PV}	£18404	1215	97%
Scenario **12**	+10% P_{load}, +10% I_{PV}	£17783	1174	96%

Table 5.5 presents the sensitivity analysis for an annual increase of 5%, 10% of the demand and an annual decrease of 5%, 10% of the solar radiation. Generally, increasing the demand and decreasing solar radiation cause a noticeable rise in fuel cost and WH_{DSL}. The highest values for the performance indices are for scenarios 14 and 16 where the increase in demand is 10%.

Table 5.5: Results of sensitivity analysis for an annual change of +5%, +10% of P_{load} and -5%, -10% of I_{PV}.

Scenario No.	Description	Fuel Cost	WH_{DSL}	PV Contribution
Scenario **13**	+5% P_{load}, -5% I_{PV}	£18238	1204	99%
Scenario **14**	+10% P_{load}, -5% I_{PV}	£19934	1316	100%
Scenario **15**	+5% P_{load}, -10% I_{PV}	£19071	1259	100%
Scenario **16**	+10% P_{load}, -10% I_{PV}	£20782	1372	100%

On the contrary, decreasing the demand and increasing the solar radiation in the sensitivity analysis causes a reduction the fuel cost and WH_{DSL}. This illustrated in Table 5.6 where the demand is decreased by 5% and 10% and solar radiation is increased by the same percentage. The PV contribution decreases and this is reasonable since the increment in solar radiation is unexploited because of the reduction in the demand. The lowest values for fuel cost, WH_{DSL} and PV contribution are for scenarios 18 and 20 where the decrease in demand is 10%. Whereas, the decrease in the demand in scenarios 17 and 19 are 5%, so the reduction in the performance indices is less than for the other two scenarios.

The last four scenarios in sensitivity analysis are presented in Table 5.7. Both demand and solar radiation are decreased by 5% and 10%. Scenarios from 20

Table 5.6: Results of sensitivity analysis for an annual change of −5%, −10% of P_{load}, 5%, 10% for I_{PV}.

Scenario No.	Description	Fuel Cost	WH_{DSL}	PV Contribution
Scenario **17**	-5% P_{load}, +5% I_{PV}	£14329	946	90%
Scenario **18**	(-10% P_{load}, +5% I_{PV}	£13118	866	86%
Scenario **19**	-5% P_{load}, +10% I_{PV}	£13951	921	87%
Scenario **20**	-10% P_{load}, +10% I_{PV}	£12754	842	83%

to 24 represent the results obtained from the reduction in demand and solar radiation.

Table 5.7: Results of sensitivity analysis for an annual change of −5%, −10% of P_{load} and I_{PV}.

Scenario No.	Description	Fuel Cost	WH_{DSL}	PV Contribution
Scenario **21**	-5% P_{load}, -5% I_{PV}	£15223	1005	96%
Scenario **22**	-5% P_{load}, -10% I_{PV}	£15844	1046	98%
Scenario **23**	-10% P_{load}, -5% I_{PV}	£13921	919	92%
Scenario **24**	-10% P_{load}, -10% I_{PV}	£14390	950	96%

Figures 5.4, 5.5 and 5.6 show the 24 scenarios concerning the sensitivity analysis of the fuel cost, WH_{DSL} and PV contribution, respectively. In Figure 5.4, the best and worst scenarios regarding fuel cost sensitivity analysis can be observed. The best scenario happens when the fuel cost is minimum and obtained by scenario 20 (-10% P_{load}, +5% I_{PV}). While the worst scenario is found when the fuel cost is maximum. This is depicted by scenario 16 where the demand is increased by 10% and solar radiation is decreased by 10%. Generally, the worst scenario happens when the increment in demand cannot be covered by the solar radiation leading to increase the reliance on the DSL.

Figure. 5.5 shows the influence of changing the demand and solar radiation in the working hours of the DSL. The figure shows the same trend as the fuel cost in the previous figure. This means when the WH_{DSL} is high this results in higher fuel cost and vice versa. Accordingly, the best and worst scenarios for this figure are the same as the ones found by the fuel cost sensitivity analysis. The worst scenario is 20 and the best scenario is 16.

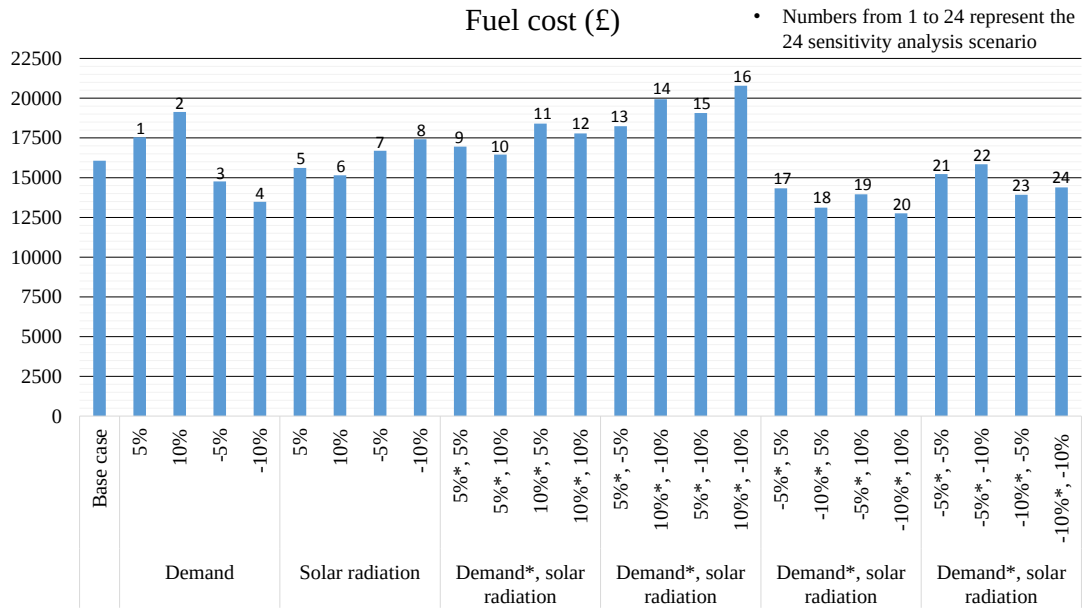

Figure 5.4: The effect of demand and solar radiation variations on the fuel cost.

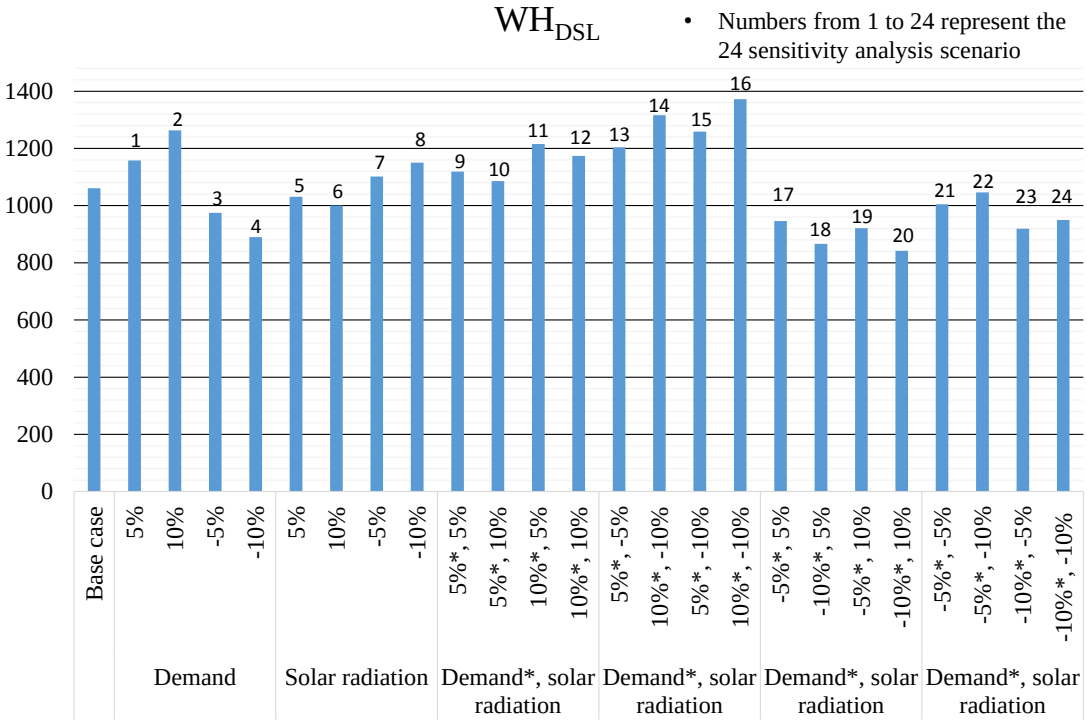

Figure 5.5: The effect of demand and solar radiation variations on DSL working hours.

Finally, the PV contribution sensitivity analysis is clarified by Figure 5.6. It is most desirable to increase the PV utilisation and this is reflected in the PV contribution. The best scenarios are when the PV contribution is 100% and they are 8, 14, 15 and 16. It is noted that all these scenarios happen when solar

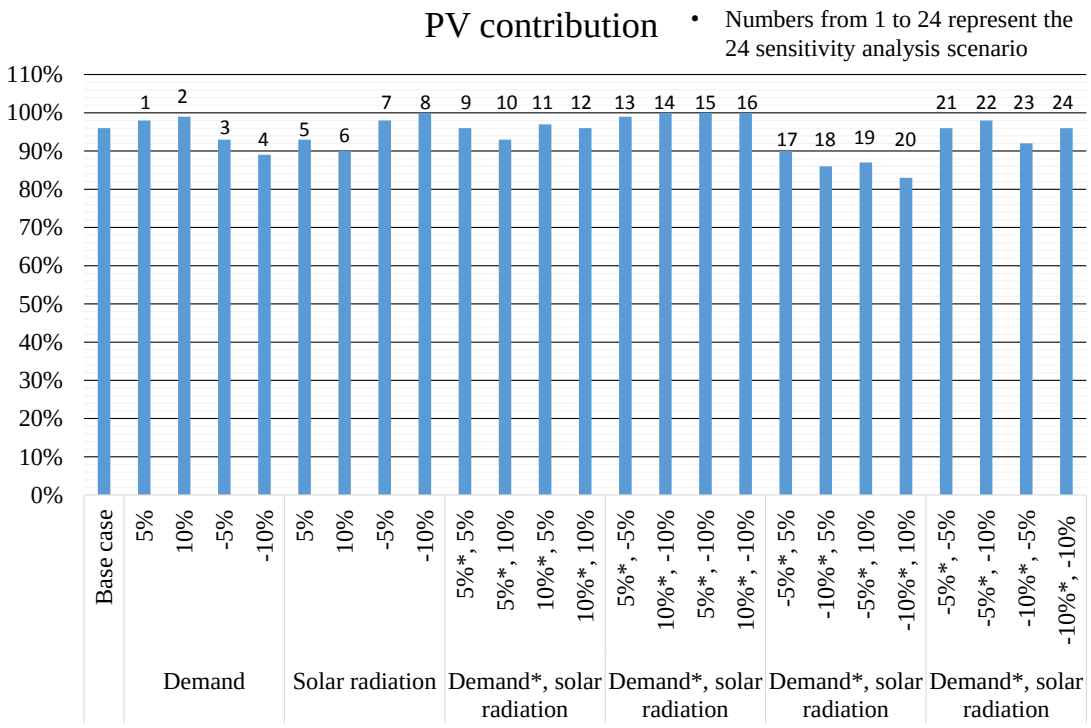

Figure 5.6: The effect of demand and solar radiation variations on PV contribution.

radiation is reduced by 10%. This means that when the annual solar radiation is less, the HES can exploit all the produced PV energy. While the worst scenario is when the PV contribution is minimum and this is scenario 20. However, this scenario is considered the best scenario for fuel cost and WH_{DSL}. This is due to the reduction in the demand by 10% meaning less dependent on the DSL. To conclude, after the sensitivity analysis is achieved, the variability in the annual demand has more effect on the DSL working hours and hence fuel cost. While this relation is the inverse with regard to the PV contribution, as the reduction in the demand leads to decrease in the PV contribution. This can be explained as the demand consumes less energy from the PV leading to more losses in PV energy.

However, the conducted sensitivity analysis is not just for investigating the effect of the demand and solar radiation uncertainty on the HES performance. The purpose of the sensitivity analysis is to use the results obtained in implementing a FLC which is explained in the following section.

5.4 MODIFY THE EMS USING FUZZY LOGIC

The results of the sensitivity analysis are exploited to implement a FLC. This controller detects the changes in the demand and solar radiation and consequently modifies the operating conditions of the DSL, FC, and EL in the EMS. A general introduction on FLC has been presented in Chapter 2. This section includes the design of the FLC, description of the fuzzy rules involved, the output of the FLC, and finally, a case study to verify the effectiveness of the FLC.

5.4.1 *The design of Fuzzy Logic Controller*

The key objective of the FLC is to modify the operating conditions of the EMS obtained previously by the integrated framework (see Chapter 4). This gives the EMS the ability to deal with the uncertainty in inputs. The DSL, FC, and EL in the HES are the target assets to modify their operating conditions. Operating these assets has a considerable effect on the BESS and HT charging and discharging process. The PV is considered ON continuously even if the solar radiation is zero, so its operating condition has not been modified. The BESS and HT rely on the above-mentioned assets for charging and discharging. Thus any change in the operating conditions of the DSL, FC, and EL will affect their performance. Figure 5.7 shows the configuration of the FLC that clearly illustrates the three steps of the FLC.

The results of the sensitivity analysis are used in the implementation of a FLC. Thereby, the fuel cost, WH_{DSL}, and the PV contribution of the 24 scenarios in Tables 5.2 to 5.7 are considered the inputs to the FLC. The input variables are fuzzified into membership functions. These membership functions are basically fuzzy sets and the degree of membership of a value is defined as how much this value is close to that set. Table 5.8 introduces the fuzzy sets that define the membership functions. The fuzzy sets are divided into three ranges: LOW, MED, and MAX. The LOW fuzzy set contains the lowest values, while the MED fuzzy

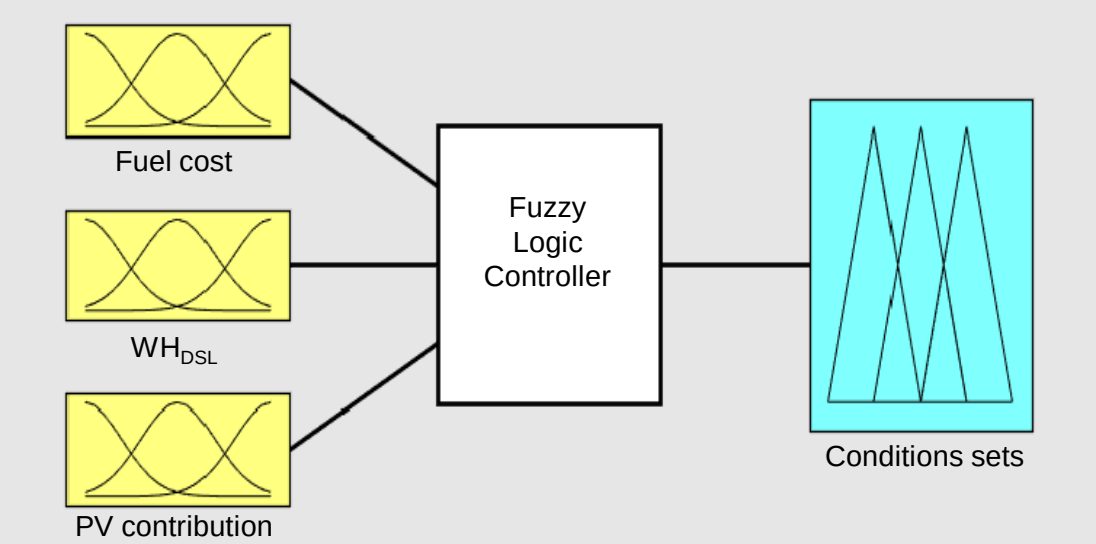

Figure 5.7: The configuration of the FLC introducing the input membership functions; fuel cost, WH_{DSL}, and PV contribution. The output membership function is the conditions sets that modify the EMS.

set is intermediate between the lowest and the highest values. The MAX fuzzy set covers the highest values of the selected performance indices.

Figure 5.8 presents the membership function for the fuel cost input fuzzy set. Figures 5.9 and 5.10 illustrate the membership functions for the WH_{DSL} and PV contribution input fuzzy sets.

After determining the input fuzzy sets (*i.e.*, fuel cost, WH_{DSL}, and PV contribution), the 24 sensitivity analysis scenarios can be classified into LOW, MED and MAX.

Table 5.9 defines each scenario in terms of fuzzy sets. By observing the fuzzy inputs in the table, it can be recognised that some scenarios share the same fuzzy sets. For example, scenarios 1, 8, 9, 11, 12, and 13 share the same input fuzzy

Table 5.8: Numerical ranges of the fuzzy sets

Fuel cost (£)	LOW	MED	MAX
	12000-16000	15000-19000	18000-21000
WH_{DSL} (hours)	LOW	MED	MAX
	800-1100	1000-1300	12000-1500
PV contribution (%)	LOW	MED	MAX
	80-91	90-96	95-100

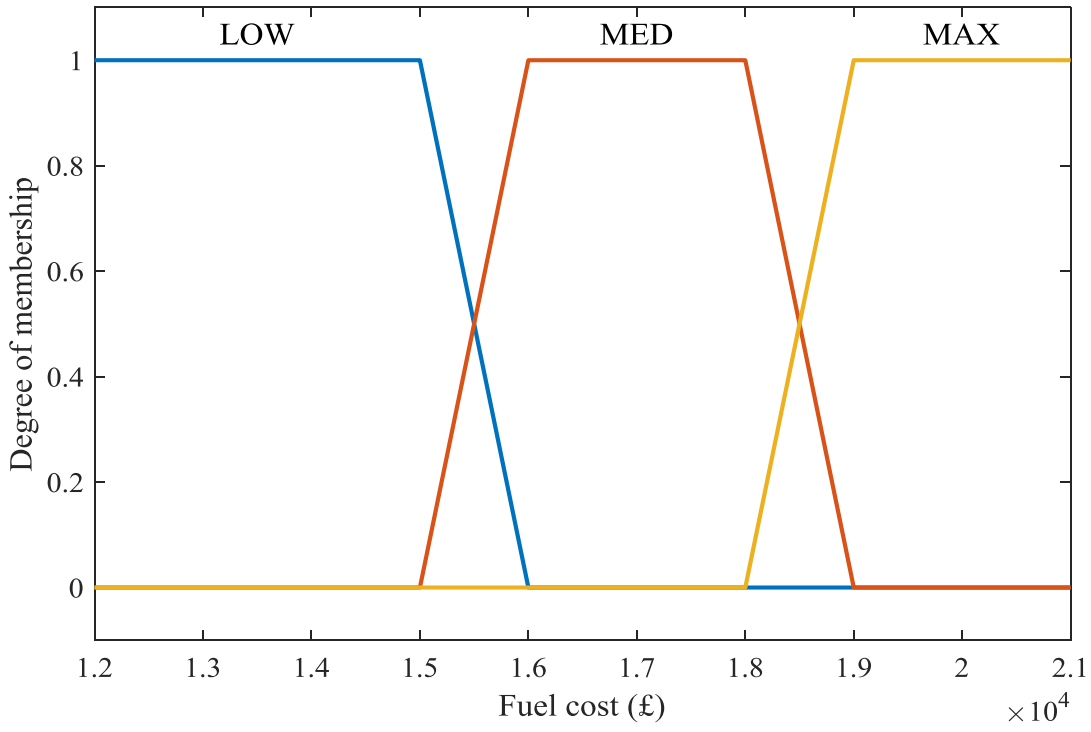

Figure 5.8: Membership function for fuel cost input fuzzy set.

sets (MED, MED, and MAX). Grouping the scenarios that have the same input

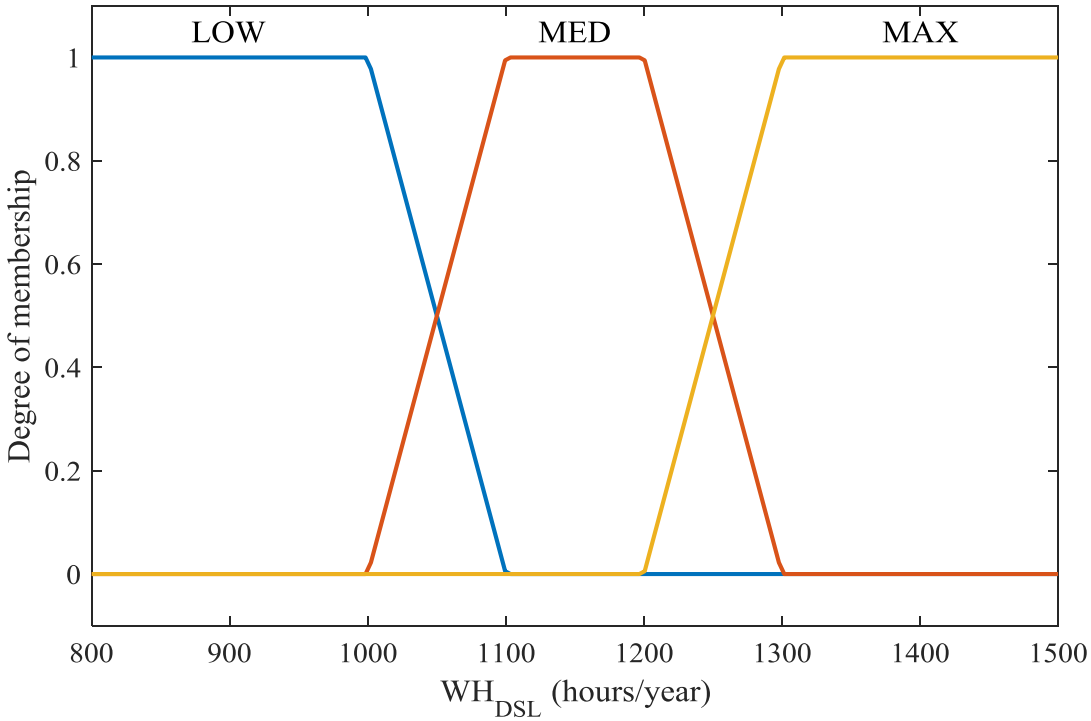

Figure 5.9: Membership function for WH_{DSL} input fuzzy set.

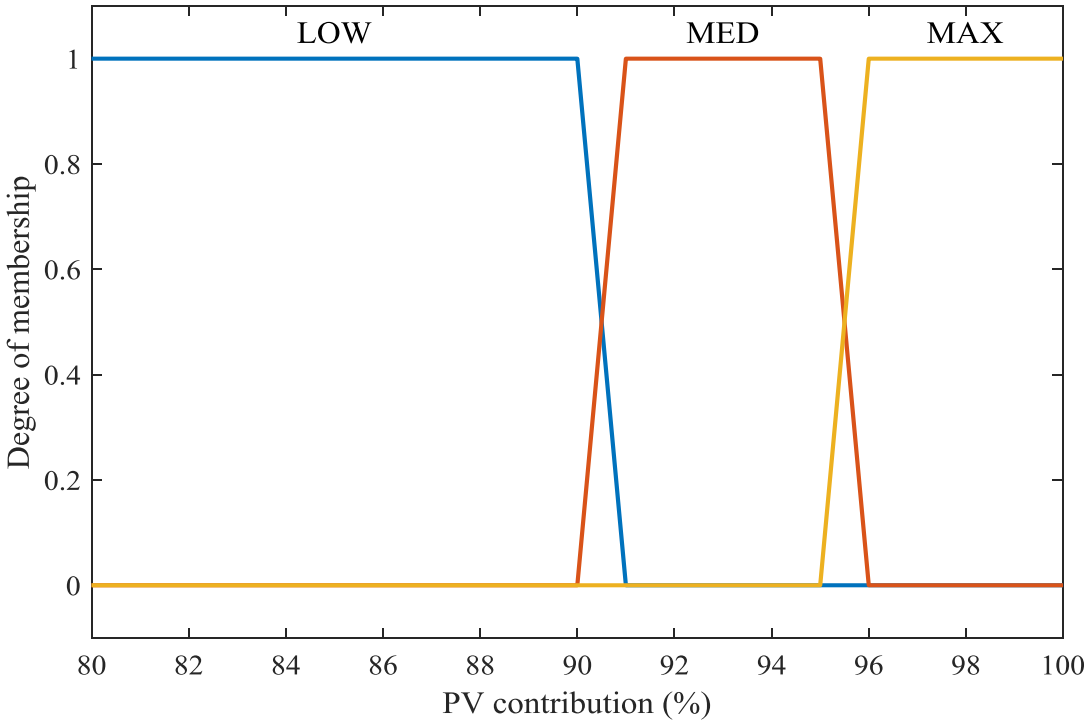

Figure 5.10: Membership function for PV contribution input fuzzy set.

fuzzy sets results in eight groups of scenarios. As a result, the fuzzy rules for the FLC are eight rules.

Table 5.10 represents the relationship between the sensitivity analysis scenarios, the ranges of the output fuzzy sets and the symbols that represent the conditions sets. The first column shows the scenarios with similar input fuzzy sets. Based on this similarity, the number of fuzzy rules needed for the FLC can be stated and equals to 8 rules. The output fuzzy sets represent the number of scenarios that have similar fuzzy input sets. The range for each output fuzzy set (*i.e.*, third column) is the total number of scenarios that have similar input fuzzy sets (*i.e.*, second column). The last column in the table is the symbols of the conditions sets representing the output fuzzy sets. To illustrate, scenarios 1, 8, 9, 11, 12, an 13 belong to the range [0 - 7] which is the output fuzzy set A. It should be noted that the number of scenarios is 6, while the range is [0 - 7], this due to the overlapping of fuzzy output sets. While scenarios 2, 14, 15, and 16 belong to the range [6 - 11] that is the output fuzzy set B, and so on. These output fuzzy

Table 5.9: The 24 sensitivity analysis scenarios interpreted into LOW, MED, and MAX with regarding to the fuzzy sets.

Scenario No.	Fuel Cost	WH_{DSL}	PV Contribution
Scenario **1**	MED	MED	MAX
Scenario **2**	MAX	MAX	MAX
Scenario **3**	LOW	LOW	MED
Scenario **4**	LOW	LOW	LOW
Scenario **5**	MED	LOW	MED
Scenario **6**	LOW	LOW	LOW
Scenario **7**	MED	LOW	MAX
Scenario **8**	MED	MED	MAX
Scenario **9**	MED	MED	MAX
Scenario **10**	MED	MED	MED
Scenario **11**	MED	MED	MAX
Scenario **12**	MED	MED	MAX
Scenario **13**	MED	MED	MAX
Scenario **14**	MAX	MAX	MAX
Scenario **15**	MAX	MAX	MAX
Scenario **16**	MAX	MAX	MAX
Scenario **17**	LOW	LOW	LOW
Scenario **18**	LOW	LOW	LOW
Scenario **19**	LOW	LOW	LOW
Scenario **20**	LOW	LOW	LOW
Scenario **21**	LOW	LOW	MAX
Scenario **22**	MED	LOW	MAX
Scenario **23**	LOW	LOW	MED
Scenario **24**	LOW	LOW	MAX

sets are translated into condition sets that replace the previous conditions in the original EMS (see Section 4.6.3) to improve the performance of HES.

These conditions sets represent the modifications made to the operating conditions of the FC, DSL, and EL. Each set of conditions modifies the operating conditions of one or more of the DSL, FC, and EL. An explanation of the conditions sets from A to H is presented in the following section.

Table 5.10: Illustration of the relationship between the sensitivity analysis scenarios, the output fuzzy sets and the condition sets.

Scenario	Sum of Scenarios	Output Fuzzy Set Ranges	Output Fuzzy Sets Symbols
1, **8**, **9**, **11**, **12**, **13**	6	[0 - 7]	A
2, **14**, **15**, **16**	4	[6 - 11]	B
3, **23**	2	[10 - 13]	C
4, **6**, **17**, **18**, **19**, **20**	6	[12 - 19]	D
5	1	[18 - 20]	E
7, **22**	2	[19 - 21]	F
10	1	[20 - 22]	G
21, **24**	2	[21 - 24]	H

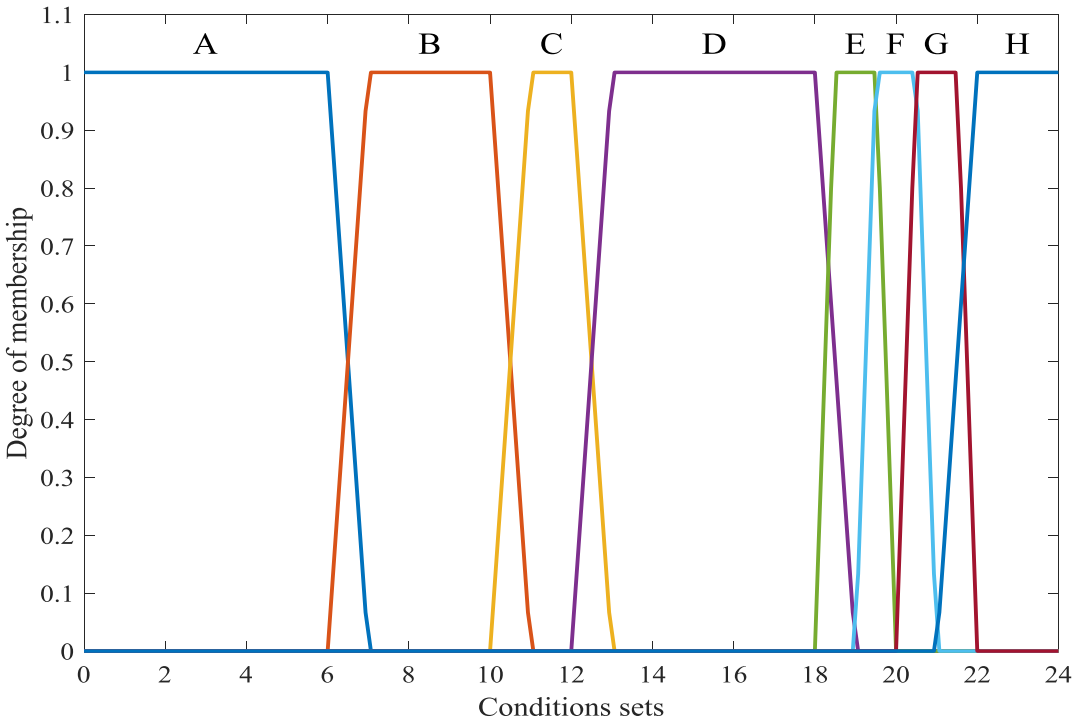

Figure 5.11: Membership function for output fuzzy sets.

5.4.2 *The Fuzzy Rules*

In the previous section, the input fuzzy sets are identified which are the fuel cost, working hours of the DSL, and the PV contribution. In addition, it has been clarified why the fuzzy rules needed are equal to eight rules. In this section, the

fuzzy rules are explained in detail. Tables 5.11 and 5.12 represent the operating conditions of EMS_{new} obtained by the integrated framework and values related to BESS soc and HT $socHT$ (see Chapter 4). These tables have been listed in this section to investigate the effectiveness of the designed FLC on the EMS.

In Table 5.11, DSL operation is controled by Conditions 14 and 15. Conditions 16, 17, and 18 responsible for EL operation. While conditions 19 - 22 are for the FC operation. These operating conditions can be modified to improve the HES performance when there are uncertainty in the demand and solar radiation.

Table 5.11: Operating conditions for EMS_{new} produced by the integrated framework described in Chapter 4.

Condition No.	Description	Operating Conditions
10	BESS charging	$P_{input}(n) \geq P_{load}(n)$ & $soc(n) < soc_{max}$
11	BESS OFF	$soc(n) \geq soc_{max}$
12	BESS discharging	$P_{input}(n) < P_{load}(n)$ & $soc(n) > soc_{DSL}$
13	BESS OFF	$soc(n) \leq soc_{min}$
14	DSL ON	$P_{input}(n) < P_{load}(n)$ & $soc(n) \leq soc_{DSL}$ & $B_{FC} = 0$
15	DSL OFF	$P_{input}(n) > P_{load}(n)$
16	EL ON	$0 < P_{PV,surplus}(n) < P_{EL,min}$ & $socHT(n) < socHT_{max}$ & $soc(n) > soc_{min}$
17	EL OFF	$P_{PV,surplus}(n) = 0$
18	EL OFF	$socHT(n) \geq socHT_{max}$
19	FC ON	$P_{input}(n) < P_{load}(n)$ & $soc_{FC} < soc(n) \leq 40\%$ & $socHT(n) > socHT_{min}$ & $B_{FC}(n-1) = 1$
20	FC ON	$P_{input}(n) < P_{load}(n)$ & $soc(n) \leq soc_{FC}$ & $socHT(n) > socHT_{min}$
21	FC OFF	$soc(n) > soc_{FC}$
22	FC OFF	$socHT(n) \leq socHT_{min}$

Table 5.12: Values of the parameters related to soc and $socHT$ mentioned in Table 5.11.

Parameter	Value	Parameter	Value
soc_{min}	20%	soc_{max}	80%
soc_{FC}	35%	soc_{DSL}	25%
$socHT_{min}$	10%	$socHT_{min}$	90%

Table 5.13 defines the changes made to the operating conditions of the FC, DSL and EL introduced in Table 5.11. The conditions sets are labeled from A to H, condition sets B, D and G are modifying the operating conditions of DSL, FC, and EL. Whereas the other sets are modifying the operating conditions of DSL and FC. DSL is the only asset among the others that has been modified in all conditions sets. The modifications done on the FC operating condition are targeting the part related to the soc and $socHT$. The first part of the condition that is dealing with the demand remained unchanged.

The derivation of the fuzzy rules is based on our experience and a series of simulations. The changes are summarized as follows:

1. The soc in the DSL operating condition for all the sets from A to H has been changed to: $soc(n) \leq soc_{FC}$ & $socHT(n) > socHT_{min}$. This ensures more utilisation of BESS energy.
2. Condition set A: the FC operating condition has been changed to $soc(n) \leq soc_{FC}$ & $socHT(n) > socHT_{min}$ OR $soc(n) = soc_{max}$ & $socHT(n) \leq socHT_{max}$. This condition allows the FC to operate whenever the soc is less than 35% without hysteresis zone. However, the FC also operates when the BESS is fully charged after checking the availability of H_2. The power generated by the FC supplies the demand without generating any surplus.
3. Condition set B: the condition $soc(n) = soc_{max}$ & $socHT(n) \leq socHT_{max}$ has been added to the FC operating condition. This allows the FC to operate when the BESS is fully charged and the power generated by the FC supplies the demand without generating any surplus.

Table 5.13: The sets of modified conditions labeled from A to H.

Condition Sets Symbols	Operating Conditions
A	DSL: $soc(n) \leq soc_{min}$ & $B_{FC}(n) = 0$
	FC: $soc(n) \leq soc_{FC}$ & $socHT(n) > socHT_{min}$ OR $soc(n) = soc_{max}$ & $socHT(n) \leq socHT_{max}$
B	DSL: $soc(n) \leq soc_{min}$ & $B_{FC}(n) = 0$
	FC: $soc_{FC} \leq soc(n) < 40\%$ & $socHT(n) > socHT_{min}$ & $B_{FC}(n-1) = 1$ OR $soc(n) \leq soc_{FC}$ & $socHT(n) > socHT_{min}$ OR $soc(n) = soc_{max}$ & $socHT(n) \leq socHT_{max}$
	EL: $85\% \leq soc(n) < socHT_{max}$ & $socHT(n-1) < socHT_{max}$ & $P_{PV,surplus}(n) = 0$
C	DSL: $soc(n) \leq soc_{min}$ & $B_{FC}(n) = 0$
	FC: $50\% < soc(n) \leq 70\%$ & $socHT(n) > socHT_{min}$ & $B_{FC(n-1)} = 1$ OR $soc(n) \leq 50\%$ & $socHT(n) > socHT_{min}$
D	DSL: $soc(n) \leq soc_{min}$ & $B_{FC}(n) = 0$
	FC: $50\% < soc(n) \leq 70\%$ & $socHT(n) > socHT_{min}$& $B_{FC}(n-1) = 1$ OR $soc(n) \leq 50\%$ & $socHT(n) > socHT_{min}$
	EL: $85\% < soc(n) \leq soc_{max}$ & $socHT(n-1) < socHT_{max}$ & $P_{PV,surplus}(n) = 0$
E	DSL: $soc(n) \leq soc_{min}$ & $B_{FC}(n) = 0$
	FC: $30\% < soc(n) < 40\%$ & $socHT(n) > socHT_{min}$ & $B_{FC}(n-1) = 1$ OR $soc(n) \leq 30\%$ & $socHT(n) > socHT_{min}$

Continued on next page

Table 5.13 – continued from previous page

Condition Sets Symbols	Operating Conditions
F	DSL: $soc(n) \leq soc_{min}$ & $B_{FC}(n) = 0$
	FC: $30\% \leq soc(n) < 40\%$ & $socHT(n) > socHT_{min}$ & $B_{FC}(n-1) = 1$) OR $soc(n) \leq 30\%$ & $socHT(n) > socHT_{min}$) OR $soc(n) = soc_{max}$ & $socHT(n) \leq socHT_{max}$
G	DSL: $soc(n) \leq soc_{min}$ & $B_{FC}(n) = 0$
	FC: $70\% < soc(n) \leq soc_{max}$ & $socHT(n) > socHT_{min}$
	EL: $85\% < soc(n) < soc_{max}$ & $socHT(n-1) < socHT_{max}$ & $P_{PV,surplus}(n) = 0$
H	DSL: $soc(n) \leq soc_{min}$ & $B_{FC}(n) = 0$
	FC: $70\% < soc(n) \leq soc_{max}$ & $socHT(n) > socHT_{min}$

4. Condition set C: the soc ranges for the FC operating condition related to hysteresis zone has been changed to 50% and 70% and the following condition has been added: $soc(n) \leq 50\%$ & $socHT(n) > socHT_{min}$. This means the FC operates when the BESS is charged to the half. In simulation this proves to reduce the DSL working hours.
5. Condition set D:
   - the changes made to the FC operating conditions are the same as in condition set C.
   - the EL operating condition has been changed to: $85\% < soc(n) \leq soc_{max}$ & $socHT(n-1) < socHT_{max}$ & $P_{PV,surplus}(n) = 0$. The EL operates

when the BESS soc between 85% and soc_{max} and there surplus PV energy equals to zero. This permits the BESS to operate the EL leading to generate more H_2.

6. Condition set E: the soc_{FC} in the FC operating condition has been changed from 35% to 30% to exploit more energy from the BESS.
7. Condition set F: the soc_{FC} in the FC operating condition from has been changed from 35% to 30% (same as in condition set E). In addition, the following condition has been added: $soc(n) = soc_{max}$ & $socHT(n) \leq socHT_{max}$, which the same as in condition set B.
8. Condition set G:
   - the second part of the FC operating condition has been changed to: $70\% < soc(n) \leq soc_{max}$ & $socHT(n) > socHT_{min}$. This means the FC operates if the soc of the BESS is between 70% and soc_{max}. The power generated by the FC supplies the demand without generating any surplus.
   - the changes that has been made to the EL operating condition is the same as in condition set D.
9. Condition set H: the changes that has been made to the FC operating condition are the same as in condition set G.

The fuzzy rules that determine the relationship between the fuzzy inputs and fuzzy outputs are outlined as follow:

- If (Fuel cost ∈ MED) and (WH_{DSL} ∈ MED) and (PV contribution ∈ MAX) then (output = A).
- If (Fuel cost ∈ MAX) and (WH_{DSL} ∈ MAX) and (PV contribution ∈ MAX) then (output = B).
- If (Fuel cost ∈ LOW) and (WH_{DSL} ∈ LOW) and (PV contribution ∈ MED) then (output = C).
- If (Fuel cost ∈ LOW) and (WH_{DSL} ∈ LOW) and (PV contribution ∈ LOW) then (output = D).

- If (Fuel cost ∈ MED) and (WH_{DSL} ∈ LOW) and (PV contribution ∈ MED) then (output = E).
- If (Fuel cost ∈ MED) and (WH_{DSL} ∈ LOW) and (PV contribution ∈ MAX) then (output = F).
- If (Fuel cost ∈ MED) and (WH_{DSL} ∈ MED) and (PV contribution ∈ MED) then (output = G).
- If (Fuel cost ∈ LOW) and (WH_{DSL} ∈ LOW) and (PV contribution ∈ MAX) then (output = H).

After determining the input fuzzy sets and the rules, the following section introduces the output fuzzy sets and the results obtained after applying the FLC. In addition, a comparison has been done to highlight the improvements on the HES made by the FLC.

5.4.3 *The Results of Fuzzy Logic Controller*

The main aim of the FLC is to modify the EMS of the HES to overcome the uncertainty in demand and solar radiation dataset. This is achieved by modifying some of the operating conditions to decrease working hours and fuel cost of the DSL and also increase the PV contribution. The FLC is designed using the Fuzzytool supported by MATLAB. The output of the FLC is a number of conditions sets alphabetically labelled from A to H. Depending on the input fuzzy sets, each output fuzzy set (*i.e.*, each set of conditions) replaces the original conditions in the EMS to generate a modified EMS. In this chapter, the operating conditions of the DSL, FC, and EL are the only conditions that supposed to be affected by the FLC (see Section 5.4.1).

Table 5.14 summarizes the output of the FLC for the 24 scenarios introduced by the sensitivity analysis. To evaluate the impact of applying the modified EMS on the performance of the HES, a comparison between the performance indices has been performed. This is illustrated in Figures 5.12, 5.13, and 5.14.

Figure 5.12 shows the values of the fuel cost for the 24 scenarios before and after applying the FLC. In general, it is observed that there are noticeable reductions

Table 5.14: The values of fuel cost, WH_{DSL}, and PV contribution of the 24 scenarios after applying the FLC.

Scenarios No.	Description	Fuel Cost	WH_{DSL}	PV Contribution
Scenario 1	+5% P_{load}	£16995	1122	100%
Scenario 2	+10% P_{load}	£18207	1202	100%
Scenario 3	-5% P_{load}	£11149	736	100%
Scenario 4	-10% P_{load}	£11921	787	100%
Scenario 5	+5% I_{PV}	£14284	943	100%
Scenario 6	+10% I_{PV}	£13989	917	100%
Scenario 7	-5% I_{PV}	£16223	1071	99%
Scenario 8	-10% I_{PV}	£17314	1143	100%
Scenario 9	+5% P_{load}, +5% I_{PV}	£16026	1058	100%
Scenario 10	+5% P_{load}, +10% I_{PV}	£15253	1007	100%
Scenario 11	+10% P_{load}, +5% I_{PV}	£17404	1149	99%
Scenario 12	+10% P_{load}, +10% I_{PV}	£16011	1057	98%
Scenario 13	+5% P_{load}, -5% I_{PV}	£18162	1199	100%
Scenario 14	+10% P_{load}, -5% I_{PV}	£19843	1310	100%
Scenario 15	+5% P_{load}, -10% I_{PV}	£19010	1255	100%
Scenario 16	+10% P_{load}, -10% I_{PV}	£20707	1367	100%
Scenario 17	-5% P_{load}, +5% I_{PV}	£13087	864	99%
Scenario 18	-10% P_{load}, +5% I_{PV}	£10800	713	100%
Scenario 19	-5% P_{load}, +10% I_{PV}	£12466	823	100%
Scenario 20	-10% P_{load}, +10% I_{PV}	£11557	763	100%
Scenario 21	-5% P_{load}, -5% I_{PV}	£14011	925	100%
Scenario 22	-5% P_{load}, -10% I_{PV}	£14557	961	100%
Scenario 23	-10% P_{load}, -5% I_{PV}	£13072	863	98%
Scenario 24	-10% P_{load}, -10% I_{PV}	£12769	843	100%

in fuel cost values. However, in some scenarios where there is a reduction in solar radiation and increase in the demand, the values are slightly improved. This is due to less availability of PV energy to cover the demand. The reduction in the fuel cost has an impact on the DSL operational cost, as well as reduce the generation of CO_2 emissions.

Figure 5.13 demonstrates the working hours of the DSL before and after applying the FLC. The scenarios where there is a reduction in demand show a significant improvement in the WH_{DSL} after applying the FLC. Since the

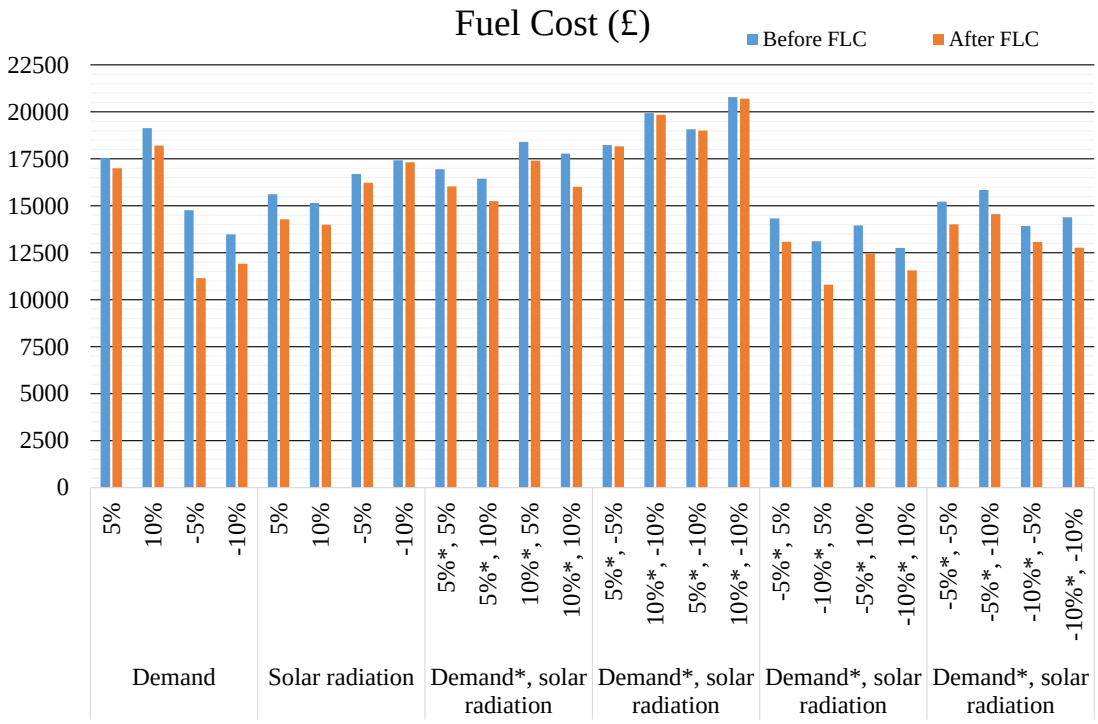

Figure 5.12: The fuel cost before and after applying the FLC.

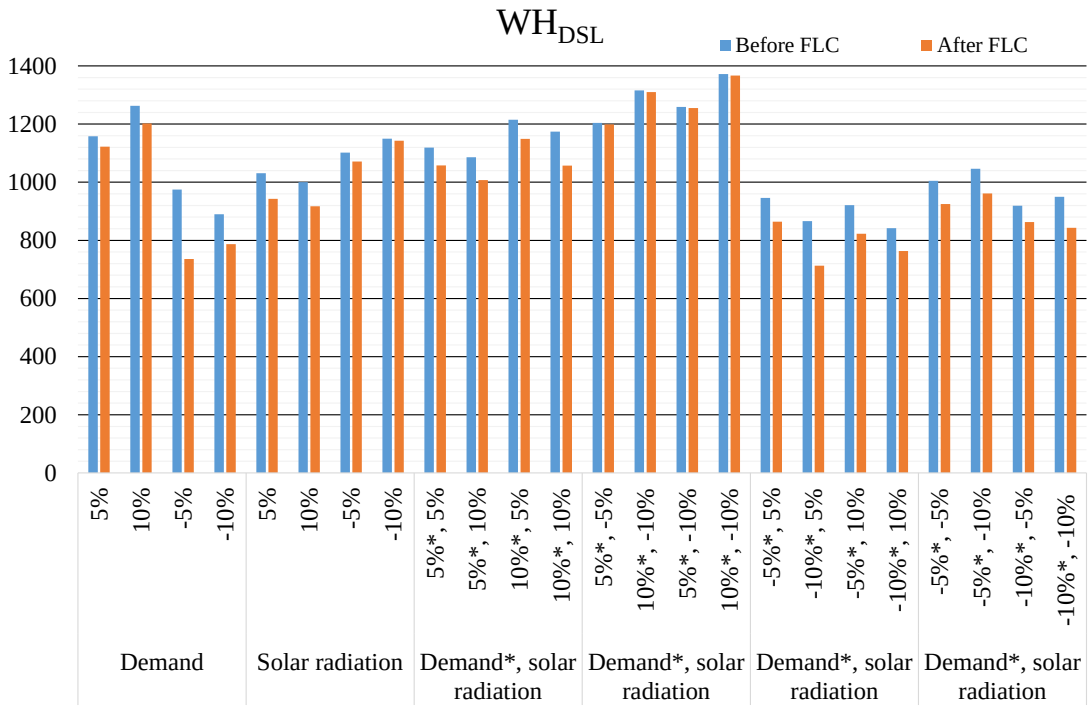

Figure 5.13: The DSL working hours before and after applying the FLC.

reduction in demand making the DSL to operate less hours. Overall, the FLC

has reduced the DSL working hours leading to reduce the replacement costs of the DSL.

Figure 5.14 illustrates the improvements in the PV contribution after applying the FLC. It is observed that for most of the scenarios, the PV contribution has been raised to 100%. There are a group of scenarios that have 100% utilisation of PV before applying the FLC. Such as, scenario 14 (+10% P_{load}, -5% I_{PV}), 15 (+5% P_{load}, -10% I_{PV}), and 16 (+10% P_{load}, -10% I_{PV}). However, the improvements that have been made by the FLC yielded in exploiting the PV energy to the maximum.

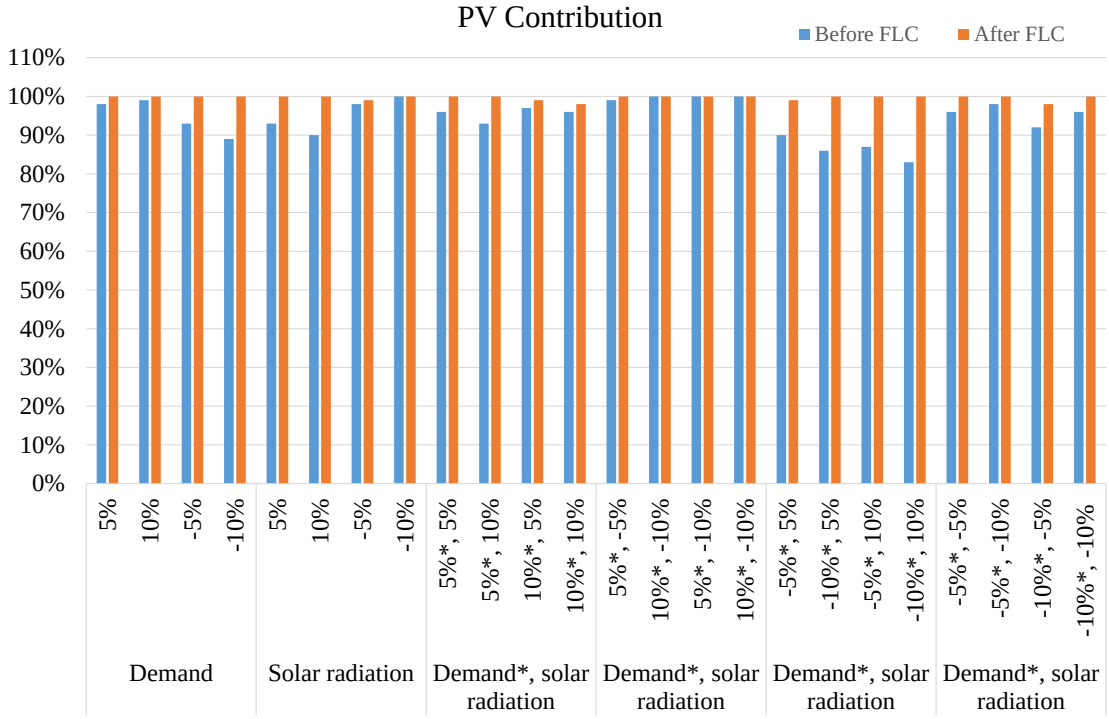

Figure 5.14: The percentage of the PV contribution before and after applying the FLC.

5.4.4 *Validation Case Study*

To validate the benefits of using the FLC, a case study is implemented for stand-alone HES. This HES is introduced in Chapter 4 and consists of PV, BESS, DSL, FC, EL, and HT. The size of the assets in the HES are presented in Section 5.2. This case study shows the improvements in the performance of the HES before

and after applying the FLC. The FLC aims at replacing the operating conditions of the DSL, FC, and EL by modified conditions. Therefore, the performance of the HES is enhanced in terms of reliability and cost. Several scenarios are selected from the 24 sensitivity analysis scenarios to demonstrate the effect of applying the FLC on the HES performance. Table 5.15 describes the selected scenarios with the performance indices before and after applying the FLC.

The scenarios selected for the case study are 2, 8, 11, 16, 18, and 24. These scenarios have been chosen to include various changes in demand and solar radiation (see Table 5.14). Scenario 2 indicates an annual increase in demand values by +5%. When comparing the performance indices for this scenario before and after applying the FLC, it is observed a reduction in the fuel cost by £ 924. Also the WH_{DSL} is decreased by 61 hours/year. On the other hand, there is a considerable increase in FC working hours. The WH_{FC} has increased by 437 hours/year. This is due to the modified condition of the FC obtained by conditions set B (see Table 5.10). This condition allows the FC to operate more than previously (see Table 5.13), leading to an increase in the FC working hours. The WH_{EL} has increased by 47 hours/year, as the modified condition for the EL enables the operation of the EL when the soc is higher than 85%. Although the decrease in the WH_{DSL} for this scenario is not significant compared to the base case (see Table 5.14), however, the improvement achieved is better than before.

Scenario 16 represents the worst case of all the sensitivity analysis scenarios. The demand values decreased by 10% and the solar radiation values increased by 10%. Before applying the FLC, the performance indices of this scenario are considered the highest among the other scenarios. The improvements in these indices after applying the FLC are minor. For instance, the fuel cost value decreased by £ 75, and the WH_{DSL} reduced by 5 hours/year. The other performance indices such as WH_{FC} and WH_{EL} increased by 5 hours/year.

Table 5.15: Different scenarios used for the case study showing the effectiveness of applying the FLC.

Scenario	Before FLC					After FLC				
	Fuel cost (£)	WH_{DSL} (hrs./year)	WH_{FC} (hrs./year)	WH_{EL} (hrs./year)	PV contr.	Fuel cost (£)	WH_{DSL} (hrs./year)	WH_{FC} (hrs./year)	WH_{EL} (hrs./year)	PV contr.
Scenario **2** +10% P_{load}	19131	1263	75	336	99%	18207	1202	512	383	100%
Scenario **8** -10% I_{PV}	17420	1150	64	309	100%	17314	1143	60	289	100%
Scenario **11** +10% P_{load} +5% I_{PV}	18404	1215	78	334	97%	17404	1149	524	384	99%
Scenario **16** +10% P_{load} -10% I_{PV}	20782	1372	51	255	100%	20707	1367	55	261	100%
Scenario **18** -10% P_{load} +5% I_{PV}	13118	866	55	246	86%	10800	713	386	566	100%
Scenario **24** -10% P_{load} -10% I_{PV}	14390	950	60	279	96%	12769	843	115	422	100%

5.5 CONCLUDING REMARKS

This chapter shows an investigation into modifying the EMS with the presence of uncertain demand and generation conditions. This investigation involves conducting a sensitivity analysis to generate several scenarios over a variation of ±5% and ±10% of demand and solar radiation. These scenarios have been utilised in implementing a FLC. The objective of such controller is managing the variations in the demand and solar radiation by modifying the operating conditions of the DSL, FC, and EL. Several scenarios were compared before and after applying the FLC. The results obtained show an improvement in the performance of the HES for most of the variations in the demand and solar radiation. The data used here (solar radiation and demand) are forecasted using Gaussian noise and done with MATLAB. In reality, the changes in these data may be unexpected. Therefore, as a future work, forecasted algorithms that provide accurate data will be used.

6

CONCLUSIONS AND FUTURE WORK

6.1 SUMMARY AND CONCLUSIONS

Microgrids have emerged to facilitate the integration of Renewable Energy Resources (RERs) and Energy Storage Systems (ESSs) in the traditional distribution systems. Effective use of diverse RER can provide a strong base for sustainable development, therefore, careful selection of the RERs and managing their operation are fundamental. This thesis aimed to investigate into sizing and energy management strategies of microgrids. The assets of a microgrid, whether grid-connected or stand-alone, have been sized from an economic point of view. The development of an efficient Energy Management Strategy (EMS) has been performed to reduce operational costs with ensuring continuous demand satisfaction. This section summarizes the main conclusions derived from this thesis.

Sizing of distributed energy resources plays a vital role in microgrid design. It offers the appropriate size of each asset to obtain the optimal microgrid operation. In the literature, various methods are used for sizing the microgrid assets, such as graphical construction, analytical, probabilistic, iterative, artificial intelligence, hybrid, and software tools. None of these methods could achieve better optimisation than the other methods on all types of problems (see Chapter 2). However, in this thesis, the analytical method was selected as the main method for the sizing of a grid-connected and stand-alone microgrids. Analytical methods have been widely applied in the literature for their capability in providing accurate results. Additionally, implementing an effective energy management strategy is critical to maintaining the balance between generation and demand. Determining the best size-EMS combination emerges from the significance of achieving a reliable,

cost-effective, and environmentally friendly microgrid design. The key features and limitations of research efforts to date in the domain of sizing methods and energy management strategies are summarised in this thesis (see Chapter 2).

An Analytical and Economic Sizing (AES) was implemented to obtain the optimal size of a grid-connected Photovoltaic (PV)-Battery Energy Storage System (BESS). Three types of BESSs are considered and the most economic combination of PV-BESS has been selected. To evaluate the microgrid with the BESSs, three case studies have been assessed and the results have shown the combination PV-Redox Flow Battery (RFB) is the most cost-effective and reliable system. Moreover, the performance of the PV-RFB combination has been examined with reference to two different scenarios; when the demand depends completely on the grid and when the PV only is installed in the microgrid. The results obtained have indicated that the combination PV-RFB outperforms the other scenarios.

The AES approach is further developed to be included in the integrated framework for sizing stand-alone Hybrid Energy System (HES). The proposed framework aims at finding the optimal size-EMS of a HES. The modified AES is responsible for determining an initial size of the HES based on initial EMS. Then, Finite Automata (FA) has been utilised to implement the initial EMS and instantiate multiple EMSs. These EMSs share the basic characteristics of the initial EMS with modifying the operating condition of the diesel generator, fuel cell and electrolyser operation. An evaluation model has been developed to assess the EMSs and select the featured conditions based on computed performance indices. The selected operating conditions are then used to form an improved EMS that replaces the initial one. Following that, the AES has been used to find the new size of the HES with the improved EMS. The results obtained by the proposed framework demonstrate a reduction in the cost, PV energy loses, and the size of the PV system to the half (see Chapter 4).

A Fuzzy Logic Controller (FLC) has been implemented to address the uncertainty in demand and solar radiation. The main aim of this controller is to detect the changes in input data and accordingly modify the operating conditions of the Diesel Generator (DSL), Fuel Cell (FC), and Electrolyser (EL). The FLC is

utilised as a decision maker to keep the HES performance within an acceptable level regardless of the changes in the input data. A sensitivity analysis has been carried out generating several scenarios. The performance indices of the generated scenarios have been used to determine the input fuzzy sets. The obtained results have demonstrated an improvement in the performance of the HES for most of the scenarios involved (see Chapter 5).

6.2 CRITICAL REVIEW AND FUTURE WORK

The objectives of this thesis include opening a new research horizons for sizing and energy management of microgrids. Therefore, many research directions can be drawn and motivated from this thesis to achieve more performance and energy efficiency. The limitations of this work and directions for future research are discussed as follows:

- *Acquiring real datasets*: the PV profiles used in this thesis are real datasets, however, the demand profiles employed with the AES to size a grid-connected microgrid are not. It was a challenge to obtain the real demand profiles for the Isle of Wight. Requesting the required demand profiles needs time and usually are not free of charge. However, in future work, including real datasets in the simulations can provide more reliable results.

- *Finite automata tools*: the FA used for implementing EMS has been performed using Simulink/state flow. However, there are available tools that can offer an automated procedure for generating multiple EMSs. This is will allow to accelerate the process of modelling EMS using FA and can go further step by including more iterations in the integrated framework. Examples on these tools are TCT [99] and PHAVer [164].

- Complexity and performance issues: the hydrogen system of the HES (FC, EL, and Hydrogen Tank (HT)) has not been considered in the calculations of the Levelised Cost of Energy (LCOE). Including the hydrogen system in the LCOE computations will increase the complexity of the simulations and

the AES will not be able to deal with the large number of parameters. In future work, Artificial Intelligence (AI) or hybrid methods could be explored to overcome the complexity resulted from increasing the number of assets in the microgrid.

We believe that the research outcomes generated by this thesis will be useful for the area of microgrid design, and continue to inspire further research and development in the above-mentioned directions.

Part II

Thesis Bibliography

BIBLIOGRAPHY

[1] "U.s. securities and exchange commission / captial markets day." https://www.sec.gov/. [Online; accessed August-2017].

[2] NREL, "Pv watts calculator." http://pvwatts.nrel.gov/pvwatts.php. Accessed 10.05.2017.

[3] OpenEI, "Us department of energy." http://en.openei.org/doe-opendata/dataset/commercial-and-residential-hourly-load-profiles-for-all-tmy3-locations-in-the-united-states/. Accessed 10.05.2017.

[4] "Pvwatts calculator." http://pvwatts.nrel.gov/. [Online; accessed December-2017].

[5] "Customer-led network revolution." http://www.networkrevolution.co.uk/project-library. [Online; accessed Februry-2018].

[6] S. Sinha and S. Chandel, "Review of recent trends in optimization techniques for solar photovoltaic-wind based hybrid energy system," *Renewable and Sustainable Energy Reviews*, vol. 50, pp. 755 – 769, 2015.

[7] B. Bhandari, K.-T. Lee, G.-Y. Lee, Y.-M. Cho, and S.-H. Ahn, "Optimization of hybrid renewable energy power systems: A review," *International Journal of Precision Engineering and Manufacturing-Green Technology*, vol. 2, pp. 99–112, Jan 2015.

[8] F. A. Khan, N. Pal, and S. Saeed, "Review of solar photovoltaic and wind hybrid energy systems for sizing strategies optimization techniques and cost analysis methodologies," *Renewable and Sustainable Energy Reviews*, vol. 92, pp. 937 – 947, 2018.

[9] K. Anoune, M. Bouya, A. Astito, and A. B. Abdellah, "Sizing methods and optimization techniques for pv-wind based hybrid renewable energy system: A review," *Renewable and Sustainable Energy Reviews*, vol. 93, pp. 652 – 673, 2018.

[10] Y. Khawaja, D. Giaouris, H. Patsios, and M. Dahidah, "Optimal cost-based model for sizing grid-connected pv and battery energy system," in *2017 IEEE Jordan Conference on Applied Electrical Engineering and Computing Technologies (AEECT)*, pp. 1–6, 2017.

[11] R. Hosseinalizadeh, H. S. G, M. Amalnick, and P. Taghipour, "Economic sizing of a hybrid (PV/WT/FC) renewable energy system (HRES) for stand-alone usages by an optimization-simulation model: Case study of iran," *Renewable and Sustainable Energy Reviews*, vol. 54, pp. 139–150, 2016.

[12] M. Mehrpooya, M. Mohammadi, and E. Ahmadi, "Techno-economic-environmental study of hybrid power supply system: A case study in iran," *Sustainable Energy Technologies and Assessments*, vol. 25, pp. 1 – 10, 2018.

[13] A. Hirsch, Y. Parag, and J. Guerrero, "Microgrids: A review of technologies, key drivers, and outstanding issues," *Renewable and Sustainable Energy Reviews*, vol. 90, pp. 402 – 411, 2018.

[14] A. C. Marques, J. A. Fuinhas, and J. P. Manso, "Motivations driving renewable energy in european countries: A panel data approach," *Energy Policy*, vol. 38, no. 11, pp. 6877 – 6885, 2010. Energy Efficiency Policies and Strategies with regular papers.

[15] J. Rogelj, M. Den Elzen, N. Höhne, T. Fransen, H. Fekete, H. Winkler, R. Schaeffer, F. Sha, K. Riahi, and M. Meinshausen, "Paris agreement climate proposals need a boost to keep warming well below 2 c," *Nature*, vol. 534, no. 7609, p. 631, 2016.

[16] F. DinÃ§er, "The analysis on photovoltaic electricity generation status, potential and policies of the leading countries in solar energy," *Renewable and Sustainable Energy Reviews*, vol. 15, no. 1, pp. 713 – 720, 2011.

[17] M. Diesendorf and B. Elliston, "The feasibility of 100systems: A response to critics," *Renewable and Sustainable Energy Reviews*, vol. 93, pp. 318 – 330, 2018.

[18] D. P. Kaundinya, P. Balachandra, and N. Ravindranath, "Grid-connected versus stand-alone systems for decentralized power-a review of literature," *Renewable and Sustainable Energy Reviews*, vol. 13, no. 8, pp. 2041 – 2050,

2009.

[19] Z. Cheng, J. Duan, and M. Chow, "To centralize or to distribute: That is the question: A comparison of advanced microgrid management systems," *IEEE Industrial Electronics Magazine*, vol. 12, pp. 6–24, March 2018.

[20] S. Parhizi, H. Lotfi, A. Khodaei, and S. Bahramirad, "State of the art in research on microgrids: A review," *IEEE Access*, vol. 3, pp. 890–925, 2015.

[21] N. Lidula and A. Rajapakse, "Microgrids research: A review of experimental microgrids and test systems," *Renewable and Sustainable Energy Reviews*, vol. 15, no. 1, pp. 186 – 202, 2011.

[22] M. F. Zia, E. Elbouchikhi, and M. Benbouzid, "Microgrids energy management systems: A critical review on methods, solutions, and prospects," *Applied Energy*, vol. 222, pp. 1033 – 1055, 2018.

[23] G. Singh, "Solar power generation by pv (photovoltaic) technology: A review," *Energy*, vol. 53, pp. 1 – 13, 2013.

[24] L. Olatomiwa, S. Mekhilef, M. Ismail, and M. Moghavvemi, "Energy management strategies in hybrid renewable energy systems: A review," *Renewable and Sustainable Energy Reviews*, vol. 62, pp. 821 – 835, 2016.

[25] A. L. Bukar and C. W. Tan, "A review on stand-alone photovoltaic-wind energy system with fuel cell: System optimization and energy management strategy," *Journal of Cleaner Production*, vol. 221, pp. 73 – 88, 2019.

[26] F. Vivas, A. D. las Heras, F. Segura, and J. AndÃºjar, "A review of energy management strategies for renewable hybrid energy systems with hydrogen backup," *Renewable and Sustainable Energy Reviews*, vol. 82, pp. 126 – 155, 2018.

[27] M. Roslan, M. Hannan, P. J. Ker, and M. Uddin, "Microgrid control methods toward achieving sustainable energy management," *Applied Energy*, vol. 240, pp. 583 – 607, 2019.

[28] J. Kumar, A. Agarwal, and V. Agarwal, "A review on overall control of dc microgrids," *Journal of Energy Storage*, vol. 21, pp. 113 – 138, 2019.

[29] C. H. Li, X. J. Zhu, G. Y. Cao, S. Sui, and M. R. Hu, "Dynamic modeling and sizing optimization of standalone photovoltaic power systems using hybrid

energy storage technology," *Renewable Energy*, vol. 34, no. 3, pp. 815–826, 2009.

[30] M. Smaoui, A. Abdelkafi, and L. Krichen, "Optimal sizing of stand-alone photovoltaic/wind/hydrogen hybrid system supplying a desalination unit," *Solar Energy*, vol. 120, pp. 263 – 276, 2015.

[31] A. Maleki and A. Askarzadeh, "Comparative study of artificial intelligence techniques for sizing of a hydrogen-based stand-alone photovoltaic/wind hybrid system," *International Journal of Hydrogen Energy*, vol. 39, no. 19, pp. 9973 – 9984, 2014.

[32] M. H. Amrollahi and S. M. T. Bathaee, "Techno-economic optimization of hybrid photovoltaic/wind generation together with energy storage system in a stand-alone micro-grid subjected to demand response," *Applied Energy*, vol. 202, pp. 66 – 77, 2017.

[33] J. Torreglosa, P. García, L. Fernández, and F. Jurado, "Hierarchical energy management system for stand-alone hybrid system based on generation costs and cascade control," *Energy Conversion and Management*, vol. 77, pp. 514 – 526, 2014.

[34] W.-M. Lin, C.-S. Tu, and M.-T. Tsai, "Energy management strategy for microgrids by using enhanced bee colony optimization," *Energies*, vol. 9, no. 1, p. 5, 2016.

[35] A. C. Luna, N. L. Diaz, M. Graells, J. C. Vasquez, and J. M. Guerrero, "Mixed-integer-linear-programming-based energy management system for hybrid pv-wind-battery microgrids: Modeling, design, and experimental verification," *IEEE Transactions on Power Electronics*, vol. 32, no. 4, pp. 2769–2783, 2017.

[36] B. Zhao, X. Zhang, P. Li, K. Wang, M. Xue, and C. Wang, "Optimal sizing, operating strategy and operational experience of a stand-alone microgrid on dongfushan island," *Applied Energy*, vol. 113, pp. 1656 – 1666, 2014.

[37] M. C. neda, A. Cano, F. Jurado, H. Sánchez, and L. M. Fernández, "Sizing optimization, dynamic modeling and energy management strategies of a stand-alone pv/hydrogen/battery-based hybrid system," *International*

Journal of Hydrogen Energy, vol. 38, no. 10, pp. 3830 – 3845, 2013.

[38] A. Maleki, F. Pourfayaz, and M. A. Rosen, "A novel framework for optimal design of hybrid renewable energy-based autonomous energy systems: A case study for namin, iran," *Energy*, vol. 98, pp. 168 – 180, 2016.

[39] Y. Khawaja, A. Allahham, D. Giaouris, C. Patsios, S. Walker, and I. Qiqieh, "An integrated framework for sizing and energy management of hybrid energy systems using finite automata," *Applied Energy*, vol. 250, pp. 257 – 272, 2019.

[40] REN21, "Renewables 2018 global status report," tech. rep., Paris: REN21 Secretariat, 2018.

[41] B. Singh, C. Pal, V. Mukherjee, P. Tiwari, and M. K. Yadav, "Distributed generation planning from power system performances viewpoints: A taxonomical survey," *Renewable and Sustainable Energy Reviews*, vol. 75, pp. 1472 – 1492, 2017.

[42] S. Upadhyay and M. Sharma, "A review on configurations, control and sizing methodologies of hybrid energy systems," *Renewable and Sustainable Energy Reviews*, vol. 38, pp. 47 – 63, 2014.

[43] X. Zhang, H. Chen, Y. Xu, W. Li, F. He, H. Guo, and Y. Huang, "Distributed generation with energy storage systems: A case study," *Applied Energy*, vol. 204, pp. 1251 – 1263, 2017.

[44] N. Lidula and A. Rajapakse, "Microgrids research: A review of experimental microgrids and test systems," *Renewable and Sustainable Energy Reviews*, vol. 15, no. 1, pp. 186 – 202, 2011.

[45] A. Banerji, D. Sen, A. K. Bera, D. Ray, D. Paul, A. Bhakat, and S. K. Biswas, "Microgrid: A review," in *2013 IEEE Global Humanitarian Technology Conference: South Asia Satellite (GHTC-SAS)*, pp. 27–35, Aug 2013.

[46] D. T. Ton and M. A. Smith, "The u.s. department of energy's microgrid initiative," *The Electricity Journal*, vol. 25, no. 8, pp. 84 – 94, 2012.

[47] *Distributed generation and Microgrid concept*, ch. Distributed generation and Microgrid concept. Institution of Engineering and Technology, 2009.

[48] A. Khodaei and M. Shahidehpour, "Microgrid-based co-optimization of generation and transmission planning in power systems," *IEEE Transactions on Power Systems*, vol. 28, pp. 1582–1590, May 2013.

[49] H. Liang and W. Zhuang, "Stochastic modeling and optimization in a microgrid: A survey," *Energies*, vol. 7, no. 4, pp. 2027–2050, 2014.

[50] H. Ibrahim and A. Ilinca, "Techno-economic analysis of different energy storage technologies," in *Energy Storage-Technologies and Applications*, InTech, 2013.

[51] O. Erdinc and M. Uzunoglu, "Optimum design of hybrid renewable energy systems: Overview of different approaches," *Renewable and Sustainable Energy Reviews*, vol. 16, no. 3, pp. 1412 – 1425, 2012.

[52] X. Luo, J. Wang, M. Dooner, and J. Clarke, "Overview of current development in electrical energy storage technologies and the application potential in power system operation," *Applied Energy*, vol. 137, pp. 511–536, 2015.

[53] A. Clerjon and F. Perdu, "Matching intermittency and electricity storage characteristics through time scale analysis: an energy return on investment comparison," *Energy Environ. Sci.*, vol. 12, pp. 693–705, 2019.

[54] T. M. Gür, "Review of electrical energy storage technologies, materials and systems: challenges and prospects for large-scale grid storage," *Energy & Environmental Science*, vol. 11, pp. 2696–2767, 2018.

[55] A. K. Arani, G. B. Gharehpetian, and M. Abedi, "Review on energy storage systems control methods in microgrids," *International Journal of Electrical Power & Energy SYstems*, vol. 107, pp. 745 – 757, 2019.

[56] M. Aneke and M. Wang, "Energy storage technologies and real life applications: A state of the art review," *Applied Energy*, vol. 179, pp. 350 – 377, 2016.

[57] M. Faisal, M. A. Hannan, P. J. Ker, A. Hussain, M. B. Mansor, and F. Blaabjerg, "Review of energy storage system technologies in microgrid applications: Issues and challenges," *IEEE Access*, vol. 6, pp. 35143–35164, 2018.

[58] D. Aydin, S. P. Casey, and S. Riffat, "The latest advancements on thermochemical heat storage systems," *Renewable and Sustainable Energy Reviews*, vol. 41, pp. 356 – 367, 2015.

[59] "Energy storage in the uk an overview," tech. rep., Renewable Energy Association, 2016.

[60] A. S. Lavine, K. M. Lovegrove, J. Jordan, G. B. Anleu, C. Chen, H. Aryafar, and A. Sepulveda, "Thermochemical energy storage swith ammonia: Aiming for the sunshot cost target," in *AIP Conference Proceedings*, vol. 1734, p. 050028, AIP Publishing, 2016.

[61] S. Twaha and M. A. Ramli, "A review of optimization approaches for hybrid distributed energy generation systems: Off-grid and grid-connected systems," *Sustainable Cities and Society*, vol. 41, pp. 320 – 331, 2018.

[62] A. H. Fathima and K. Palanisamy, "Optimization in microgrids with hybrid energy systems: A review," *Renewable and Sustainable Energy Reviews*, vol. 45, pp. 431–446, 2015.

[63] P. Nema, R. Nema, and S. Rangnekar, "A current and future state of art development of hybrid energy system using wind and pv-solar: A review," *Renewable and Sustainable Energy Reviews*, vol. 13, no. 8, pp. 2096–2103, 2009.

[64] B. Madaci, R. Chenni, E. Kurt, and K. E. Hemsas, "Design and control of a stand-alone hybrid power system," *International Journal of Hydrogen Energy*, vol. 41, no. 29, pp. 12485 – 12496, 2016. Special Issue on 3rd European Conference on Renewable Energy Systems (ECRES 2015), 7-10 October 2015, Kemer, Antalya, Turkey.

[65] S. Guo, Q. Liu, J. Sun, and H. Jin, "A review on the utilization of hybrid renewable energy," *Renewable and Sustainable Energy Reviews*, vol. 91, pp. 1121 – 1147, 2018.

[66] W. Zhou, C. Lou, Z. Li, L. Lu, and H. Yang, "Current status of research on optimum sizing of stand-alone hybrid solar-wind power generation systems," *Applied Energy*, vol. 87, no. 2, pp. 380 – 389, 2010.

[67] D. Giaouris, A. I. Papadopoulos, C. Ziogou, D. Ipsakis, S. Voutetakis, S. Papadopoulou, P. Seferlis, F. Stergiopoulos, and C. Elmasides, "Performance investigation of a hybrid renewable power generation and storage system using systemic power management models," *Energy*, vol. 61, pp. 621 – 635, 2013.

[68] J. Lagorse, D. Paire, and A. Miraoui, "A multi-agent system for energy management of distributed power sources," *Renewable Energy*, vol. 35, no. 1, pp. 174 – 182, 2010.

[69] M. Trifkovic, M. Sheikhzadeh, K. Nigim, and P. Daoutidis, "Modeling and control of a renewable hybrid energy system with hydrogen storage," *IEEE Transactions on Control Systems Technology*, vol. 22, no. 1, pp. 169–179, 2014.

[70] J.-H. Cho, M.-G. Chun, and W.-P. Hong, "Structure optimization of stand-alone renewable power systems based on multi object function," *Energies*, vol. 9, no. 8, p. 649, 2016.

[71] W. Zhou, C. Lou, Z. Li, L. Lu, and H. Yang, "Current status of research on optimum sizing of stand-alone hybrid solar-wind power generation systems," *Applied Energy*, vol. 87, no. 2, pp. 380 – 389, 2010.

[72] D. Saheb-Koussa, M. Koussa, M. Belhamel, and M. Haddadi, "Economic and environmental analysis for grid-connected hybrid photovoltaic-wind power system in the arid region," *Energy Procedia*, vol. 6, pp. 361 – 370, 2011. Impact of Integrated Clean Energy on the Future of the Mediterranean Environment.

[73] R. Luna-Rubio, M. Trejo-Perea, D. Vargas-VÃ¡zquez, and G. RÃos-Moreno, "Optimal sizing of renewable hybrids energy systems: A review of methodologies," *Solar Energy*, vol. 86, no. 4, pp. 1077 – 1088, 2012. ISRES 2010.

[74] S. M. Dawoud, X. Lin, and M. I. Okba, "Hybrid renewable microgrid optimization techniques: A review," *Renewable and Sustainable Energy Reviews*, vol. 82, pp. 2039 – 2052, 2018.

[75] G. Tina, S. Gagliano, and S. Raiti, "Hybrid solar/wind power system probabilistic modelling for long-term performance assessment," *Solar Energy*,

vol. 80, no. 5, pp. 578 – 588, 2006.

[76] P. Zhou, R. Jin, and L. Fan, "Reliability and economic evaluation of power system with renewables: A review," *Renewable and Sustainable Energy Reviews*, vol. 58, pp. 537 – 547, 2016.

[77] M. Bazilian, I. Onyeji, M. Liebreich, I. MacGill, J. Chase, J. Shah, D. Gielen, D. Arent, D. Landfear, and S. Zhengrong, "Re-considering the economics of photovoltaic power," *Renewable Energy*, vol. 53, pp. 329–338, 2013.

[78] K. Branker, M. Pathak, and J. Pearce, "A review of solar photovoltaic levelized cost of electricity," *Renewable and Sustainable Energy Reviews*, vol. 15, no. 9, pp. 4470–4482, 2011.

[79] C. S. Lai and M. D. McCulloch, "Levelized cost of electricity for solar photovoltaic and electrical energy storage," *Applied Energy*, vol. 190, pp. 191 – 203, 2017.

[80] A. Kaabeche, M. Belhamel, and R. Ibtiouen, "Sizing optimization of grid-independent hybrid photovoltaic/wind power generation system," *Energy*, vol. 36, no. 2, pp. 1214 – 1222, 2011.

[81] B. Mozafari and S. Mohammadi, "Optimal sizing of energy storage system for microgrids," *Sadhana*, vol. 39, pp. 819–841, Aug 2014.

[82] J. M. Guerrero, J. C. Vasquez, J. Matas, L. G. de Vicuna, and M. Castilla, "Hierarchical control of droop-controlled ac and dc microgrids-a general approach toward standardization," *IEEE Transactions on Industrial Electronics*, vol. 58, pp. 158–172, Jan 2011.

[83] P. P. Vergara, J. C. López, J. M. Rey, L. C. P. da Silva, and M. J. Rider, *Energy Management in Microgrids*, pp. 195–216. Cham: Springer International Publishing, 2019.

[84] D. E. Olivares, A. Mehrizi-Sani, A. H. Etemadi, C. A. Cañzares, R. Iravani, M. Kazerani, A. H. Hajimiragha, O. Gomis-Bellmunt, M. Saeedifard, R. Palma-Behnke, G. A. Jiménez-Estévez, and N. D. Hatziargyriou, "Trends in microgrid control," *IEEE Transactions on Smart Grid*, vol. 5, pp. 1905–1919, July 2014.

[85] C. Ziogou, D. Ipsakis, P. Seferlis, S. Bezergianni, S. Papadopoulou, and S. Voutetakis, "Optimal production of renewable hydrogen based on an efficient energy management strategy," *Energy*, vol. 55, pp. 58 – 67, 2013.

[86] D. Solow, "Linear and nonlinear programming," *Wiley Encyclopedia of Computer Science and Engineering*, 2007.

[87] J. P. Torreglosa, P. G.-T. no, L. M. Fernández-Ramirez, and F. Jurado, "Control based on techno-economic optimization of renewable hybrid energy system for stand-alone applications," *Expert Systems with Applications*, vol. 51, pp. 59 – 75, 2016.

[88] E. Eriksson and E. Gray, "Optimization and integration of hybrid renewable energy hydrogen fuel cell energy systems –a critical review," *Applied Energy*, vol. 202, pp. 348–364, 2017.

[89] A. Askarzadeh, "A memory-based genetic algorithm for optimization of power generation in a microgrid," *IEEE Transactions on Sustainable Energy*, vol. 9, pp. 1081–1089, July 2018.

[90] M. Manbachi and M. Ordonez, "Ami-based energy management for islanded ac/dc microgrids utilizing energy conservation and optimization," *IEEE Transactions on Smart Grid*, vol. 10, pp. 293–304, Jan 2019.

[91] J. E. Hopcroft, *Introduction to automata theory, languages, and computation*. Pearson Education India, 2008.

[92] M. Skoldstam, K. Akesson, and M. Fabian, "Modeling of discrete event systems using finite automata with variables," in *2007 46th IEEE Conference on Decision and Control*, pp. 3387–3392, 2007.

[93] P. J. G. Ramadge and W. M. Wonham, "The control of discrete event systems," *Proceedings of the IEEE*, vol. 77, no. 1, pp. 81–98, 1989.

[94] M. Skoldstam, K. Akesson, and M. Fabian, "Modeling of discrete event systems using finite automata with variables," in *2007 46th IEEE Conference on Decision and Control*, pp. 3387–3392, 2007.

[95] J. Prosser, J. Selinsky, H. Kwatny, and M. Kam, "Supervisory control of electric power transmission networks," *IEEE Transactions on Power Systems*, vol. 10, no. 2, pp. 1104–1110, 1995.

[96] M. S. Lee and J. T. Lim, "Restoration strategy for power distribution networks using optimal supervisory control," *IEE Proceedings-Generation, Transmission and Distribution*, vol. 151, no. 3, pp. 367–372, 2004.

[97] A. Afzalian, A. Saadatpoor, and W. M. Wonham, "Discrete-event system modeling and supervisory control for under-load tap-changing transformers," in *IEEE Conference on Computer Aided Control System Design, IEEE International Conference on Control Applications, IEEE International Symposium on Intelligent Control*, pp. 1867–1872, 2006.

[98] A. A. Afzalian, S. A. N. Niaki, M. R. Iravani, and W. M. Wonham, "Discrete-event systems supervisory control for a dynamic flow controller," *IEEE Transactions on Power Delivery*, vol. 24, no. 1, pp. 219–230, 2009.

[99] L. Feng and W. M. Wonham, "Tct: A computation tool for supervisory control synthesis," in *2006 8th International Workshop on Discrete Event Systems*, pp. 388–389, 2006.

[100] A. Kharrazi, Y. Mishra, and V. Sreeram, "Discrete-event systems supervisory control for a custom power park," *IEEE Transactions on Smart Grid*, vol. PP, no. 99, pp. 1–1, 2017.

[101] W. H. Sadid, S. A. Abobakr, and G. Zhu, "Discrete-event systems-based power admission control of thermal appliances in smart buildings," *IEEE Transactions on Smart Grid*, vol. 8, no. 6, pp. 2665–2674, 2017.

[102] Z. Roumila, D. Rekioua, and T. Rekioua, "Energy management based fuzzy logic controller of hybrid system wind/photovoltaic/diesel with storage battery," *International Journal of Hydrogen Energy*, vol. 42, no. 30, pp. 19525 – 19535, 2017.

[103] M. Cirstea, A. Dinu, J. Khor, and M. McCormick, "Fuzzy logic fundamentals," in *Neural and Fuzzy Logic Control of Drives and Power Systems* (M. Cirstea, A. Dinu, J. Khor, and M. McCormick, eds.), pp. 113 – 122, Oxford: Newnes, 2002.

[104] S. A. Kalogirou, "Chapter eleven - designing and modeling solar energy systems," in *Solar Energy Engineering* (S. A. Kalogirou, ed.), pp. 553 – 664, Boston: Academic Press, 2009.

[105] S. A. Soliman, *Modern optimization techniques with applications in electric power systems*. Energy systems, New York, NY: Springer, 2012.

[106] A. Keshtkar and S. Arzanpour, "An adaptive fuzzy logic system for residential energy management in smart grid environments," *Applied Energy*, vol. 186, pp. 68 – 81, 2017.

[107] L. Suganthi, S. Iniyan, and A. A. Samuel, "Applications of fuzzy logic in renewable energy systems - a review," *Renewable and Sustainable Energy Reviews*, vol. 48, pp. 585 – 607, 2015.

[108] D. Arcos-Aviles, J. Pascual, F. Guinjoan, L. Marroyo, P. Sanchis, and M. P. Marietta, "Low complexity energy management strategy for grid profile smoothing of a residential grid-connected microgrid using generation and demand forecasting," *Applied Energy*, vol. 205, pp. 69 – 84, 2017.

[109] G. Kyriakarakos, A. I. Dounis, K. G. Arvanitis, and G. Papadakis, "A fuzzy logic energy management system for polygeneration microgrids," *Renewable Energy*, vol. 41, pp. 315 – 327, 2012.

[110] A. Gheibi, S. Mohammadi, and M. maghfoori, "Maximum power point tracking of photovoltaic generation based on the type 2 fuzzy logic control method," *Energy Procedia*, vol. 12, pp. 538 – 546, 2011. The Proceedings of International Conference on Smart Grid and Clean Energy Technologies (ICSGCE 2011.

[111] M. Macedo, J. Galo, L. Almeida, and A. Lima, "Methodology for the calculation of the factor of priority for smart grid implantation using fuzzy logic," *International Journal of Electrical Power & Energy Systems*, vol. 78, pp. 563 – 568, 2016.

[112] P. Bajpai and V. Dash, "Hybrid renewable energy systems for power generation in stand-alone applications: A review," *Renewable and Sustainable Energy Reviews*, vol. 16, no. 5, pp. 2926 – 2939, 2012.

[113] M. D. Al-falahi, S. Jayasinghe, and H. Enshaei, "A review on recent size optimization methodologies for standalone solar and wind hybrid renewable energy system," *Energy Conversion and Management*, vol. 143, pp. 252 – 274, 2017.

[114] T. Markvart, "Sizing of hybrid photovoltaic-wind energy systems," *Solar Energy*, vol. 57, no. 4, pp. 277 – 281, 1996.

[115] B. S. Borowy and Z. M. Salameh, "Methodology for optimally sizing the combination of a battery bank and pv array in a wind/pv hybrid system," *IEEE Transactions on Energy Conversion*, vol. 11, pp. 367–375, June 1996.

[116] D. K. Khatod, V. Pant, and J. Sharma, "Analytical approach for well-being assessment of small autonomous power systems with solar and wind energy sources," *IEEE Transactions on Energy Conversion*, vol. 25, pp. 535–545, June 2010.

[117] M. Bortolini, M. Gamberi, and A. Graziani, "Technical and economic design of photovoltaic and battery energy storage system," *Energy Conversion and Management*, vol. 86, pp. 81–92, 2014.

[118] A. Kanase-Patil, R. Saini, and M. Sharma, "Sizing of integrated renewable energy system based on load profiles and reliability index for the state of uttarakhand in india," *Renewable Energy*, vol. 36, no. 11, pp. 2809 – 2821, 2011.

[119] D. Q. Hung, N. Mithulananthan, and R. Bansal, "An optimal investment planning framework for multiple distributed generation units in industrial distribution systems," *Applied Energy*, vol. 124, pp. 62 – 72, 2014.

[120] Z. Wissem, K. Gueorgui, and K. HÃ©di, "Modeling and technical-economic optimization of an autonomous photovoltaic system," *Energy*, vol. 37, no. 1, pp. 263 – 272, 2012. 7th Biennial International Workshop, Advances in Energy Studies.

[121] S. S. KOLA, "A review on optimal allocation and sizing techniques for dg in distribution systems," *International Journal of Renewable Energy Research (IJRER)*, vol. 8, no. 3, pp. 1236–1256, 2018.

[122] U. Akram, M. Khalid, and S. Shafiq, "Optimal sizing of a wind/solar/battery hybrid grid-connected microgrid system," *IET Renewable Power Generation*, vol. 12, no. 1, pp. 72–80, 2017.

[123] S. Diaf, D. Diaf, M. Belhamel, M. Haddadi, and A. Louche, "A methodology for optimal sizing of autonomous hybrid pv/wind system," *Energy Policy*,

vol. 35, no. 11, pp. 5708 – 5718, 2007.

[124] R. Hosseinalizadeh, H. S. G, M. S. Amalnick, and P. Taghipour, "Economic sizing of a hybrid (pv-wt-fc) renewable energy system (hres) for stand-alone usages by an optimization-simulation model: Case study of iran," *Renewable and Sustainable Energy Reviews*, vol. 54, pp. 139 – 150, 2016.

[125] M. Smaoui, A. Abdelkafi, and L. Krichen, "Optimal sizing of stand-alone photovoltaic/wind/hydrogen hybrid system supplying a desalination unit," *Solar Energy*, vol. 120, pp. 263 – 276, 2015.

[126] F. A. Bhuiyan, A. Yazdani, and S. L. Primak, "Optimal sizing approach for islanded microgrids," *IET Renewable Power Generation*, vol. 9, no. 2, pp. 166–175, 2015.

[127] M. Das, M. A. Singh, A. Biswas, and K. K. Sharma, "Design and analysis of hybrid renewable energy system: A review," in *AIP Conference Proceedings*, vol. 1998, p. 020007, AIP Publishing, 2018.

[128] G. M. Tina and S. Gagliano, "Probabilistic modelling of hybrid solar/wind power system with solar tracking system," *Renewable Energy*, vol. 36, no. 6, pp. 1719 – 1727, 2011.

[129] S. Upadhyay and M. Sharma, "A review on configurations, control and sizing methodologies of hybrid energy systems," *Renewable and Sustainable Energy Reviews*, vol. 38, pp. 47 – 63, 2014.

[130] A. Mellit, S. Kalogirou, L. Hontoria, and S. Shaari, "Artificial intelligence techniques for sizing photovoltaic systems: A review," *Renewable and Sustainable Energy Reviews*, vol. 13, no. 2, pp. 406 – 419, 2009.

[131] D. Abbes, A. Martinez, and G. Champenois, "Life cycle cost, embodied energy and loss of power supply probability for the optimal design of hybrid power systems," *Mathematics and Computers in Simulation*, vol. 98, pp. 46 – 62, 2014.

[132] G. Merei, C. Berger, and D. U. Sauer, "Optimization of an off-grid hybrid pv-wind-diesel system with different battery technologies using genetic algorithm," *Solar Energy*, vol. 97, pp. 460 – 473, 2013.

[133] M. Combe, A. Mahmoudi, M. H. Haque, and R. Khezri, "Cost-effective sizing of an ac mini-grid hybrid power system for a remote area in south australia," *IET Generation, Transmission Distribution*, vol. 13, no. 2, pp. 277–287, 2019.

[134] A. Maleki, H. Hafeznia, M. A. Rosen, and F. Pourfayaz, "Optimization of a grid-connected hybrid solar-wind-hydrogen chp system for residential applications by efficient metaheuristic approaches," *Applied Thermal Engineering*, vol. 123, pp. 1263 – 1277, 2017.

[135] T. Khatib, A. Mohamed, and K. Sopian, "Optimization of a pv/wind microgrid for rural housing electrification using a hybrid iterative/genetic algorithm: Case study of kuala terengganu, malaysia," *Energy and Buildings*, vol. 47, pp. 321 – 331, 2012.

[136] T. Zhou and W. Sun, "Optimization of battery-supercapacitor hybrid energy storage station in wind/solar generation syatem," *IEEE Transactions on Sustainable Energy*, vol. 5, pp. 408–415, April 2014.

[137] Y. A. Katsigiannis, P. S. Georgilakis, and E. S. Karapidakis, "Hybrid simulated annealingtabu search method for optimal sizing of autonomous power systems with renewables," *IEEE Transactions on Sustainable Energy*, vol. 3, pp. 330–338, July 2012.

[138] A. Arabali, M. Ghofrani, M. Etezadi-Amoli, and M. S. Fadali, "Stochastic performance assessment and sizing for a hybrid power system of solar/wind/energy storage," *IEEE Transactions on Sustainable Energy*, vol. 5, pp. 363–371, April 2014.

[139] S. Sinha and S. Chandel, "Review of software tools for hybrid renewable energy systems," *Renewable and Sustainable Energy Reviews*, vol. 32, pp. 192 – 205, 2014.

[140] R. Sen and S. C. Bhattacharyya, "Off-grid electricity generation with renewable energy technologies in india: An application of homer," *Renewable Energy*, vol. 62, pp. 388 – 398, 2014.

[141] M. A. Ramli, A. Hiendro, K. Sedraoui, and S. Twaha, "Optimal sizing of grid-connected photovoltaic energy system in saudi arabia," *Renewable*

Energy, vol. 75, pp. 489 – 495, 2015.

[142] R. Rajbongshi, D. Borgohain, and S. Mahapatra, "Optimization of pv-biomass-diesel and grid base hybrid energy systems for rural electrification by using homer," *Energy*, vol. 126, pp. 461 – 474, 2017.

[143] "Isle of wight council." https://www.iow.gov.uk/Residents/Environment-Planning-and-Waste/Future-Energy-Initiatives/Renewable-Energy/Renewable-Energy-on-the-Island. [Online; accessed June-2016].

[144] M. Jarnut, S. Werminski, and B. Waskowicz, "Comparative analysis of selected energy storage technologies for prosumer-owned microgrids," *Renewable and Sustainable Energy Reviews*, vol. 74, pp. 925–937, 2017.

[145] M. Bortolini, M. Gamberi, A. Graziani, and F. Pilati, "Economic and enviromental bi-objective design of an off-grid photovoltaic-battery-diesel generator hybrid energy system," *Energy Conversion and Management*, vol. 106, pp. 1024 – 1038, 2015.

[146] M. Bortolini, M. Gamberi, A. Graziani, C. Mora, and A. Regattieri, "Multi-parameter analysis for the technical and economic assessment of photovoltaic systems in the main european union countries," *Energy Conversion & Management*, vol. 74, pp. 117–128, 2013.

[147] A. Chel, G. Tiwari, and A. Chandra, "Simplified method of sizing and life cycle cost assessment of building integrated photovoltaic system," *Energy and Buildings*, vol. 41, no. 11, pp. 1172 – 1180, 2009.

[148] S. Diaf, M. Belhamel, M. Haddadi, and A. Louche, "Technical and economic assessment of hybrid photovoltaic/wind system with battery storage in corsica island," *Energy Policy*, vol. 36, pp. 743 – 754, 2008.

[149] ScottishPower, "Prices your domestic gas and electricity pricing information, 2015." https://www.scottishpower.co.uk/pdf/SCP1492-Jan-15.pdf. Accessed 02.05.2017.

[150] A. Castillo and D. F. Gayme, "Grid-scale energy storage applications in renewable energy integration: A survey," *Energy Conversion and Management*, vol. 87, pp. 885 – 894, 2014.

[151] I. Pawel, "The cost of storage - how to calculate the levelized cost of stored energy (lcoe) and applications to renewable energy generation," *Energy Procedia*, vol. 46, pp. 68–77, 2014.

[152] T. Bocklisch, "Hybrid energy storage systems for renewable energy applications," *Energy Procedia*, vol. 73, pp. 103 – 111, 2015.

[153] J. Carroll and D. Long, "Theory of finite automata with an introduction to formal languages," 1989.

[154] S. Lafortune, "Discrete event systems: Modeling, observation, and control," *Annual Review of Control, Robotics, and Autonomous Systems*, vol. 2, no. 1, pp. 141–159, 2019.

[155] C. G. Cassandras and S. Lafortune, eds., *Languages and Automata*, pp. 53 – 131. Boston, MA: Springer US, 2008.

[156] D. Giaouris, A. I. Papadopoulos, S. Voutetakis, S. Papadopoulou, and P. Seferlis, "A power grand composite curves approach for analysis and adaptive operation of renewable energy smart grids," *Clean Technologies and Environmental Policy*, vol. 17, no. 5, pp. 1171–1193, 2015.

[157] D. Giaouris, A. I. Papadopoulos, P. Seferlis, S. Papadopoulou, S. Voutetakis, F. Stergiopoulos, and C. Elmasides, "Optimum energy management in smart grids based on power pinch analysis," *CHEMICAL ENGINEERING*, vol. 39, 2014.

[158] C. Wang and M. H. Nehrir, "Power management of a stand-alone wind/photovoltaic/fuel cell energy system," *IEEE Transactions on Energy Conversion*, vol. 23, no. 3, pp. 957–967, 2008.

[159] O. Schmidt, A. Gambhir, I. Staffell, A. Hawkes, J. Nelson, and S. Few, "Future cost and performance of water electrolysis: An expert elicitation study," *International Journal of Hydrogen Energy*, vol. 42, no. 52, pp. 30470 – 30492, 2017.

[160] C.-H. Li, X.-J. Zhu, G.-Y. Cao, S. Sui, and M.-R. Hu, "Dynamic modeling and sizing optimization of stand-alone photovoltaic power systems using hybrid energy storage technology," *Renewable Energy*, vol. 34, no. 3, pp. 815 – 826, 2009.

[161] "The price of fuel." https://www.petrolprices.com/the-price-of-fuel.html. [Online; accessed December-2017].

[162] A. Askarzadeh, "Distribution generation by photovoltaic and diesel generator systems: Energy management and size optimization by a new approach for a stand-alone application," *Energy*, vol. 122, pp. 542 – 551, 2017.

[163] M. Bortolini, M. Gamberi, A. Graziani, and F. Pilati, "Economic and environmental bi-objective design of an off-grid photovoltaic/battery/diesel generator hybrid energy system," *Energy Conversion and Management*, vol. 106, pp. 1024–1038, 2015.

[164] G. Frehse, "Phaver: Algorithmic verification of hybrid systems past hytech," in *International workshop on hybrid systems: computation and control*, pp. 258–273, Springer, 2005.